NORSAR

NORSAR Scientific Report No. 1-2002

Semiannual Technical Summary

1 July - 31 December 2001

Frode Ringdal (ed.)

Kjeller, February 2002

SECURITY CLASSIFICATION OF THIS PAGE

REPORT DOCUMENTATION PAGE

Form Approved OMB No. 0704-0188

1a. REPORT SECURITY CLASSIFICATION Unclassified	1b. RESTRICTIVE MARKINGS Not applicable
2a. SECURITY CLASSIFICATION AUTHORITY Not Applicable	3. DISTRIBUTION / AVAILABILITY OF REPORT Approved for public release; distribution unlimited
2b. DECLASSIFICATION / DOWNGRADING SCHEDULE	
4. PERFORMING ORGANIZATION REPORT NUMBER(S) Scientific Rep. 1-2002	5. MONITORING ORGANIZATION REPORT NUMBER(S) Scientific Rep. 1-2002
6a. NAME OF PERFORMING ORGANIZATION NORSAR 6b. OFFICE SYMBOL (*If applicable*)	7a. NAME OF MONITORING ORGANIZATION HQ/AFTAC/TTS
6c. ADDRESS (*City, State, and ZIP Code*) Post Box 51 N-2027 Kjeller, Norway	7b. ADDRESS (*City, State, and ZIP Code*) Patrick AFB, FL 32925-6001
8a. NAME OF FUNDING / SPONSORING ORGANIZATION Defense Threat Reduction Agency/NTPO 8b. OFFICE SYMBOL (*If applicable*) DTRA/NTPO	9. PROCUREMENT INSTRUMENT IDENTIFICATION NUMBER Contract No. F08650-01-C-0055
8c. ADDRESS (*City, State, and ZIP Code*) 1515 Wilson Blvd., Suite 720 Arlington, VA 22209	10. SOURCE OF FUNDING NUMBERS PROGRAM ELEMENT NO.: R&D PROJECT NO.: NORSAR Phase 3 TASK NO.: SOW Task 5.0 WORK UNIT ACCESSION NO.: Sequence No. 004A2
11. TITLE (*Include Security Classification*) Semiannual Technical Summary, 1 July - 31 December 2001 (Unclassified)	
12. PERSONAL AUTHOR(S)	
13a. TYPE OF REPORT Scientific Summary 13b. TIME COVERED FROM 1 Jul 01 TO 31 Dec 01	14. DATE OF REPORT (*Year, Month, Day*) 2002 Feb 15. PAGE COUNT 121
16. SUPPLEMENTARY NOTATION	

17. COSATI CODES			18. SUBJECT TERMS (*Continue on reverse if necessary and identify by block number*)
FIELD	GROUP	SUB-GROUP	
8	11		NORSAR, Norwegian Seismic Array

19. ABSTRACT (*Continue on reverse if necessary and identify by block number*)

This report describes the research activities carried out at NORSAR under Contract No. F08650-01-C-0055 for the period 1 July - 31 December 2001. In addition, it provides summary information on operation and maintenance (O&M) activities at the Norwegian National Data Center (NDC) during the same period. Research activities described in this report, as well as transmission of selected data to the United States NDC, are funded by the United States Department of Defense. The O&M activities, including operation of transmission links within Norway and to Vienna, Austria, are being funded jointly by the CTBTO/PTS and the Norwegian Government, with the understanding that the funding of IMS-related activities will gradually be transferred to the CTBTO/PTS. The O&M statistics presented in this report are included for the purpose of completeness, and in order to maintain consistency with earlier reporting practice.

(cont.)

20. DISTRIBUTION / AVAILABILITY OF ABSTRACT ☐ UNCLASSIFIED/UNLIMITED ☐ SAME AS RPT. ☐ DTIC USERS	21. ABSTRACT SECURITY CLASSIFICATION
22a. NAME OF RESPONSIBLE INDIVIDUAL Lt. Col. William S. Jones	22b. TELEPHONE (*Include Area Code*) (407) 494-7985 22c. OFFICE SYMBOL AFTAC/TTS

DD Form 1473, JUN 86 *Previous editions are obsolete.* SECURITY CLASSIFICATION OF THIS PAGE

Abstract (cont.)

The seismic arrays operated by the Norwegian NDC comprise the Norwegian Seismic Array (NOA), the Norwegian Regional Seismic Array (NORES), the Arctic Regional Seismic Array (ARCES) and the Spitsbergen Regional Array (SPITS). This report also presents statistics for additional seismic stations which through cooperative agreements with institutions in the host countries provide continuous data to the NORSAR Data Processing Center (NPDC). These stations comprise the Finnish Regional Seismic Array (FINES), the Hagfors array in Sweden and the regional seismic array in Apatity, Russia.

The NOA Detection Processing system has been operated throughout the period with an average uptime of 100.00%. A total of 2004 seismic events have been reported in the NOA monthly seismic bulletin from July through December 2001. On-line detection processing and data recording at the NDC of NORES, ARCES and FINES data have been conducted throughout the period. Data from two small-aperture arrays at sites in Spitsbergen and Apatity, Kola Peninsula, as well as the Hagfors array in Sweden, have also been recorded and processed. Processing statistics for the arrays for the reporting period are given.

A summary of the activities related to the GSETT-3 experiment and experience gained at the Norwegian NDC during the reporting period is provided in Section 4. Norway is now contributing primary station data from two seismic arrays: ARCES and NOA and one auxiliary array (SPITS). These data are being provided to the IDC via the global communications infrastructure (GCI). Continuous data from all three arrays are in addition being transmitted to the US NDC. The performance of the data transmission to the US NDC has been satisfactory during the reporting period.

The PrepCom has encouraged states that operate IMS-designated stations to continue to do so on a voluntary basis and in the framework of the GSETT-3 experiment until the stations have been certified for formal inclusion in IMS. So far among the Norwegian stations, the NOA and the ARCES array (PS27 and PS28 respectively) have been certified. We envisage continuing the provision of data from these and other Norwegian IMS-designated stations in accordance with current procedures.

Summaries of six scientific and technical contributions are presented in Chapter 6 of this report.

Section 6.1 contains a study of the estimated global and regional detection capability of the IMS primary seismic network. The study makes use of the Threshold Monitoring (TM) method. The TM method is capable of using actual seismic data for a given time interval as the basis for the detectability calculations. In cases when a seismic station did not provide data during the time period under study, an estimated background noise level can be assigned. These noise estimates and signal/noise variances can be based on results from earlier studies, or they can be taken from stations assumed to have similar noise and signal characteristics.

We have found that the 35 stations of the primary seismic IMS network operational as of July 2001 have a three-station detection capability that is quite close to the projected performance of the 49 stations of the network. The largest difference of about 0.5 m_b units is found in southwest Asia. This can be explained by the fact that most of the sensitive array stations of the network are already in place. Another uncertainty is the noise levels assigned to the planned stations and to the stations that did not provide real noise data during the period under investigation. The

assignment of realistic noise levels for planned stations is therefore a topic requiring additional studies.

This study also confirms the results provided by Kværna and Ringdal (1999) that large earthquakes and the corresponding coda energy can temporarily, over tens of minutes, significantly reduce the detection capability of the IMS network. During such conditions the use of high-frequency regional data, combined with less stringent event formation criteria (1 or 2 station only) will be important for CTBT verification purposes.

Section 6.2 is a study of travel times and attenuation relations of regional seismic phases in the Barents Sea region. A database containing 42 events in the Barents Sea region has been compiled and analyzed with the aim of evaluating crustal models, travel times and attenuation relations in the context of performing regional detection threshold monitoring of this region. The 42 events are mostly located around the circumference of the study area due to the virtually aseismic nature of the Barents Sea itself. Regional P_n and S_n phases were observable for most events in the database, while P_g and L_g phases were only observable for events with ray paths within continental crust. This corroborates a number of previous observations of L_g-wave blockage across the Barents Sea. Three existing velocity models were evaluated, with a model having slightly lower S-velocities than earlier assumed in the upper mantle giving the overall best fit to the observed arrivals. In order to estimate magnitudes, short term average (STA) and spectral amplitude values were calculated in several frequency bands for all phase arrivals in the data base. There were no significant differences between spectral and STA amplitudes, so the latter were used as this parameter is more efficient to calculate in real-time processing. An inversion was performed in order to determine a P_n and S_n attenuation relation specific for this region. The resulting magnitudes based on P_n and S_n phases gave an internally consistent, reasonably stable set of values, which can be calibrated towards any existing global or regional scale. An attenuation relation was also determined for the L_g phase, but the low number of amplitude readings in this case renders the results less reliable.

Section 6.3 is a study of experimental Site-Specific Threshold Monitoring (SSTM) applied to the Lop Nor test site in China. This study is a follow-up on similar experimental studies applied to Novaya Zemlya and the "Kursk" accident site in the Barents Sea. These two previous case studies have been reported upon in earlier Semiannual Reports, and have made use of seismic stations at regional distances, mostly from the Fennoscandian array network. In the case of Lop Nor, we have applied a combination of 3-component stations and arrays, at both regional and teleseismic ranges. Our efforts so far, as reported in this contribution, comprise mainly a study of available seismic stations, selected among those stations which are most sensitive to seismic events in the Lop Nor general area, and tuning of the signal parameters of these stations so as to prepare processing recipes for the application of the threshold monitoring tool.

We have selected a total of 17 seismic stations, including both IMS stations (mostly arrays at teleseismic distances) and other available stations (mostly of the three-component type, and situated in the regional distance range). It appears that the combined threshold monitoring level of this station network is close to or better than m_b 3.0 for the Lop Nor test site. This is quite encouraging, taking into account that the IMS network is not yet well developed in central and eastern Asia. Once the full IMS network becomes available, this capability should improve considerably.

Section 6.4 is a study of seismicity of the Spitsbergen archipelago. Spitsbergen and the adjacent areas are parts of a geologically complex region with moderate to high earthquake activity. The

main seismicity in the area is associated with the North-Atlantic Ridge, and especially the Knipovich Ridge. In addition, some coal mines are located in the area of Spitsbergen, causing occasional induced seismicity. We have compared maps of seismic events in and near Spitsbergen for the period 1964 - 1998 as taken from ISC bulletins with a corresponding map for 1998-2001 using the solutions from the NORSAR Reviewed Regional Seismic Bulletin. Even though the NORSAR regional bulletin covers a much shorter time interval than the ISC bulletin, the observed seismicity patterns in the two plots are remarkably similar. In particular, a segment of the mid-atlantic ridge to the west can be observed, and pronounced seismic zones in Nordaustlandet (northeast) and Heerland (southeast) can also be identified on both maps. We have pursued further the location calibration of the Spitsbergen area, and have adapted the Barents regional velocity model to this area by adding a sedimentary layer of 2 km. This has resulted in encouraging improvements in locating events with known (ground truth) locations.

Section 6.5 is a comparison of various location procedures applied to the Kara Sea seismic event of 16 August 1997. This event has been the subject of considerable discussion, and in particular it has been difficult to obtain a reliable focal depth estimate from available seismic recordings. We have undertaken a sequence of location experiments to compare the results of a) using different velocity models to describe the travel times of the phases and b) to make a comparison between the use of a linearized location algorithm (HYPOSAT – Schweitzer, 2001) and a fully non-linear scheme (shakeNA – Sambridge and Kennett, 2001). For direct comparisons between the two methods we have used a standard least-squares misfit criterion, but we have also examined the influence of more robust choices for data misfit when using the non-linear location scheme.

This study has shown both the importance of S wave information in assessing the depth of regional events, and the need to get a good regional velocity model for both P and S in order to place the strongest constraints on the location of the event.

The conclusions from our experiment of comparing the different data centre solutions with our results are that using only a limited data set but an adequate travel-time model one can locate the event in the Kara Sea relatively close to our HYPOSAT-based location. However, in this case there is very little depth resolution. The relative small error ellipses are a problem which arises when using only a limited number of data. Then the data errors do not usually follow a normal distribution but are biased in one direction and suggest an unreasonably high resolution and accuracy.

The location estimates for the whole data set from the different techniques agree quite well, with some overlap of the estimated confidence regions. The study concludes that the event cannot be shallower than 10 km and is most likely in the lower crust around 20-30 km depth. Such deep crustal events are often attributed to the long-term effects of ice-unloading from the last glaciation and have previously been observed at Novaya Zemlya (*e.g.* Marshall *et al.*, 1989). The assertion that this event was not an underwater explosion is supported by the occurrence of an aftershock in the same epicentral area about four hours later and the fact that the observed seismic signals do not show bubble pulse reverberations, typical for underwater explosions.

Section 6.6 presents some results derived from studying the seismic signals generated by the accident of the Russian submarine “Kursk” on 12 August 2000. Two seismic events, which occurred about 2 minutes and 16 seconds apart, were associated with this accident. The first of these two events (Kursk-1) was about two magnitude units smaller than the second one (Kursk-

2), which had a local magnitude of about 3.5 (Ringdal *et al.*, 2000).

To get a better understanding of the accident, we have tried to estimate the relative location between these two events. We have applied a signal correlation analysis procedure to measure, with high accuracy, the time difference between the two events for various phases recorded at six seismic stations. We then applied the master-event location technique and inverted the time differences to obtain a relative horizontal location between the two events. The application of the master-event analysis suggests that the submarine moved about 145 m to the north-west during the 135.8 s between the two events. The azimuth of this movement is estimated at 302°. After the accident not only the exact position of the Kursk submarine became known but also the direction in which the submarine was lying on the sea bottom. This direction was reported as 288°. This is in good agreement with the results in the study about the relative movement of the submarine during the time interval between Kursk-1 and Kursk-2. An estimate of the uncertainty involved in the calculations is also provided.

Frode Ringdal

AFTAC Project Authorization	:	T/0155/PKO
ARPA Order No.	:	4138 AMD # 53
Program Code No.	:	0F10
Name of Contractor	:	Stiftelsen NORSAR
Effective Date of Contract	:	1 Feb 2001 (T/0155/PKO)
Contract Expiration Date	:	31 December 2005
Project Manager	:	Frode Ringdal +47 63 80 59 00
Title of Work	:	The Norwegian Seismic Array (NORSAR) Phase 3
Amount of Contract	:	$ 3,383,445
Period Covered by Report	:	1 July - 31 December 2001

The research presented in this report was supported by the Defense Threat Reduction Agency and was monitored by AFTAC, Patrick AFB, FL32925, under contract no. F08650-01-C-0055.

The operational activities of the seismic field systems and the Norwegian National Data Center (NDC) are currently jointly funded by the Norwegian Government and the CTBTO/PTS, with the understanding that the funding of IMS-related activities will gradually be transferred to the CTBTO/PTS.

NORSAR Contribution No. 758

Table of Contents

1 Summary

This report describes the research activities carried out at NORSAR under Contract No. F08650-01-C-0055 for the period 1 July - 31 December 2001. In addition, it provides summary information on operation and maintenance (O&M) activities at the Norwegian National Data Center (NDC) during the same period. Research activities described in this report, as well as transmission of selected data to the United States NDC, are funded by the United States Department of Defense. The O&M activities, including operation of transmission links within Norway and to Vienna, Austria are being funded jointly by the CTBTO/PTS and the Norwegian Government, with the understanding that the funding of all IMS-related activities will gradually be transferred to the CTBTO/PTS. The O&M statistics presented in this report are included for the purpose of completeness, and in order to maintain consistency with earlier reporting practice.

The seismic arrays operated by the Norwegian NDC comprise the Norwegian Seismic Array (NOA), the Norwegian Regional Seismic Array (NORES), the Arctic Regional Seismic Array (ARCES) and the Spitsbergen Regional Array (SPITS). This report also presents statistics for additional seismic stations which through cooperative agreements with institutions in the host countries provide continuous data to the NORSAR Data Processing Center (NPDC). These stations comprise the Finnish Regional Seismic Array (FINES), the Hagfors array in Sweden and the regional seismic array in Apatity, Russia.

The NOA Detection Processing system has been operated throughout the period with an average uptime of 100.00%. A total of 2004 seismic events have been reported in the NOA monthly seismic bulletin from July through December 2001. On-line detection processing and data recording at the NDC of NORES, ARCES and FINES data have been conducted throughout the period. Data from two small-aperture arrays at sites in Spitsbergen and Apatity, Kola Peninsula, as well as the Hagfors array in Sweden, have also been recorded and processed. Processing statistics for the arrays for the reporting period are given.

A summary of the activities related to the GSETT-3 experiment and experience gained at the Norwegian NDC during the reporting period is provided in Section 4. Norway is now contributing primary station data from two seismic arrays: ARCES and NOA and one auxiliary array (SPITS). These data are being provided to the IDC via the global communications infrastructure (GCI). Continuous data from all three arrays are in addition being transmitted to the US NDC. The performance of the data transmission to the US NDC has been satisfactory during the reporting period.

The PrepCom has encouraged states that operate IMS-designated stations to continue to do so on a voluntary basis and in the framework of the GSETT-3 experiment until the stations have been certified for formal inclusion in IMS. So far among the Norwegian stations, the NOA and the ARCES array (PS27 and PS28 respectively) have been certified. We envisage continuing the provision of data from these and other Norwegian IMS-designated stations in accordance with current procedures.

Summaries of six scientific and technical contributions are presented in Chapter 6 of this report.

Section 6.1 contains a study of the estimated global and regional detection capability of the IMS primary seismic network. The study makes use of the Threshold Monitoring (TM) method. The TM method is capable of using actual seismic data for a given time interval as the basis for the detectability calculations. In cases when a seismic station did not provide data during the time

period under study, an estimated background noise level can be assigned. These noise estimates and signal/noise variances can be based on results from earlier studies, or they can be taken from stations assumed to have similar noise and signal characteristics.

We have found that the 35 stations of the primary seismic IMS network operational as of July 2001 have a three-station detection capability that is quite close to the projected performance of the 49 stations of the network. The largest difference of about 0.5 m_b units is found in southwest Asia. This can be explained by the fact that most of the sensitive array stations of the network are already in place. Another uncertainty is the noise levels assigned to the planned stations and to the stations that did not provide real noise data during the period under investigation. The assignment of realistic noise levels for planned stations is therefore a topic requiring additional studies.

This study also confirms the results provided by Kværna and Ringdal (1999) that large earthquakes and the corresponding coda energy can temporarily, over tens of minutes, significantly reduce the detection capability of the IMS network. During such conditions the use of high-frequency regional data, combined with less stringent event formation criteria (1 or 2 station only) will be important for CTBT verification purposes.

Section 6.2 is a study of travel times and attenuation relations of regional seismic phases in the Barents Sea region. A database containing 42 events in the Barents Sea region has been compiled and analyzed with the aim of evaluating crustal models, travel times and attenuation relations in the context of performing regional detection threshold monitoring of this region. The 42 events are mostly located around the circumference of the study area due to the virtually aseismic nature of the Barents Sea itself. Regional P_n and S_n phases were observable for most events in the database, while P_g and L_g phases were only observable for events with ray paths within continental crust. This corroborates a number of previous observations of L_g-wave blockage across the Barents Sea. Three existing velocity models were evaluated, with a model having slightly lower S-velocities than earlier assumed in the upper mantle giving the overall best fit to the observed arrivals. In order to estimate magnitudes, short term average (STA) and spectral amplitude values were calculated in several frequency bands for all phase arrivals in the data base. There were no significant differences between spectral and STA amplitudes, so the latter were used as this parameter is more efficient to calculate in real-time processing. An inversion was performed in order to determine a P_n and S_n attenuation relation specific for this region. The resulting magnitudes based on P_n and S_n phases gave an internally consistent, reasonably stable set of values, which can be calibrated towards any existing global or regional scale. An attenuation relation was also determined for the L_g phase, but the low number of amplitude readings in this case renders the results less reliable.

Section 6.3 is a study of experimental Site-Specific Threshold Monitoring (SSTM) applied to the Lop Nor test site in China. This study is a follow-up on similar experimental studies applied to Novaya Zemlya and the "Kursk" accident site in the Barents Sea. These two previous case studies have been reported upon in earlier Semiannual Reports, and have made use of seismic stations at regional distances, mostly from the Fennoscandian array network. In the case of Lop Nor, we have applied a combination of 3-component stations and arrays, at both regional and teleseismic ranges. Our efforts so far, as reported in this contribution, comprise mainly a study of available seismic stations, selected among those stations which are most sensitive to seismic events in the Lop Nor general area, and tuning of the signal parameters of these stations so as to prepare processing recipes for the application of the threshold monitoring tool.

We have selected a total of 17 seismic stations, including both IMS stations (mostly arrays at teleseismic distances) and other available stations (mostly of the three-component type, and situated in the regional distance range). It appears that the combined threshold monitoring level of this station network is close to or better than m_b 3.0 for the Lop Nor test site. This is quite encouraging, taking into account that the IMS network is not yet well developed in central and eastern Asia. Once the full IMS network becomes available, this capability should improve considerably.

Section 6.4 is a study of seismicity of the Spitsbergen archipelago. Spitsbergen and the adjacent areas are parts of a geologically complex region with moderate to high earthquake activity. The main seismicity in the area is associated with the North-Atlantic Ridge, and especially the Knipovich Ridge. In addition, some coal mines are located in the area of Spitsbergen, causing occasional induced seismicity. We have compared maps of seismic events in and near Spitsbergen for the period 1964 - 1998 as taken from ISC bulletins with a corresponding map for 1998-2001 using the solutions from the NORSAR Reviewed Regional Seismic Bulletin. Even though the NORSAR regional bulletin covers a much shorter time interval than the ISC bulletin, the observed seismicity patterns in the two plots are remarkably similar. In particular, a segment of the mid-atlantic ridge to the west can be observed, and pronounced seismic zones in Nordaustlandet (northeast) and Heerland (southeast) can also be identified on both maps. We have pursued further the location calibration of the Spitsbergen area, and have adapted the Barents regional velocity model to this area by adding a sedimentary layer of 2 km. This has resulted in encouraging improvements in locating events with known (ground truth) locations.

Section 6.5 is a comparison of various location procedures applied to the Kara Sea seismic event of 16 August 1997. This event has been the subject of considerable discussion, and in particular it has been difficult to obtain a reliable focal depth estimate from available seismic recordings. We have undertaken a sequence of location experiments to compare the results of a) using different velocity models to describe the travel times of the phases and b) to make a comparison between the use of a linearized location algorithm (HYPOSAT – Schweitzer, 2001) and a fully non-linear scheme (shakeNA – Sambridge and Kennett, 2001). For direct comparisons between the two methods we have used a standard least-squares misfit criterion, but we have also examined the influence of more robust choices for data misfit when using the non-linear location scheme.

This study has shown both the importance of S wave information in assessing the depth of regional events, and the need to get a good regional velocity model for both P and S in order to place the strongest constraints on the location of the event.

The conclusions from our experiment of comparing the different data centre solutions with our results are that using only a limited data set but an adequate travel-time model one can locate the event in the Kara Sea relatively close to our HYPOSAT-based location. However, in this case there is very little depth resolution. The relative small error ellipses are a problem which arises when using only a limited number of data. Then the data errors do not usually follow a normal distribution but are biased in one direction and suggest an unreasonably high resolution and accuracy.

The location estimates for the whole data set from the different techniques agree quite well, with some overlap of the estimated confidence regions. The study concludes that the event cannot be shallower than 10 km and is most likely in the lower crust around 20-30 km depth. Such deep crustal events are often attributed to the long-term effects of ice-unloading from the last glacia-

tion and have previously been observed at Novaya Zemlya (*e.g.* Marshall *et al.*, 1989). The assertion that this event was not an underwater explosion is supported by the occurrence of an aftershock in the same epicentral area about four hours later and the fact that the observed seismic signals do not show bubble pulse reverberations, typical for underwater explosions.

Section 6.6 presents some results derived from studying the seismic signals generated by the accident of the Russian submarine "Kursk" on 12 August 2000. Two seismic events, which occurred about 2 minutes and 16 seconds apart, were associated with this accident. The first of these two events (Kursk-1) was about two magnitude units smaller than the second one (Kursk-2), which had a local magnitude of about 3.5 (Ringdal *et al.*, 2000).

To get a better understanding of the accident, we have tried to estimate the relative location between these two events. We have applied a signal correlation analysis procedure to measure, with high accuracy, the time difference between the two events for various phases recorded at six seismic stations. We then applied the master-event location technique and inverted the time differences to obtain a relative horizontal location between the two events. The application of the master-event analysis suggests that the submarine moved about 145 m to the north-west during the 135.8 s between the two events. The azimuth of this movement is estimated at 302°. After the accident not only the exact position of the Kursk submarine became known but also the direction in which the submarine was lying on the sea bottom. This direction was reported as 288°. This is in good agreement with the results in this study about the relative movement of the submarine during the time interval between Kursk-1 and Kursk-2. An estimate of the uncertainty involved in the calculations is also provided.

Frode Ringdal

2 Operation of International Monitoring System (IMS) Stations in Norway

2.1 PS27 — Primary Seismic Station NOA

The average recording time was 100%, the same as for the previous reporting period.

Monthly uptimes for the NORSAR on-line data recording task, taking into account all factors (field installations, transmissions line, data center operation) affecting this task were as follows:

July 2001	:	100%
August	:	100%
September	:	100%
October	:	100%
November	:	100%
December	:	100%

Fig. 2.1.1 shows the uptime for the data recording task, or equivalently, the availability of NORSAR data in our tape archive, on a day-by-day basis for the reporting period.

J. Torstveit

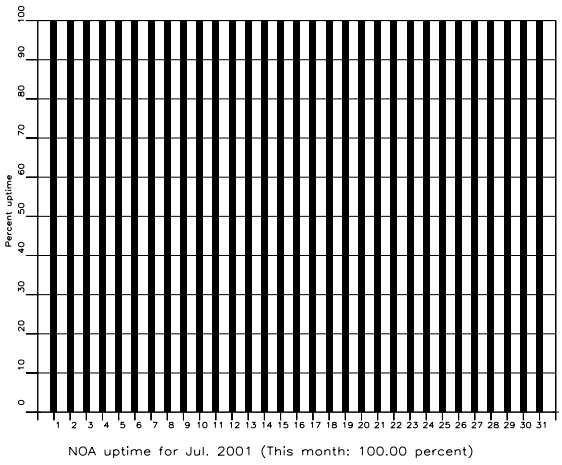

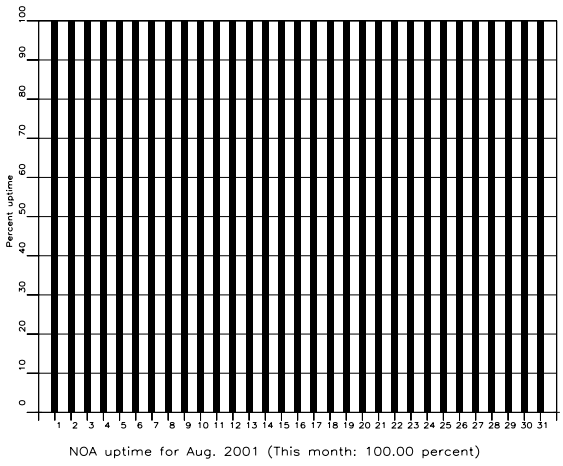

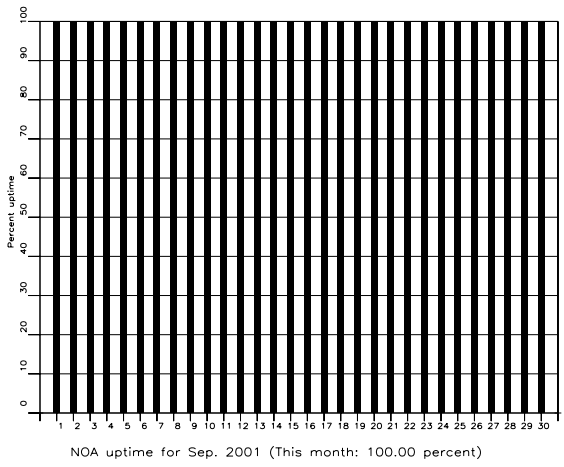

Fig. 2.1.1. *The figure shows the uptime for the data recording task, or equivalently, the availability of NOA data in our tape archive, on a day-by-day basis, for the reporting period. (Page 1 of 2, July-Sep 2001).*

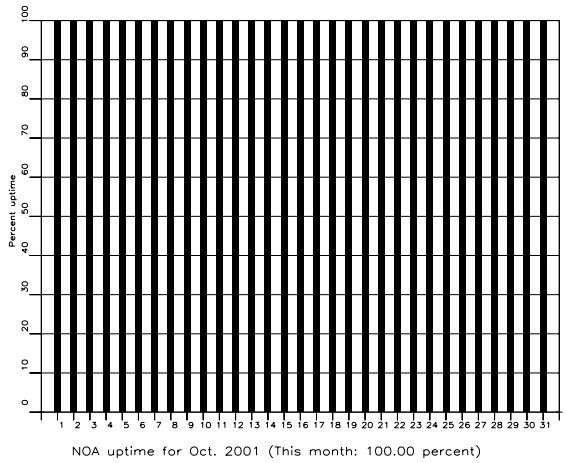

NOA uptime for Oct. 2001 (This month: 100.00 percent)

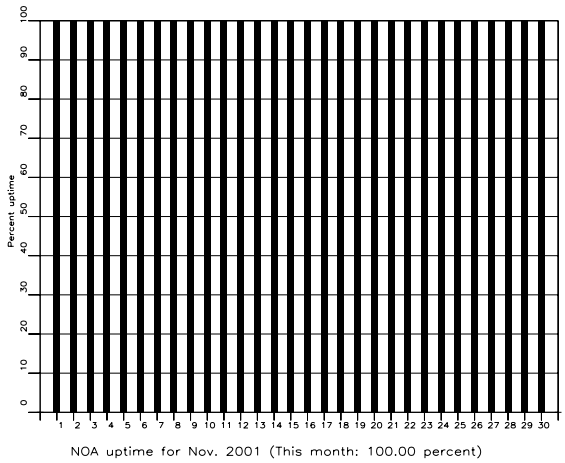

NOA uptime for Nov. 2001 (This month: 100.00 percent)

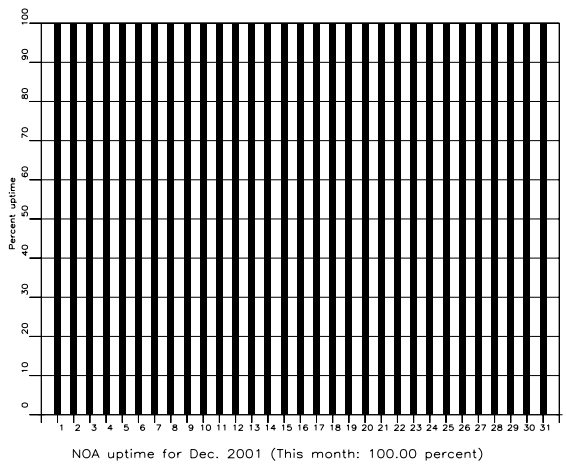

NOA uptime for Dec. 2001 (This month: 100.00 percent)

Fig. 2.1.1. *(cont.) (Page 2 of 2, Oct-Dec 2001).*

NOA Event Detection Operation

In Table 2.1.1 some monthly statistics of the Detection and Event Processor operation are given. The table lists the total number of detections (DPX) triggered by the on-line detector, the total number of detections processed by the automatic event processor (EPX) and the total number of events accepted after analyst review (teleseismic phases, core phases and total).

	Total DPX	Total EPX	Accepted Events		Sum	Daily
			P-phases	Core Phases		
Jul 2001	7,589	1,077	359	62	421	13.6
Aug	10,045	1,550	250	129	379	12.2
Sep	8,228	832	225	78	303	10.1
Oct	10,728	856	249	91	340	11.0
Nov	12,043	942	204	70	274	9.1
Dec	11,867	908	228	59	287	9.3
	60,500	6,165	1,515	489	2,004	10.9

Table 2.1.1. *Detection and Event Processor statistics, 1 July - 31 December 2001.*

NOA detections

The number of detections (phases) reported by the NORSAR detector during day 182, 2001, through day 365, 2001, was 60,500, giving an average of 329 detections per processed day (184 days processed).

B. Paulsen
U. Baadshaug

2.2 PS28 — Primary Seismic Station ARCES

The average recording time was 99.20% as compared to 99.74% for the previous period. Table 2.2.1 lists the reasons for and time periods of the main downtimes in the reporting period.

Date	Time		Cause
11 Jul	2241	-	Power failure
12 Jul		- 1836	
18 Jul	1835	-	Power failure
19 Jul		- 0221	
20 Jul	1634	- 2357	Power failure

Table 2.2.1. *The main interruptions in recording of ARCES data at NDPC, 1 July - 31 December 2001.*

Monthly uptimes for the ARCES on-line data recording task, taking into account all factors (field installations, transmission lines, data center operation) affecting this task were as follows:

July 2001	:	95.18%
August	:	100%
September	:	100%
October	:	100%
November	:	100%
December	:	100%

J. Torstveit

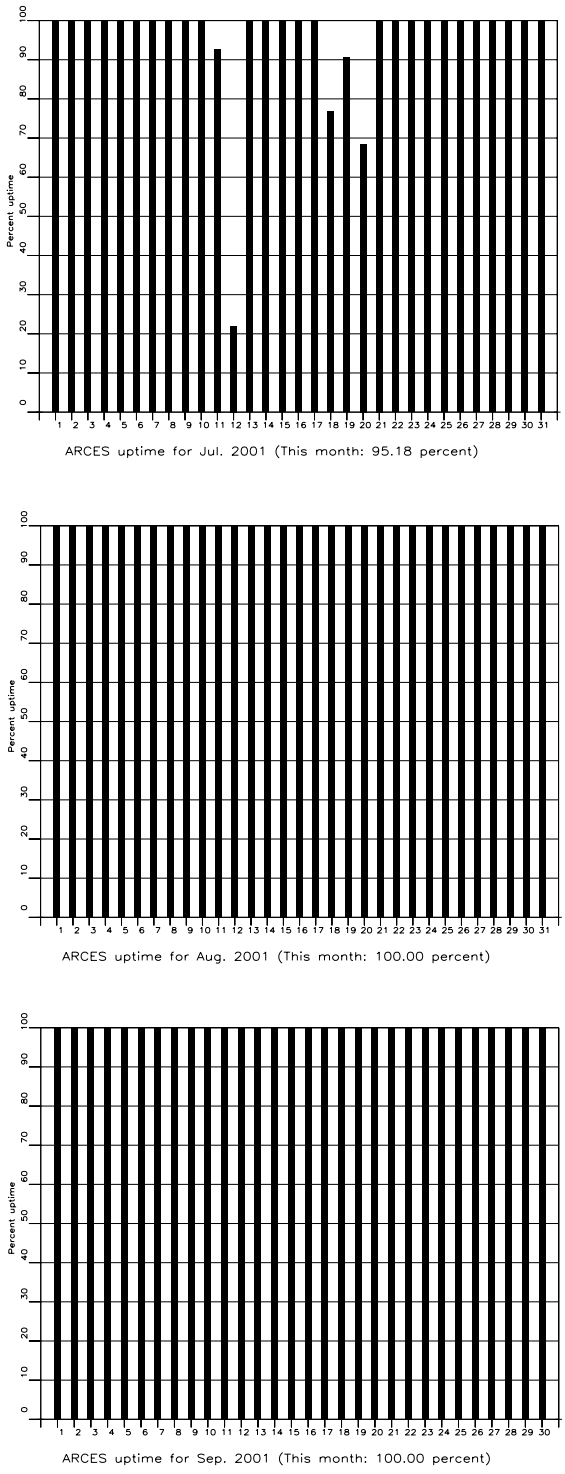

Fig. 2.2.1. *The figure shows the uptime for the data recording task, or equivalently, the availability of ARCES data in our tape archive, on a day-by-day basis, for the reporting period. (Page 1 of 2, Jul-Sep 2001)*

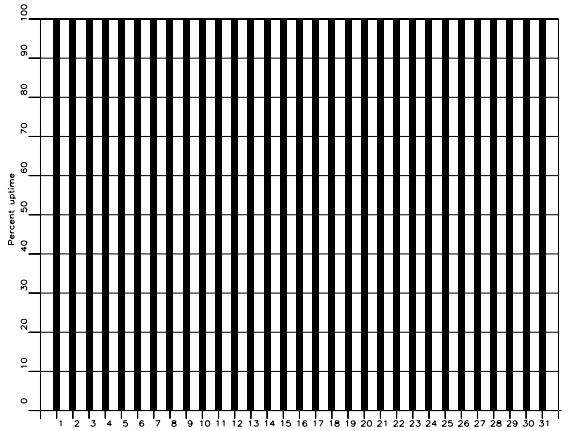

ARCES uptime for Oct. 2001 (This month: 100.00 percent)

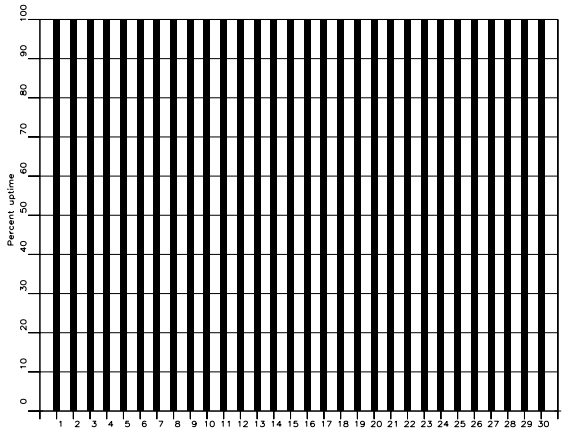

ARCES uptime for Nov. 2001 (This month: 100.00 percent)

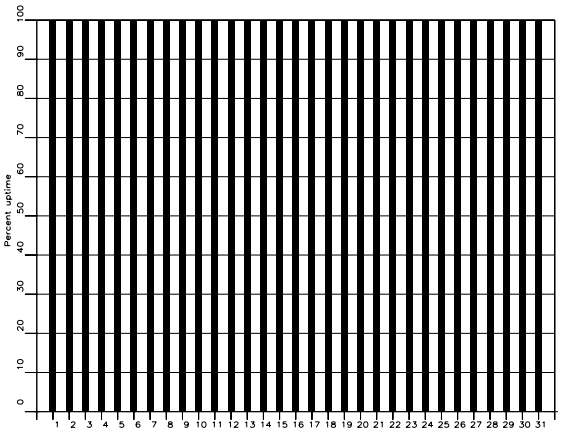

ARCES uptime for Dec. 2001 (This month: 100.00 percent)

Fig. 2.2.1 *(cont.) (Page 2 of 2, Oct-Dec 2001).*

Event Detection Operation

ARCES detections

The number of detections (phases) reported during day 182, 2001, through day 365, 2001, was 145,357, giving an average of 790 detections per processed day (184 days processed).

Events automatically located by ARCES

During days 182, 2001, through 365, 2001, 11,215 local and regional events were located by ARCES, based on automatic association of P- and S-type arrivals. This gives an average of 61.0 events per processed day (184 days processed). 44% of these events are within 300 km, and 76% of these events are within 1000 km.

U. Baadshaug

2.3 AS72 — Auxiliary Seismic Station Spitsbergen

The average recording time was 99.99% as compared to 93.52% for the previous reporting period.

Monthly uptimes for the Spitsbergen on-line data recording task, taking into account all factors (field installations, transmissions line, data center operation) affecting this task were as follows:

July 2001	:	100%
August	:	100%
September	:	100%
October	:	99.97%
November	:	99.99%
December	:	99.97%

J. Torstveit

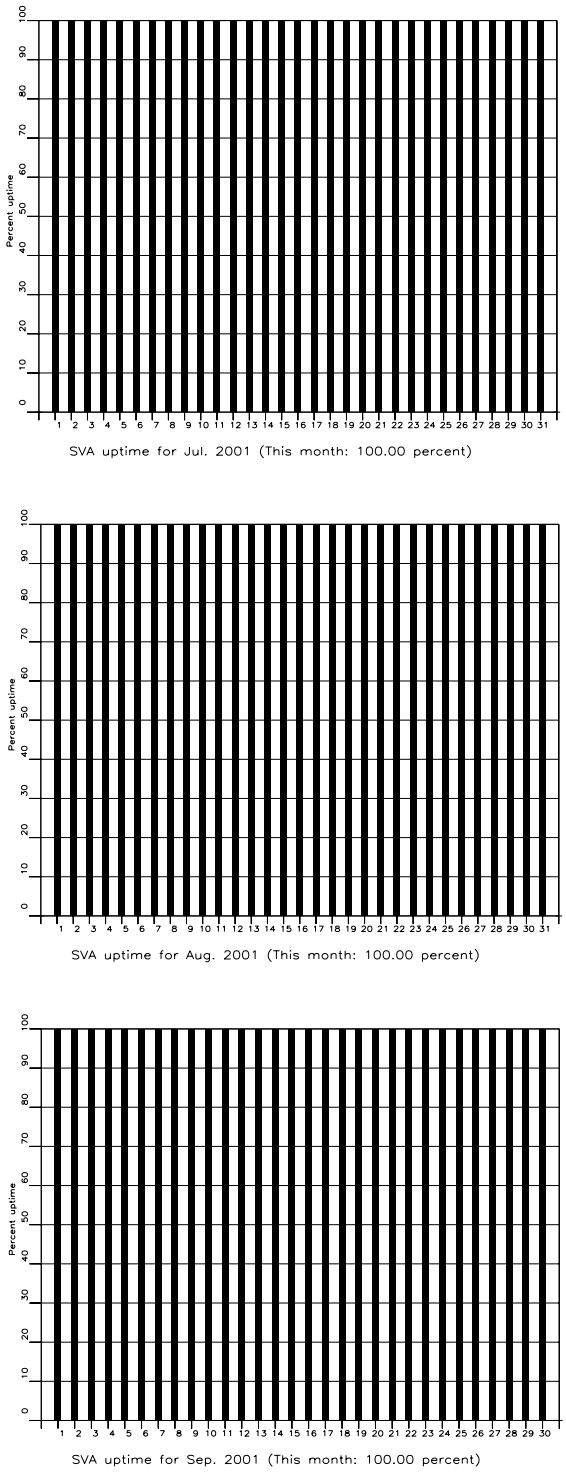

Fig. 2.3.1. *The figure shows the uptime for the data recording task, or equivalently, the availability of Spitsbergen data in our tape archive, on a day-by-day basis, for the reporting period. (Page 1 of 2, Jul-Sep 2001).*

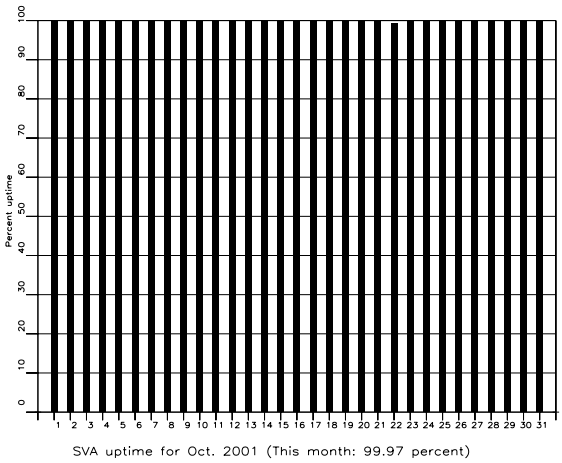

SVA uptime for Oct. 2001 (This month: 99.97 percent)

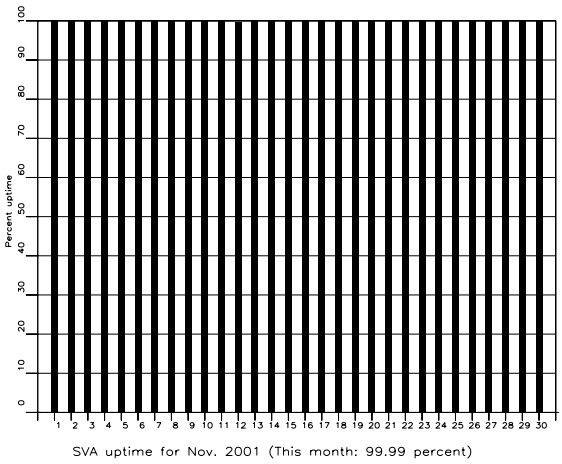

SVA uptime for Nov. 2001 (This month: 99.99 percent)

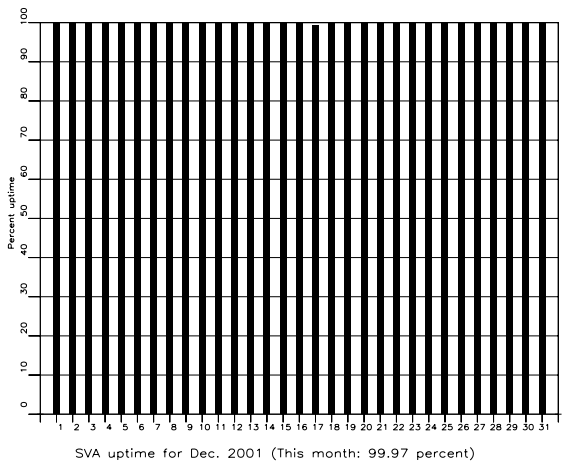

SVA uptime for Dec. 2001 (This month: 99.97 percent)

Fig. 2.3.1 *(cont.) (Page 2 of 2, Oct-Dec 2001).*

Event Detection Operation

Spitsbergen array detections

The number of detections (phases) reported from day 182, 2001, through day 365, 2001, was 400,191, giving an average of 2175 detections per processed day (184 days processed).

Events automatically located by the Spitsbergen array

During days 182, 2001, through 365, 2001, 42,476 local and regional events were located by the Spitsbergen array, based on automatic association of P- and S-type arrivals. This gives an average of 184.0 events per processed day (184 days processed). 60% of these events are within 300 km, and 82% of these events are within 1000 km.

U. Baadshaug

2.4 AS73 — Auxiliary Seismic Station at Jan Mayen

The IMS auxiliary seismic network will include a three-component station on the Norwegian island of Jan Mayen. The station location given in the protocol to the Comprehensive Nuclear-Test-Ban Treaty is 70.9˚N, 8.7˚W.

The University of Bergen has operated a seismic station at this location since 1970. An investment in the new station at Jan Mayen will be made in due course and in accordance with PrepCom program and budget decisions. In the meanwhile data from the existing seismic station on Jan Mayen are being transmitted to the NDC at Kjeller and to the University of Bergen via a VSAT link installed in April 2000.

S. Mykkeltveit

2.5 IS37 — Infrasound Station at Karasjok

The IMS infrasound network will include a station at Karasjok in northern Norway. The coordinates given for this station are 69.5˚N, 25.5˚E. These coordinates coincide with those of the primary seismic station PS28.

A site survey for this station was carried out during June/July 1998 as a cooperative effort between the Provisional Technical Secretariat of the CTBTO and NORSAR. Analysis of the data collected at several potential locations for this station in and around Karasjok has been completed. The results of this analysis have lead to a recommendation on the exact location of the infrasound station. This location needs to be surveyed in detail. The next step will be to approach the local authorities to obtain the permissions needed to establish the station. Station installation is now expected to take place in the year 2003.

S. Mykkeltveit

2.6 RN49 — Radionuclide Station on Spitsbergen

The IMS radionuclide network will include a station at Longyearbyen on the island of Spitsbergen, with location 78.2˚N, 16.4˚E, as given in the protocol to the Comprehensive Nuclear-Test-Ban Treaty. These coordinates coincide with those of the auxiliary seismic station AS72. According to PrepCom decision, this station will also be among those IMS radionuclide stations that will have a capability of monitoring for the presence of relevant noble gases upon entry into force of the CTBT.

A site survey for this station was carried out in August of 1999 by NORSAR, in cooperation with the Norwegian Radiation Protection Authority. The site survey report to the PTS contained a recommendation to establish this station at Platåberget, some 20 km away from the Treaty location. The PrepCom approved the corresponding coordinate change in its meeting in May 2000. The station installation was part of PrepCom's work program and budget for the year 2000. The infrastructure for housing the station equipment has been established, and a noble gas detection system, based on the Swedish "SAUNA" design, was installed at this site in May 2001. A particulate station ("ARAME" design) was installed at the same location in September 2001. Currently, the two systems are undergoing testing and evaluation.

S. Mykkeltveit

3 Contributing Regional Seismic Arrays

3.1 NORES

Average recording time was 70.32% as compared to 99.98% for the previous period.

The outage between 16 August and 9 October was due to a thunderstorm that caused major damage to the equipment.

Monthly uptimes for the NORES on-line data recording task, taking into account all factors (field installations, transmissions line, data center operation) affecting this task were as follows:

July 2001	:	100%
August	:	50.70%
September	:	0%
October	:	72.55%
November	:	98.65%
December	:	100%

Fig. 3.1.1 shows the uptime for the data recording task, or equivalently, the availability of NORES data in our tape archive on a day-by-day basis for the reporting period.

J. Torstveit

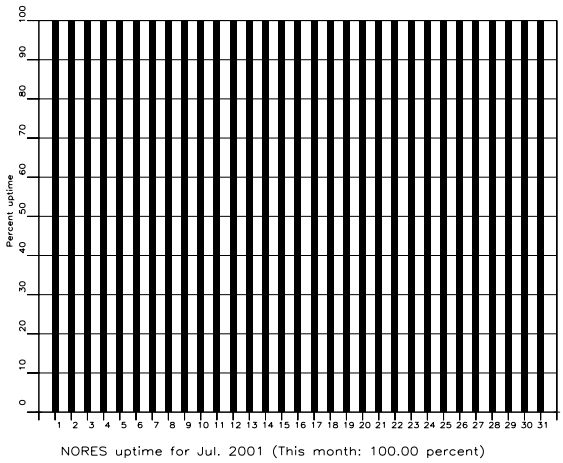

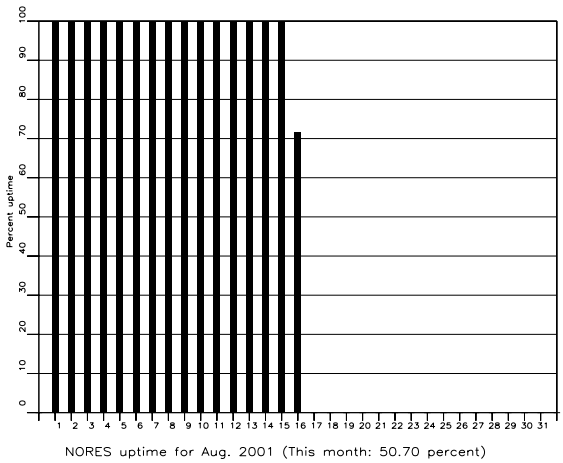

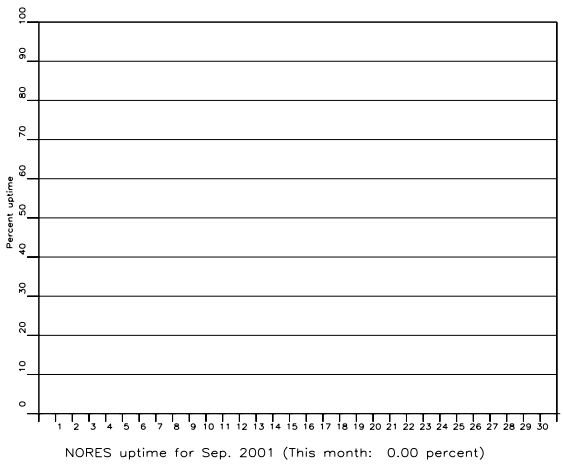

Fig. 3.1.1. *The figure shows the uptime for the data recording task, or equivalently, the availability of NORES data in our tape archive, on a day-by-day basis, for the reporting period (Page 1 of 2, Jul-Sep 2001).*

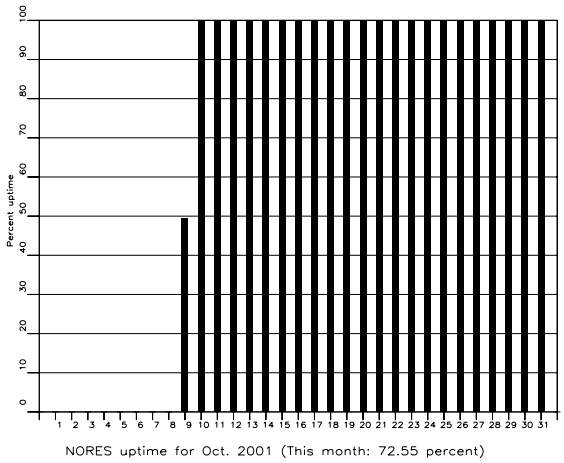

NORES uptime for Oct. 2001 (This month: 72.55 percent)

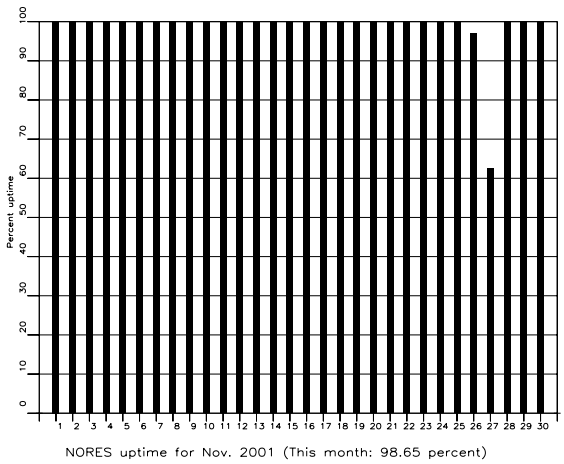

NORES uptime for Nov. 2001 (This month: 98.65 percent)

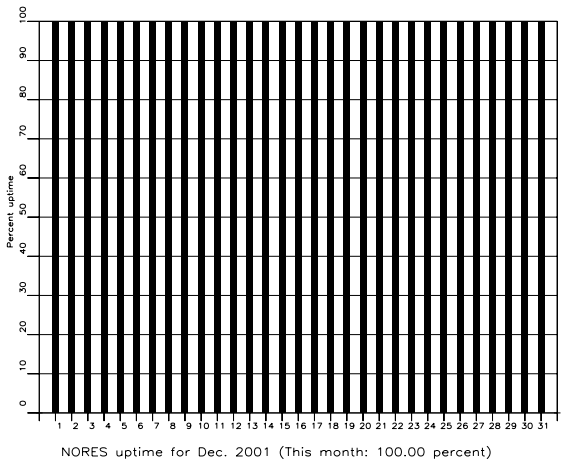

NORES uptime for Dec. 2001 (This month: 100.00 percent)

Fig. 3.1.1 *(cont.) (Page 2 of 2, Oct-Dec 2001).*

NORES Event Detection Operation

NORES detections

The number of detections (phases) reported from day 182, 2001, through day 365, 2001, was 95,065, giving an average of 726 detections per processed day (131 days processed; the processing of NORES data was suspended for a total of 53 days, due to severe clock problems following a thunderstorm).

Events automatically located by NORES

During days 182, 2001, through 365, 2001, 2351 local and regional events were located by NORES, based on automatic association of P- and S-type arrivals. This gives an average of 17.9 events per processed day (131 days processed). 43% of these events are within 300 km, and 75% of these events are within 1000 km.

U. Baadshaug

3.2 Hagfors (IMS Station AS101)

The average recording time was 99.91% as compared to 99.90% for the previous reporting period.

Table 3.2.1 lists the reasons for and times of the main outages in the reporting period.

Date	Time	Cause
14 Aug	0832 - 1050	Installation of new station

Table 3.2.1. *The main interruptions in Hagfors recordings at the Norwegian NDC, 1 July - 31 December 2001.*

The Hagfors array was refurbished in August through the installation of entirely new equipment deployed at new site locations. The “old” array continues its operation in parallel with the “new” array. All data reported here refer to the “old” Hagfors array.

Monthly uptimes for the Hagfors on-line data recording task, taking into account all factors (field installations, transmissions line, data center operation) affecting this task were as follows:

July 2001	:	99.99%
August	:	99.55%
September	:	100%
October	:	100%
November	:	99.94%
December	:	99.98%

J. Torstveit

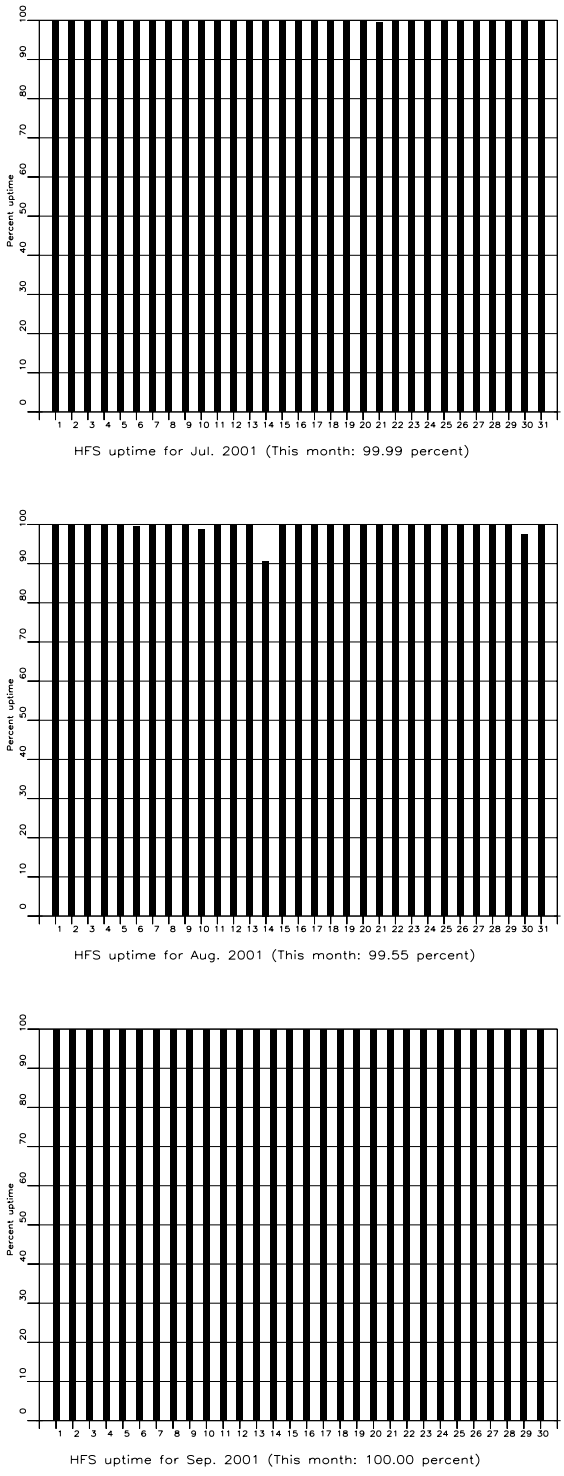

Fig. 3.2.1. *The figure shows the uptime for the data recording task, or equivalently, the availability of Hagfors data in our tape archive, on a day-by-day basis, for the reporting period (Page 1 of 2, Jul-Sep 2001).*

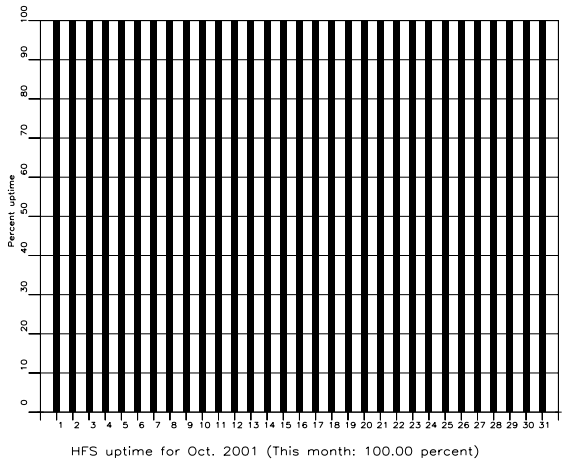

HFS uptime for Oct. 2001 (This month: 100.00 percent)

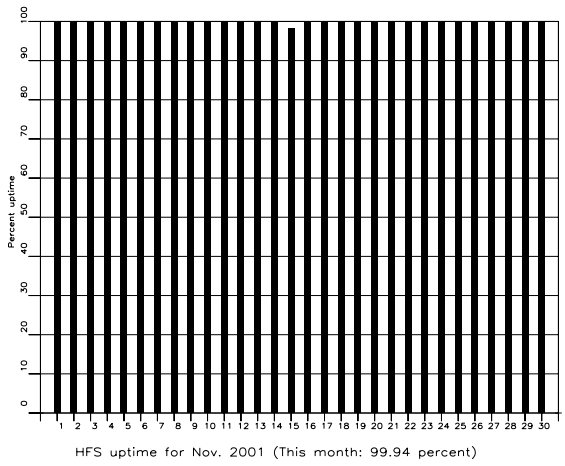

HFS uptime for Nov. 2001 (This month: 99.94 percent)

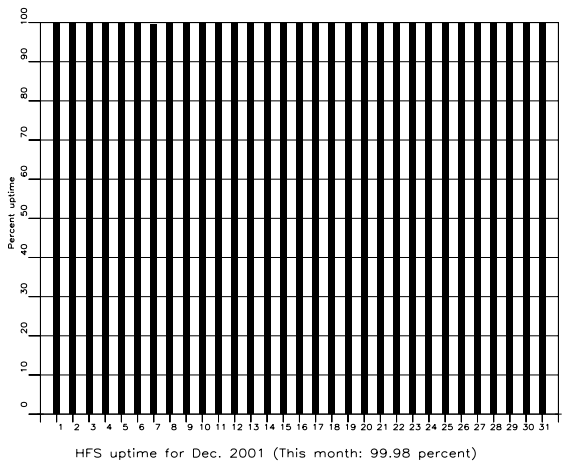

HFS uptime for Dec. 2001 (This month: 99.98 percent)

Fig. 3.2.1 *(cont.) (Page 2 of 2, Oct-Dec 2001).*

Hagfors Event Detection Operation

Hagfors array detections

The number of detections (phases) reported from day 182, 2001, through day 365, 2001, was 103,399, giving an average of 562 detections per processed day (184 days processed).

Events automatically located by the Hagfors array

During days 182, 2001, through 365, 2001, 2952 local and regional events were located by the Hagfors array, based on automatic association of P- and S-type arrivals. This gives an average of 16.0 events per processed day (184 days processed). 56% of these events are within 300 km, and 83% of these events are within 1000 km.

U. Baadshaug

3.3 FINES (IMS station PS17)

The average recording time was 99.99% as compared to 99.51% for the previous reporting period.

Monthly uptimes for the FINES on-line data recording task, taking into account all factors (field installations, transmissions line, data center operation) affecting this task were as follows:

July 2001	:	99.99%
August	:	100%
September	:	100%
October	:	100%
November	:	99.96%
December	:	100%

Fig. 3.3.1 shows the uptime for the data recording task, or equivalently, the availability of FINES data in our tape archive on a day-by-day basis for the reporting period.

J. Torstveit

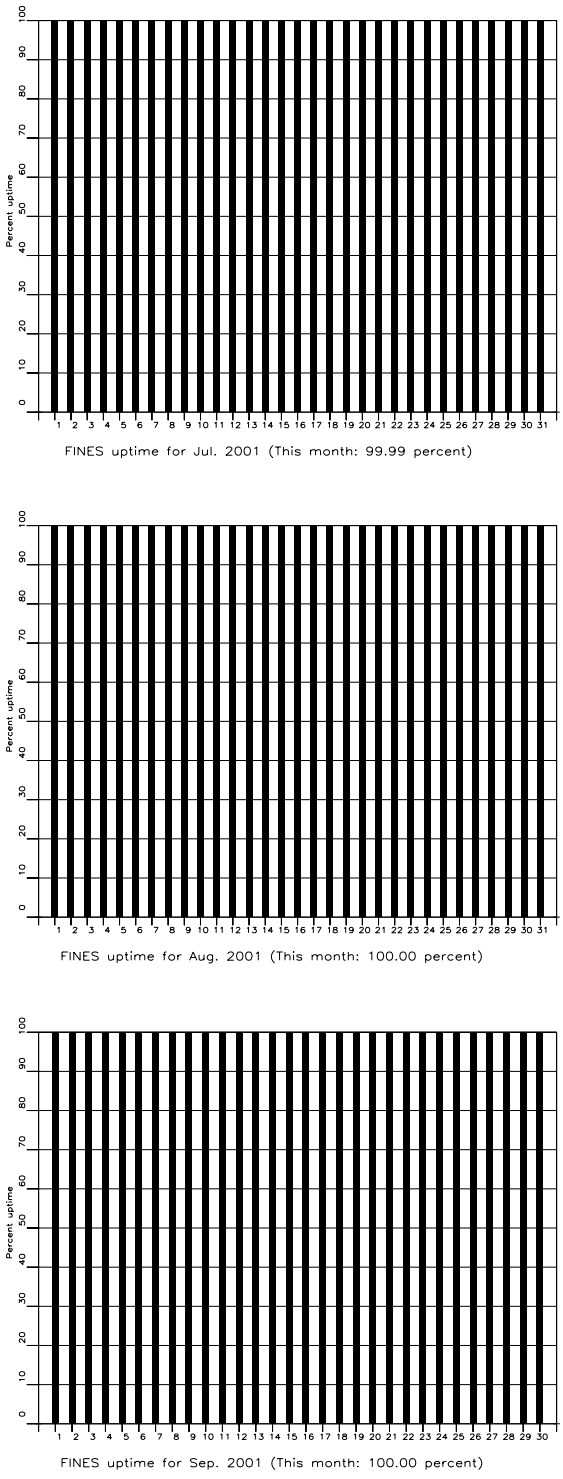

Fig. 3.3.1. *The figure shows the uptime for the data recording task, or equivalently, the availability of FINES data in our tape archive, on a day-by-day basis, for the reporting period (Page 1 of 2, Jul-Sep 2001).*

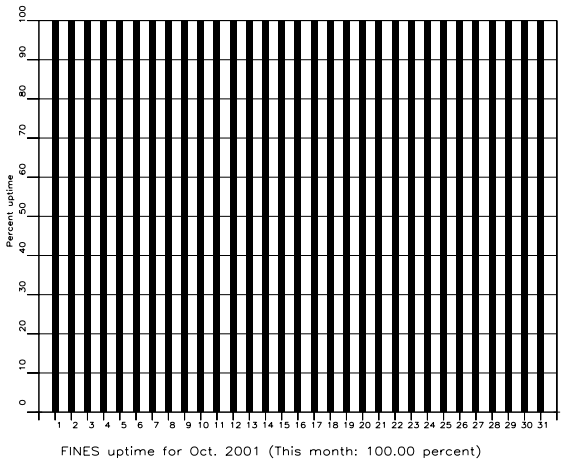

FINES uptime for Oct. 2001 (This month: 100.00 percent)

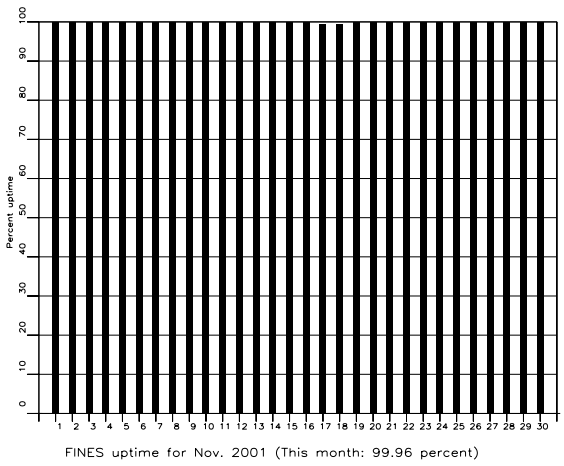

FINES uptime for Nov. 2001 (This month: 99.96 percent)

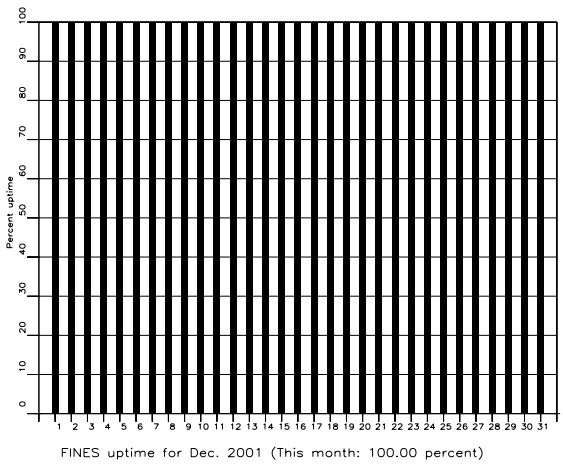

FINES uptime for Dec. 2001 (This month: 100.00 percent)

Fig. 3.3.1 *(cont.) (Page 2 of 2, Oct-Dec 2001)*

FINES Event Detection Operation

FINES detections

The number of detections (phases) reported during day 182, 2001, through day 365, 2001, was 41,957, giving an average of 228 detections per processed day (184 days processed).

Events automatically located by FINES

During days 182, 2001, through 365, 2001, 2381 local and regional events were located by FINES, based on automatic association of P- and S-type arrivals. This gives an average of 12.9 events per processed day (184 days processed). 79% of these events are within 300 km, and 88% of these events are within 1000 km.

U. Baadshaug

3.4 Apatity

The average recording time was 98.31% in the reporting period compared to 99.92% during the previous period.

Table 3.4.1 lists the reasons for and times of the main outages during the reporting period .

Date	Time			Cause
02 Jul	1528	-	1724	Stop in Apatity
01 Oct	0723	-	0958	Stop in Apatity
01 Oct	1153	-		Stop in Apatity
02 Oct		-	0414	
02 Oct	1120	-		Stop in Apatity
03 Oct		-	1347	
05 Nov	1207	-	1458	Stop in Apatity
28 Nov	1326	-		Stop in Apatity
29 Nov		-	0848	
29 Nov	0925	-	1008	Stop in Apatity
29 Nov	1245	-	1300	Stop in Apatity

Table 3.4.1. *The main interruptions in Apatity recordings at the NDC, 1 July - 31 December 2001.*

Monthly uptimes for the Apatity on-line data recording task, taking into account all factors (field installations, transmissions line, data center operation) affecting this task were as follows:

July 2001	:	99.74%
August	:	100%
September	:	100%
October	:	94.06%
November	:	96.09%
December	:	99.95%

J. Torstveit

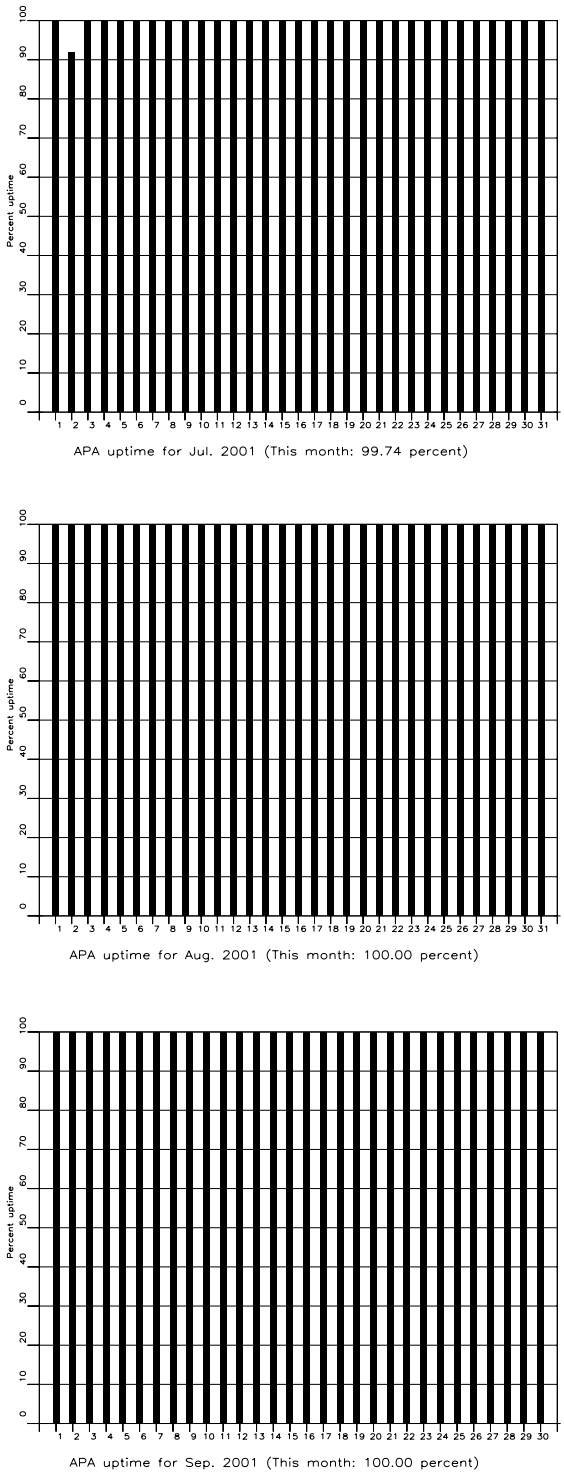

Fig. 3.4.1. *The figure shows the uptime for the data recording task, or equivalently, the availability of Apatity data in our tape archive, on a day-by-day basis, for the reporting period (Page 1 of 2, Jul-Sep 2001).*

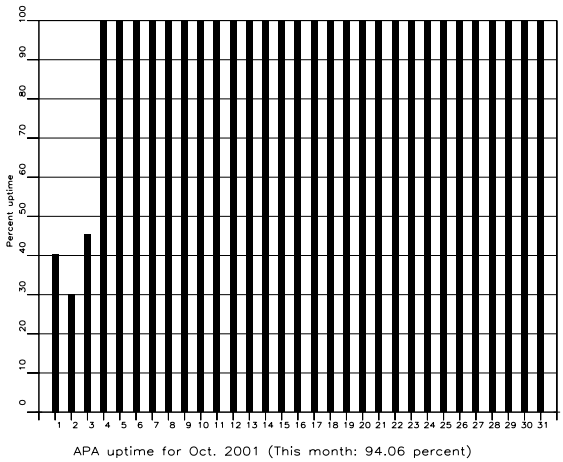

APA uptime for Oct. 2001 (This month: 94.06 percent)

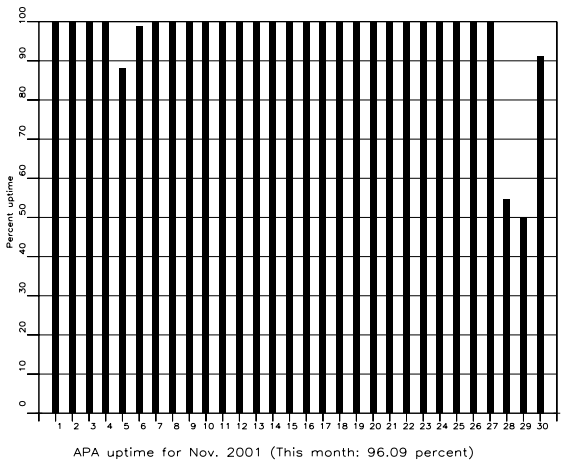

APA uptime for Nov. 2001 (This month: 96.09 percent)

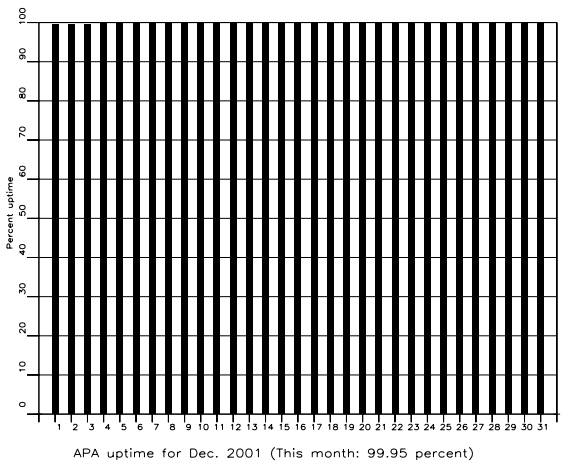

APA uptime for Dec. 2001 (This month: 99.95 percent)

Fig. 3.4.1 *(cont.) (Page 2 of 2, Oct-Dec 2001)*

Apatity Event Detection Operation

Apatity array detections

The number of detections (phases) reported from day 182, 2001, through day 365, 2001, was 229,833, giving an average of 1200 detections per processed day (184 days processed).

As described in earlier reports, the data from the Apatity array are transferred by one-way (simplex) radio links to Apatity city. The transmission suffers from radio disturbances that occasionally result in a large number of small data gaps and spikes in the data. In order for the communication protocol to correct such errors by requesting retransmission of data, a two-way radio link would be needed (duplex radio). However, it should be noted that noise from cultural activities and from the nearby lakes cause most of the unwanted detections. These unwanted detections are "filtered" in the signal processing, as they give seismic velocities that are outside accepted limits for regional and teleseismic phase velocities.

Events automatically located by the Apatity array

During days 182, 2001, through 365, 2001, 2246 local and regional events were located by the Apatity array, based on automatic association of P- and S-type arrivals. This gives an average of 12.2 events per processed day (184 days processed). 42% of these events are within 300 km, and 73% of these events are within 1000 km.

U. Baadshaug

3.5 Regional Monitoring System Operation and Analysis

The Regional Monitoring System (RMS) was installed at NORSAR in December 1989 and was operated at NORSAR from 1 January 1990 for automatic processing of data from ARCES and NORES. A second version of RMS that accepts data from an arbitrary number of arrays and single 3-component stations was installed at NORSAR in October 1991, and regular operation of the system comprising analysis of data from the 4 arrays ARCES, NORES, FINES and GERES started on 15 October 1991. As opposed to the first version of RMS, the one in current operation also has the capability of locating events at teleseismic distance.

Data from the Apatity array were included on 14 December 1992, and from the Spitsbergen array on 12 January 1994. Detections from the Hagfors array were available to the analysts and could be added manually during analysis from 6 December 1994. After 2 February 1995, Hagfors detections were also used in the automatic phase association.

Since 24 April 1999, RMS has processed data from all the seven regional arrays ARCES, NORES, FINES, GERES (until January 2000), Apatity, Spitsbergen, and Hagfors. Starting 19 September 1999, waveforms and detections from the NORSAR array have also been available to the analyst.

Phase and event statistics

Table 3.5.1 gives a summary of phase detections and events declared by RMS. From top to bottom the table gives the total number of detections by the RMS, the number of detections that are associated with events automatically declared by the RMS, the number of detections that are not associated with any events, the number of events automatically declared by the RMS, and finally the total number of events worked on interactively (in accordance with criteria that vary over time; see below) and defined by the analyst.

New criteria for interactive event analysis were introduced from 1 January 1994. Since that date, only regional events in areas of special interest (e.g, Spitsbergen, since it is necessary to acquire new knowledge in this region) or other significant events (e.g, felt earthquakes and large industrial explosions) were thoroughly analyzed. Teleseismic events of special interest are also analyzed.

To further reduce the workload on the analysts and to focus on regional events in preparation for Gamma-data submission during GSETT-3, a new processing scheme was introduced on 2 February 1995. The GBF (Generalized Beamforming) program is used as a pre-processor to RMS, and only phases associated to selected events in northern Europe are considered in the automatic RMS phase association. All detections, however, are still available to the analysts and can be added manually during analysis.

	Jul 01	Aug 01	Sep 01	Oct 01	Nov 01	Dec 01	Total
Phase detections	194113	180434	163008	165445	135244	159879	998123
- Associated phases	7043	6003	4657	5588	3252	5029	31572
- Unassociated phases	187070	174431	158351	159857	131992	154850	966551
Events automatically declared by RMS	1718	1329	1050	1270	561	1127	7055
No. of events defined by the analyst	80	104	103	62	98	80	527

Table 3.5.1. *RMS phase detections and event summary.*

U. Baadshaug
B. Paulsen

4 NDC and Field Activities

4.1 NDC Activitities

NORSAR is functioning as the Norwegian National Data Center (NDC) for CTBT verification. Six monitoring stations, comprising altogether 119 field instruments, will be located on Norwegian territory as part of the future IMS as described elsewhere in this report. The four seismic IMS stations are all in operation today, and three of them are currently providing data to the IDC. The radionuclide station at Spitsbergen is currently operating in a testing mode, whereas the infrasound station in northern Norway will need to be established within the next few years. Data recorded by the Norwegian stations is being transmitted in real time to the Norwegian NDC, and provided to the IDC through the Global Communications Infrastructure (GCI). Norway is connected to the GCI with a frame relay link to Vienna.

Operating the Norwegian IMS stations will require increased resources and additional personnel both at the NDC and in the field. It will require establishing new and strictly defined procedures as well as increased emphasis on regularity of data recording and timely data transmission to the IDC in Vienna. Anticipating these requirements, a new organizational unit has been established at NORSAR to form a core group for the future Norwegian NDC for treaty monitoring. The NDC will carry out all the technical tasks required in support of Norway's treaty obligations. NORSAR will also carry out assessments of events of special interest, and advise the Norwegian authorities in technical matters relating to treaty compliance.

Verification functions; information received from the IDC

After the CTBT enters into force, the IDC will provide data for a large number of events each day, but will not assess whether any of them are likely to be nuclear explosions. Such assessments will be the task of the States Parties, and it is important to develop the necessary national expertise in the participating countries. An important task for the Norwegian NDC will thus be to make independent assessments of events of particular interest to Norway, and to communicate the results of these analyses to the Norwegian Ministry of Foreign Affairs.

Monitoring the Arctic region

Norway will have monitoring stations of key importance for covering the Arctic, including Novaya Zemlya, and Norwegian experts have a unique competence in assessing events in this region. On several occasions in the past, seismic events near Novaya Zemlya have caused political concern, and NORSAR specialists have contributed to clarifying these issues.

International cooperation

After entry into force of the treaty, a number of countries are expected to establish national expertise to contribute to the treaty verification on a global basis. Norwegian experts have been in contact with experts from several countries with the aim to establish bilateral or multilateral cooperation in this field. One interesting possibility for the future is to establish NORSAR as a regional center for European cooperation in the CTBT verification activities.

NORSAR event processing

The automatic routine processing of NORSAR events as described in NORSAR Sci. Rep. No. 2-93/94, has been running satisfactorily. The analyst tools for reviewing and updating the solutions have been continuously modified to simplify operations and improve results. NORSAR is currently applying teleseismic detection and event processing using the large-aperture NORSAR array as well as regional monitoring using the network of small-aperture arrays in Fennoscandia and adjacent areas.

Certification of PS28

On 8 November 2001 the IMS station PS28-ARCES was formally certified. PTS personnel visited the station during the winter of 2000, and carried out a detailed technical evaluation. As a result of this inspection and subsequent discussions between NORSAR and the PTS, it was concluded that PS28 needed only one enhancement in order to be certified: to install a centralized authentication process at the central array recording facility. After this was done during the fall of 2001 and subsequently verified by the PTS, station certification was granted.

Communication topology

Norway has elected to use the option for an independent subnetwork, which will connect the IMS stations AS72, AS73, PS28, IS37 and RN49 operated by NORSAR to the GCI at NOR_NDC. A contract has been concluded and VSAT antennas have been installed at each station in the network. Under the same contract, VSAT antennas for 6 of the PS27 subarrays have been installed for intra-array communication. The seventh subarray is connected to the central recording facility via a leased land line. The central recording facility for PS27 is connected directly to the GCI (Basic Topology). All the VSAT communication is functioning satisfactorily.

The Norwegian NDC has been cooperating with institutions in other countries for transmission of IMS data to the Prototype IDC during GSETT-3. Details on this can be found in Section 4.2.

Jan Fyen

4.2 Status Report: Norway's Participation in GSETT-3

Introduction

This contribution is a report for the period July - December 2001 on activities associated with Norway's participation in the GSETT-3 experiment, which provides data to the International Data Centre (IDC) in Vienna on an experimental basis until the participating stations have been commissioned as part of the International Monitoring System (IMS) network defined in the protocol to the Comprehensive Nuclear-Test-Ban Treaty. This report represents an update of contributions that can be found in previous editions of NORSAR's Semiannual Technical Summary. It is noted that as of 31 December 2001, two out of the three Norwegian seismic stations providing data to the IDC have been formally certified and thus commissioned as part of the IMS network.

Norwegian GSETT-3 stations and communications arrangements

During the reporting interval 1 July - 31 December 2001, Norway has provided data to the GSETT-3 experiment from the three seismic stations shown in Fig. 4.2.1. The NORSAR array (PS27, station code NOA) is a 60 km aperture teleseismic array, comprised of 7 subarrays, each containing six vertical short period sensors and a three-component broadband instrument. ARCES is a 25-element regional array with an aperture of 3 km, whereas the Spitsbergen array (station code SPITS) has 9 elements within a 1-km aperture. ARCES and SPITS both have a broadband three-component seismometer at the array center.

The intra-array communication for NOA has been achieved by a land line for subarray NC6 and VSAT links based on TDMA technology for the other 6 subarrays. The central recording facility of NOA is at NOR_NDC.

Continuous ARCES data have been transmitted from the ARCES site to NOR_NDC using a 64 kbits/s VSAT satellite link, based on BOD technology.

Continuous SPITS data have been transmitted to NOR_NDC via a VSAT terminal located at Platåberget in Longyearbyen (which is the site of the IMS radionuclide monitoring station RN49 installed during 2001).

Seven-day station buffers have been established at the ARCES and SPITS sites and at all NOA subarray sites, as well as at NOR_NDC for ARCES, SPITS and NOA (central array station buffer).

The NOA and ARCES arrays are primary stations in the GSETT-3 network and the IMS, which implies that data from these stations are transmitted continuously to the receiving international data center. Since October 1999, these data have been transmitted (from NOR_NDC) via the Global Communications Infrastructure (GCI) to the IDC in Vienna, whereas transmission of the same data to the Prototype International Data Center (PIDC) in Arlington, VA, was discontinued on 7 February 2000. The SPITS array is an auxiliary station in GSETT-3 and the IMS, and the SPITS data have been available to both the IDC and the PIDC throughout the reporting period on a request basis via use of the AutoDRM protocol (Kradolfer, 1993; Kradolfer, 1996). The Norwegian stations are thus participating in GSETT-3 with the same status (primary/auxiliary seismic stations) they have in the IMS defined in the protocol to the Comprehensive Nuclear-Test-Ban Treaty. In addition, continuous data from all three arrays are being transmitted to the US NDC.

Uptimes and data availability

Figs. 4.2.2 - 4.2.3 show the monthly uptimes for the Norwegian GSETT-3 primary stations ARCES and NOA, respectively, for the period 1 July - 31 December 2001, given as the hatched (taller) bars in these figures. These barplots reflect the percentage of the waveform data that are available in the NOR_NDC tape archives for these two arrays. The downtimes inferred from these figures thus represent the cumulative effect of field equipment outages, station site to NOR_NDC communication outage, and NOR_NDC data acquisition outages.

Figs. 4.2.2-4.2.3 also give the data availability for these two stations as reported by the PIDC in the PIDC Station Status reports. The main reason for the discrepancies between the NOR_NDC and PIDC data availabilities as observed from these figures is the difference in the ways the two data centers report data availability for arrays: Whereas NOR_NDC reports an

array station to be up and available if at least one channel produces useful data, the PIDC uses weights where the reported availability (capability) is based on the number of actually operating channels. The PIDC receives its ARCES and NOA data via the IDC in Vienna.

Use of the AutoDRM protocol

NOR_NDC's AutoDRM has been operational since November 1995 (Mykkeltveit & Baadshaug, 1996). The PIDC started actively and routinely using NOR_NDC's AutoDRM service after SPITS changed its station status from primary to auxiliary on 1 October 1996. The monthly number of requests by the PIDC for SPITS data for the period July - December 2001 is shown in Fig. 4.2.4.

NDC automatic processing and data analysis

These tasks have proceeded in accordance with the descriptions given in Mykkeltveit and Baadshaug (1996). For the period July - December 2001, NOR_NDC derived information on 524 supplementary events in northern Europe and submitted this information to the Finnish NDC as the NOR_NDC contribution to the joint Nordic Supplementary (Gamma) Bulletin, which in turn is forwarded to the PIDC. These events are plotted in Fig. 4.2.5.

Data forwarding for GSETT-3 stations in other countries

NOR_NDC continued to provide communications for the GSETT-3 auxiliary station at Nilore, Pakistan, through a VSAT satellite link between NOR_NDC and Pakistan's NDC in Nilore. The PIDC as well as the IDC obtain data from the Hagfors array (HFS) in Sweden through requests to the AutoDRM server at NOR_NDC (in the same way requests for Spitsbergen array data are handled, see above). Fig. 4.2.6 shows the monthly number of requests for HFS data from the two PIDC accounts "pipeline" and "testbed".

Current developments and future plans

NOR_NDC is continuing the efforts towards improving and hardening all critical data acquisition and data forwarding hardware and software components, so as to meet future requirements related to operation of IMS stations to the maximum extent possible.

The PrepCom has tasked its Working Group B with overseeing, coordinating, and evaluating the GSETT-3 experiment. The PrepCom has also encouraged states that operate IMS-designated stations to continue to do so on a voluntary basis and in the framework of the GSETT-experiment until such time that the stations have been certified for formal inclusion in IMS. The NOA array was formally certified by the PTS on 28 July 2000, and a contract with the PTS in Vienna currently provides partial funding for operation and maintenance of this station. The ARCES array was formally certified by the PTS on 8 November 2001. It is expected that a contract will be signed with the PTS for operation and maintenance of this station, with an effective date of 1 January 2002. Provided that adequate funding continues to be made available (from the PTS and the Norwegian Ministry of Foreign Affairs), we envisage continuing the provision of data from all Norwegian IMS-designated seismic stations without interruption to the IDC in Vienna.

U. Baadshaug
S. Mykkeltveit
J. Fyen

References

Kradolfer, U. (1993): Automating the exchange of earthquake information. *EOS, Trans., AGU*, 74, 442.

Kradolfer, U. (1996): AutoDRM — The first five years, *Seism. Res. Lett.*, 67, 4, 30-33.

Mykkeltveit, S. & U. Baadshaug (1996): Norway's NDC: Experience from the first eighteen months of the full-scale phase of GSETT-3. *Semiann. Tech. Summ., 1 October 1995 - 31 March 1996*, NORSAR Sci. Rep. No. 2-95/96, Kjeller, Norway.

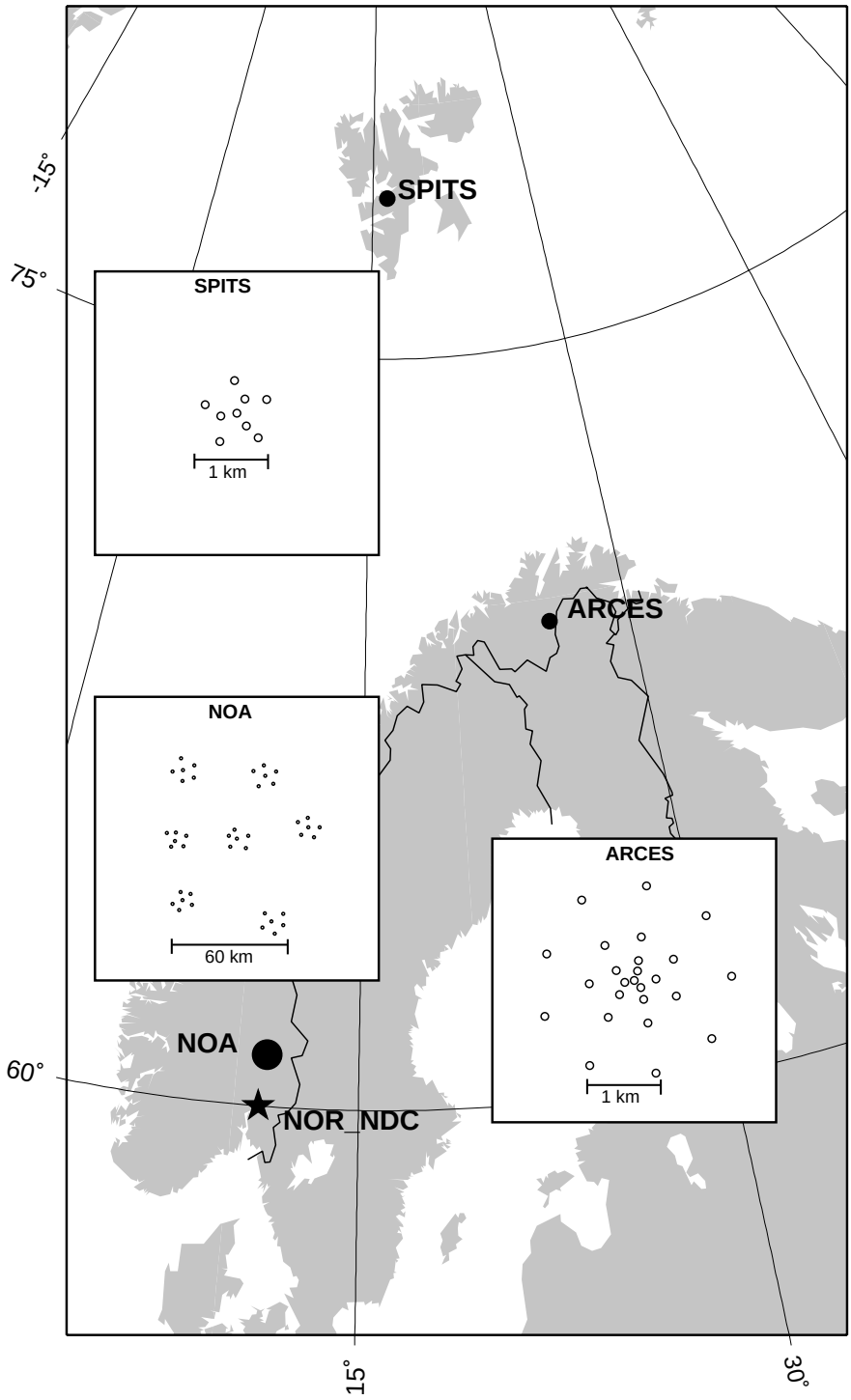

Fig. 4.2.1. The figure shows the locations and configurations of the three Norwegian seismic array stations that have provided data to the GSETT-3 experiment during the period 1 July - 31 December 2001. The data from these stations are transmitted continuously and in real time to the Norwegian NDC (NOR_NDC). The stations NOA and ARCES have participated in GSETT-3 as primary stations, whereas SPITS has contributed as an auxiliary station.

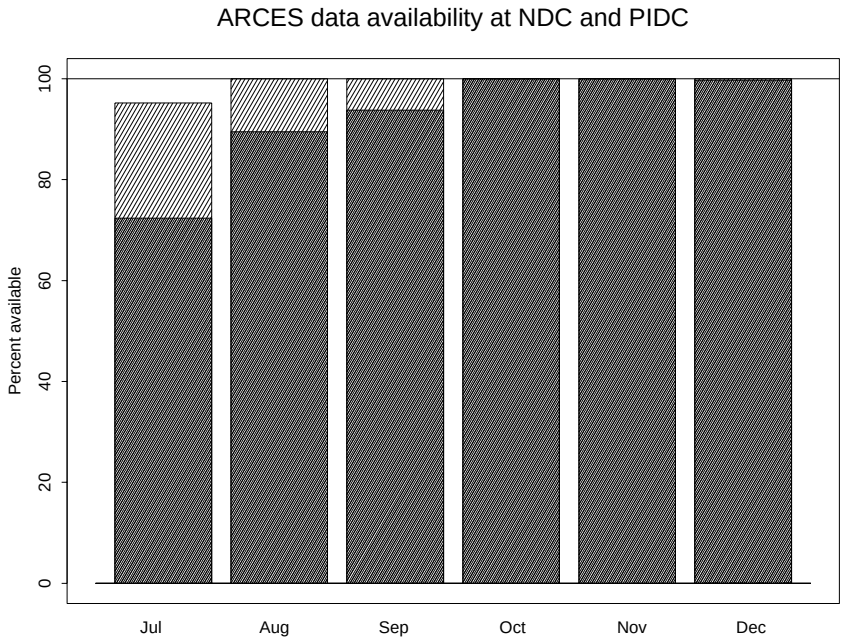

Fig. 4.2.2. The figure shows the monthly availability of ARCES array data for the period June - December 2001 at NOR_NDC and the PIDC. See the text for explanation of differences in definition of the term "data availability" between the two centers. The higher values (hatched bars) represent the NOR_NDC data availability.

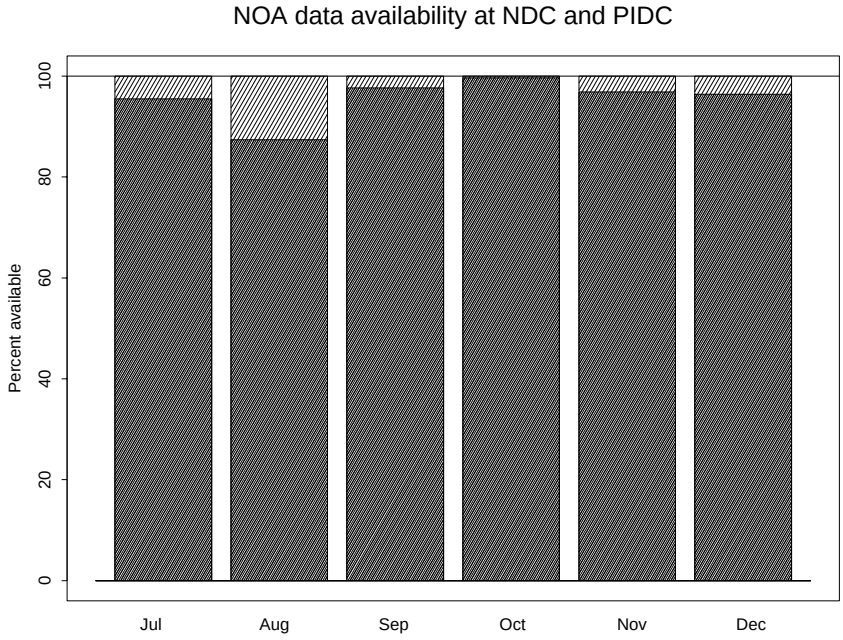

Fig. 4.2.3. The figure shows the monthly availability of NORSAR array data for the period June - December 2001 at NOR_NDC and the PIDC. See the text for explanation of differences in definition of the term "data availability" between the two centers. The higher values (hatched bars) represent the NOR_NDC data availability.

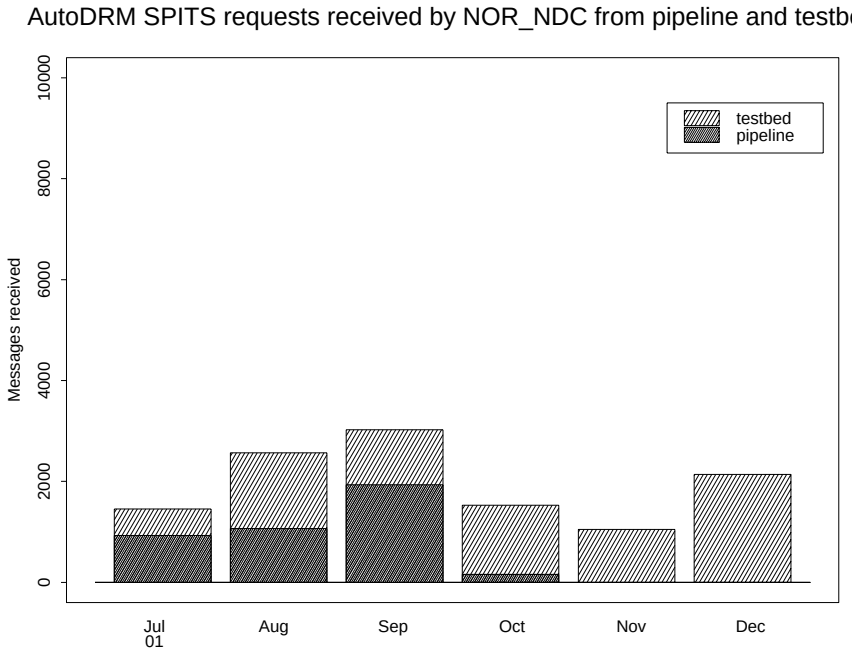

Fig. 4.2.4. The figure shows the monthly number of requests received by NOR_NDC from the PIDC for SPITS waveform segments during July - December 2001.

Reviewed Supplementary events

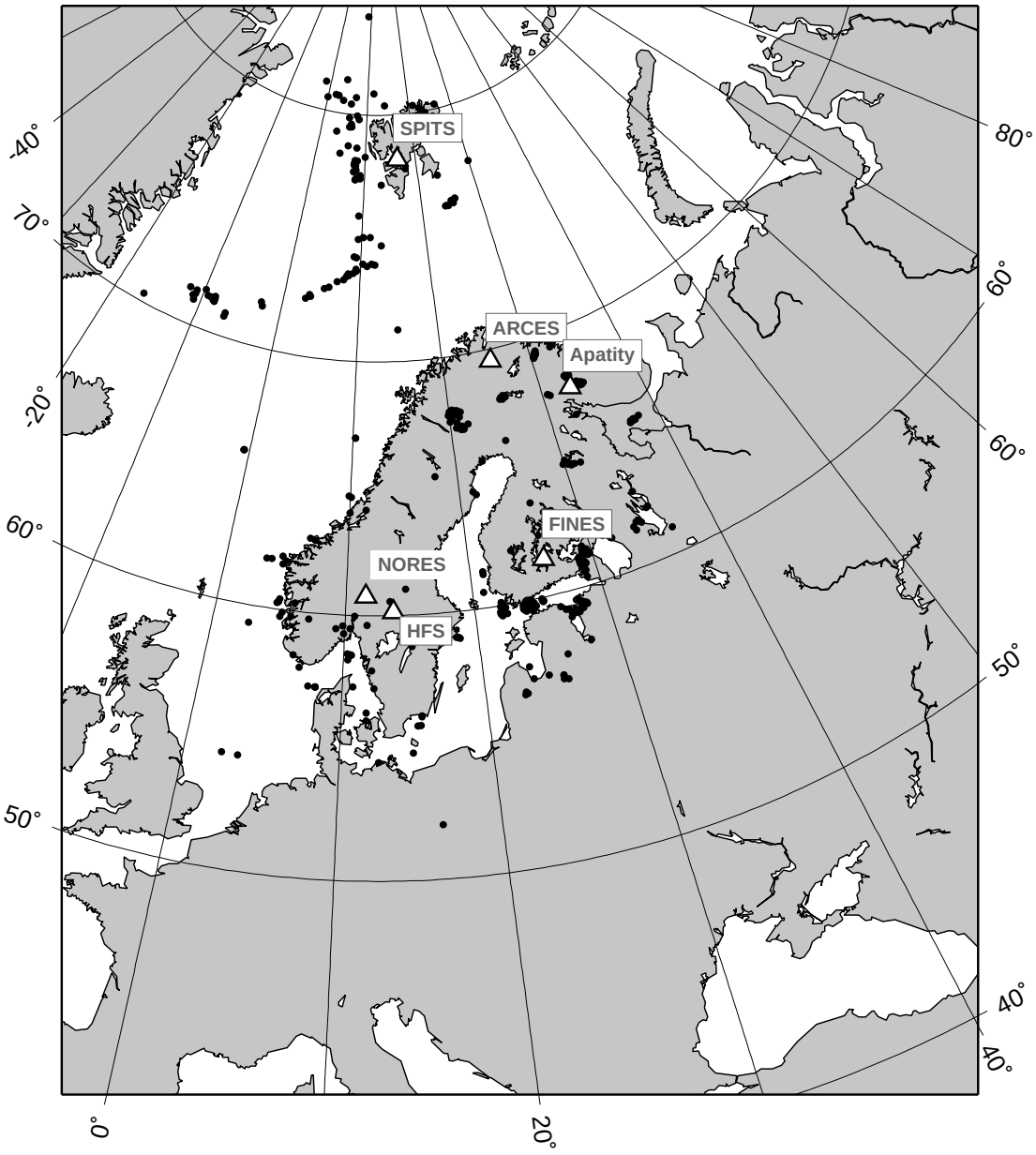

Fig. 4.2.5. The map shows the 524 events in and around Norway contributed by NOR_NDC during July - December 2001 as supplementary (Gamma) events to the PIDC, as part of the Nordic supplementary data compiled by the Finnish NDC. The map also shows the seismic stations used in the data analysis to define these events.

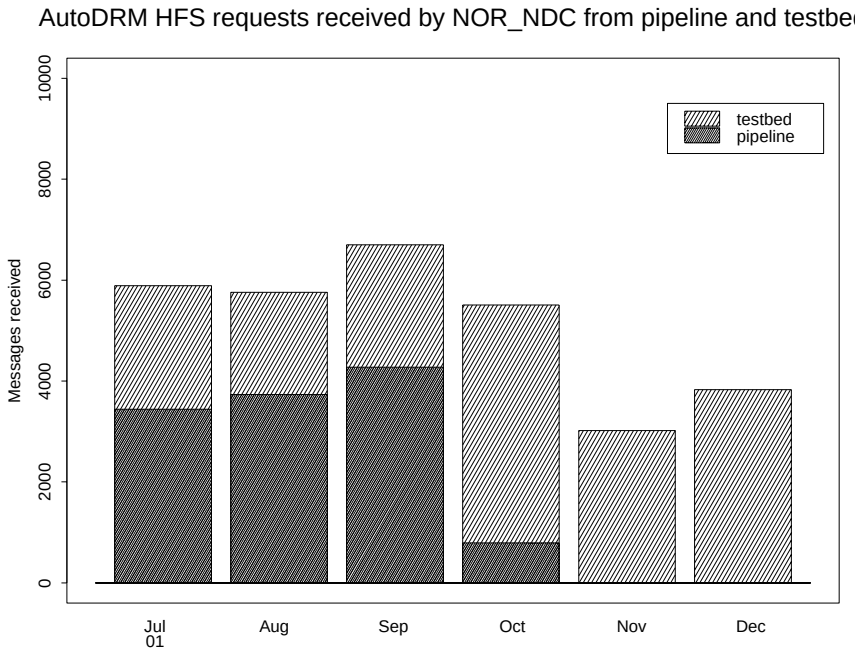

Fig. 4.2.6. The figure shows the monthly number of requests received by NOR_NDC from the PIDC for HFS waveform segments during July - December 2001.

4.3 Field Activities

The activities at the NORSAR Maintenance Center (NMC) at Hamar currently includes work related to operation and maintenance of the following IMS seismic stations: the NOA teleseismic array (PS27), the ARCES array (PS28) and the Spitsbergen array (AS72). Some preparatory work has also been carried out in connection with the seismic station on Jan Mayen (AS73), the infrasound station at Karasjok (IS37) and the radionuclide station at Spitsbergen (RN49). NORSAR also acts as a consultant for the operation and maintenance of the Hagfors array in Sweden (AS101).

In addition to the above activities, which are directly related to the International Monitoring System, NORSAR's field staff are continuing, within available resources, to maintain the small-aperture NORES array, which is co-located with NOA subarray 06C. These efforts are given low priority, since there is no requirement for specific uptimes at NORES.

NORSAR carries out the field activities relating to IMS stations in a manner generally consistent with the requirements specified in the appropriate IMS Operational Manuals, which are currently being developed by Working Group B of the Preparatory Commission. For seismic stations these specifications are contained in the Operational Manual for Seismological Monitoring and the International Exchange of Seismological Data (CTBT/WGB/TL-11/2), currently available in a draft version.

All regular maintenance on the NORSAR field systems is conducted on a one-shift-per-day, five-day-per-week basis. The maintenance tasks include:

- Operating and maintaining the seismic sensors and the accociated digitizers, authentication devices and other electronics components.
- Maintaining the power supply to the field sites as well as backup power supplies .
- Operating and maintaining the VSATs, the data acquisition systems and the intra-array data transmission systems.
- Assisting the NDC in evaluating the data quality and making the necessary changes in gain settings, frequency response and other operating characteristics as required.
- Carrying out preventive, routine and emergency maintenance to ensure that all field systems operate properly.
- Maintaining a computerized record of the utilization, status, and maintenance history of all site equipment.
- Providing appropriate security measures to protect against incidents such as intrusion, theft and vandalism at the field installations.

Details of the daily maintenance activities are kept locally. As part of its contract with CTBTO/PTS, NORSAR submits, when applicable problem reports, outage notification reports and equipment status reports. The contents of these reports, and the circumstances under which they will be submitted, are specified in the draft Operational Manual.

P.W. Larsen
K.A. Løken

5 Documentation Developed

Gibbons, S., C. Lindholm, T. Kværna & F. Ringdal (2002): Analysis of cavity-decoupled chemical explosions, **In**: *NORSAR Sci. Rep. 2-2002*, 1 January - 30 June 2002, Kjeller, Norway.

Kværna, T., E. Hicks & F. Ringdal (2002): Site-Specific Generalized Beamforming (SSGBF) applied to the Lop Nor test site, **In**: *NORSAR Sci. Rep. 2-2001*, 1 July - 31 December 2001, Kjeller, Norway.

Kværna, T., E. Hicks, J. Schweitzer & F. Ringdal (2002): Regional Seismic Threshold Monitoring, **In**: *NORSAR Sci. Rep. 2-2001*, 1 July - 31 December 2001, Kjeller, Norway.

Kværna, T., F. Ringdal, J. Schweitzer & L. Taylor (2002): Optimized Seismic Threshold Monitoring — Part 1: Regional Processing, *PAGEOPH* 159, 969-987.

Kværna, T., F. Ringdal, J. Schweitzer & L. Taylor (2002): Optimized Seismic Threshold Monitoring — Part 2: Teleseismic Processing, *PAGEOPH* 159, 989-1004.

Ringdal, F. (2002): Technical Summary, *NORSAR Sci. Rep. 1-2002*, Kjeller Norway.

Ringdal, F. (2002): Seismic Event Location Calibration, **In**: *NORSAR Sci. Rep. 2-2002*, 1 January - 30 June 2002, Kjeller, Norway.

Ringdal, F., T. Kværna, E. Kremenetskaya, V. Asming, S. Mykkeltveit, C. Lindholm & J. Schweitzer (2002): Research in regional seismic monitoring, **In**: *NORSAR Sci. Rep. 2-2002*, 1 January - 30 June 2002, Kjeller, Norway.

Schweitzer, J. & T. Kværna (2002): Design study for the refurbishment of the SPITS Array (AS72), **In**: NORSAR Sci. Rep. 2-2002, 1 January - 30 June 2002, Kjeller, Norway.

6 Summary of Technical Reports / Papers Published

6.1 Estimating global and regional IMS detection capability

Introduction

The primary seismic network of the International Monitoring System (IMS) for verifying compliance with the Comprehensive Nuclear Test Ban Treaty (CTBT) consists of 49 stations (see Fig. 6.1.1), out of which 35 are installed and operational as of July 2001. These stations are the key element of the IMS as they are used for detecting events that might be violations of the CTBT. We have in this study used the threshold monitoring (TM) method (Kværna and Ringdal, 1999, Ringdal and Kværna, 1989, 1992) to assess the detection capability of the IMS seismic network. The TM method is capable of using actual seismic data for a given time interval as the basis for the detectability calculations. In cases when a seismic station did not provide data during the time period under study, an estimated background noise level can be assigned. These noise estimates can be based on results from earlier studies, or they can be taken from stations assumed to have similar noise characteristics.

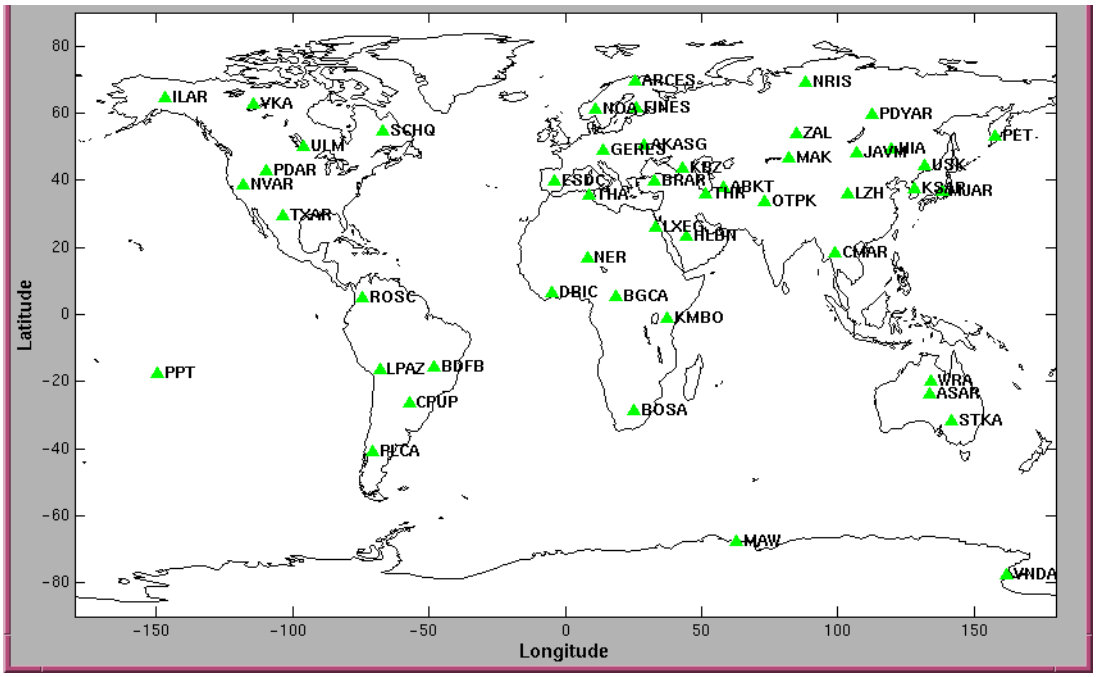

Fig. 6.1.1. Station configuration of the full IMS primary seismic network.

The detection capability of the full IMS primary seismic network

We have used the time interval 10:20-11:00 on 29 June 2001 as the basis for estimating the detection capability of the full IMS primary seismic network. This time interval does not contain any major seismic events and most of the stations have relatively quiet noise conditions. Fig. 6.1.2 shows the short-term-averages (STAs) representing the noise levels at each of the IMS primary seismic stations operational as of 29 June 2001. For stations not providing data during this time interval, a typical constant noise level has been assigned. These stations have the label *const* at the top of each panel.

The noise levels assigned for the planned primary seismic stations are shown in Fig. 6.1.3.

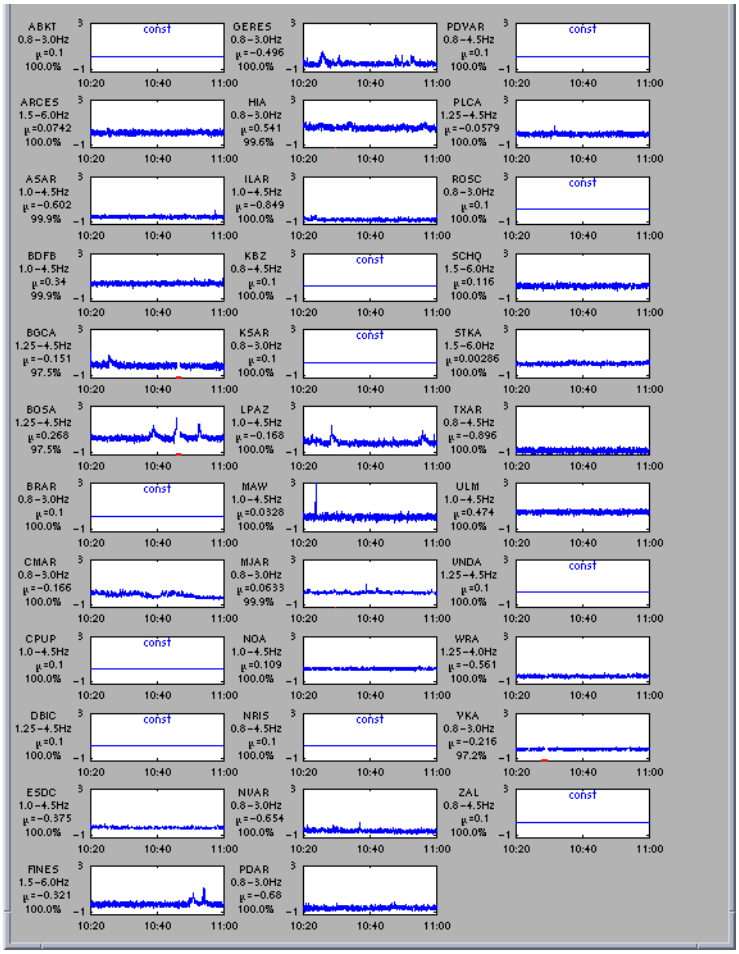

Fig. 6.1.2. Real or estimated noise levels of current IMS primary seismic stations for the time period 10:20-11:00 on 29 June 2001.

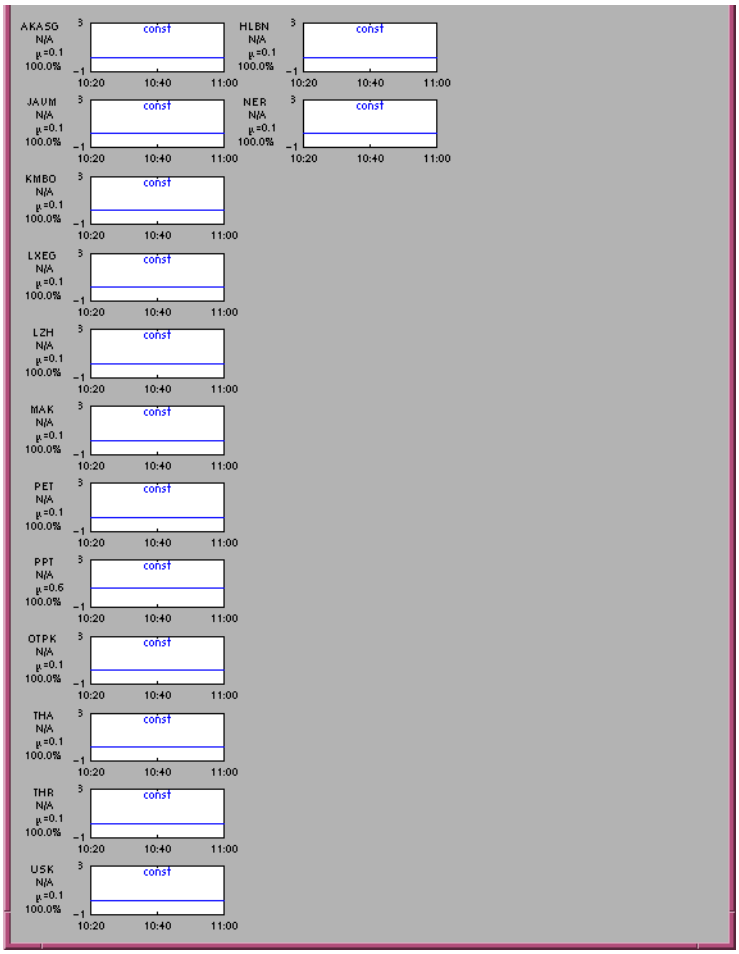

Fig. 6.1.3. Noise levels assigned for the planned IMS primary seismic stations.

We have used the average noise levels shown in Figs. 6.1.2 and 6.1.3 to calculate the three-station network detection capability at the 90% confidence level of the full IMS primary seismic network. The results are shown in Fig. 6.1.4. Very good detection capability is found in northern Europe and North America where several high performance seismic arrays are installed. The results shown in Fig. 6.1.4 agree well with the statistical simulations provided by the NetSim program (Sereno et. al, 1990).

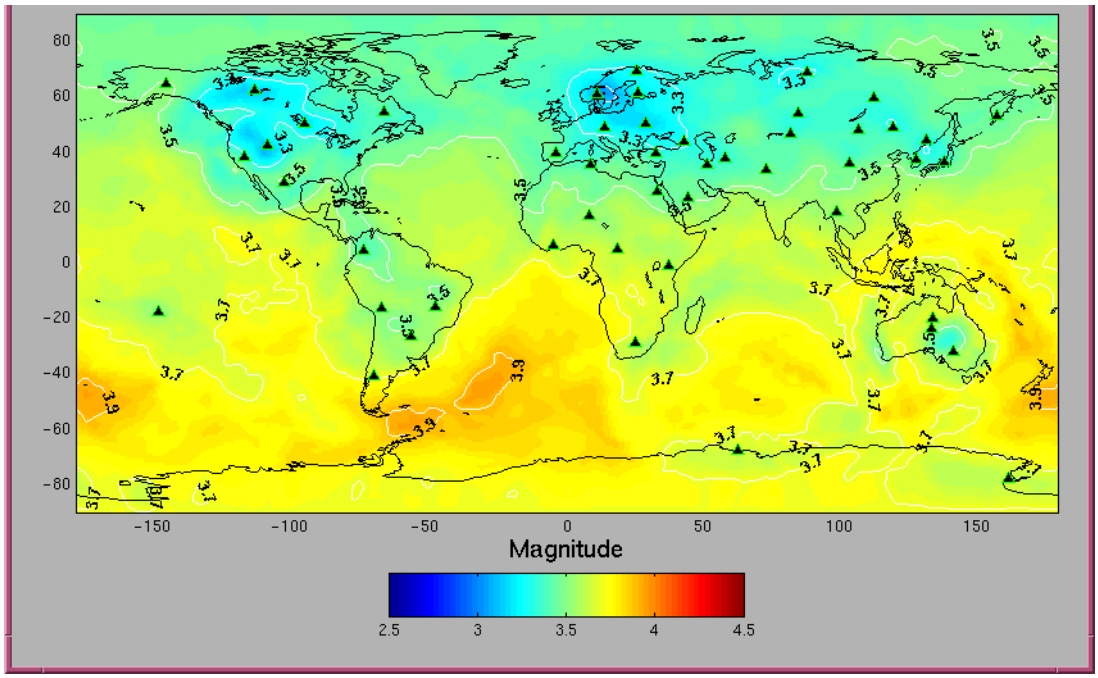

Fig. 6.1.4. Three station detection capability of the full IMS primary network.

The detection capability of the IMS primary seismic network as of July 2001

It is of particular interest to compare the detection capability of the current IMS network with the projected performance of the 49 stations of the full network. As of 7 July 2001 the primary seismic IMS network consisted of 35 stations, but several of these stations did not provide any data. We have in Fig. 6.1.5 plotted the background noise levels for a time interval without any significant seismic signals, and we see that several stations are down or providing data gaps. The corresponding three-station detection capability is shown in Fig. 6.1.6, and we again notice the good detectability associated with the high performance arrays in northern Europe, North America and Australia.

We have in Fig. 6.1.7 plotted the difference in detectability between the current IMS primary seismic and the projected performance of the full network. The average difference is only 0.06 magnitude units, and the largest differences are found in southwest Asia with a maximum value of 0.47. The constant noise levels assigned to the planned or non-operational stations are taken from typical noise levels at stations assumed to have similar noise characteristics. The relatively large uncertainty associated with the assigned constant noise levels is also reflected in the detectability estimates.

Fig. 6.1.5. Noise levels of current IMS primary seismic stations on 7 July 2001.

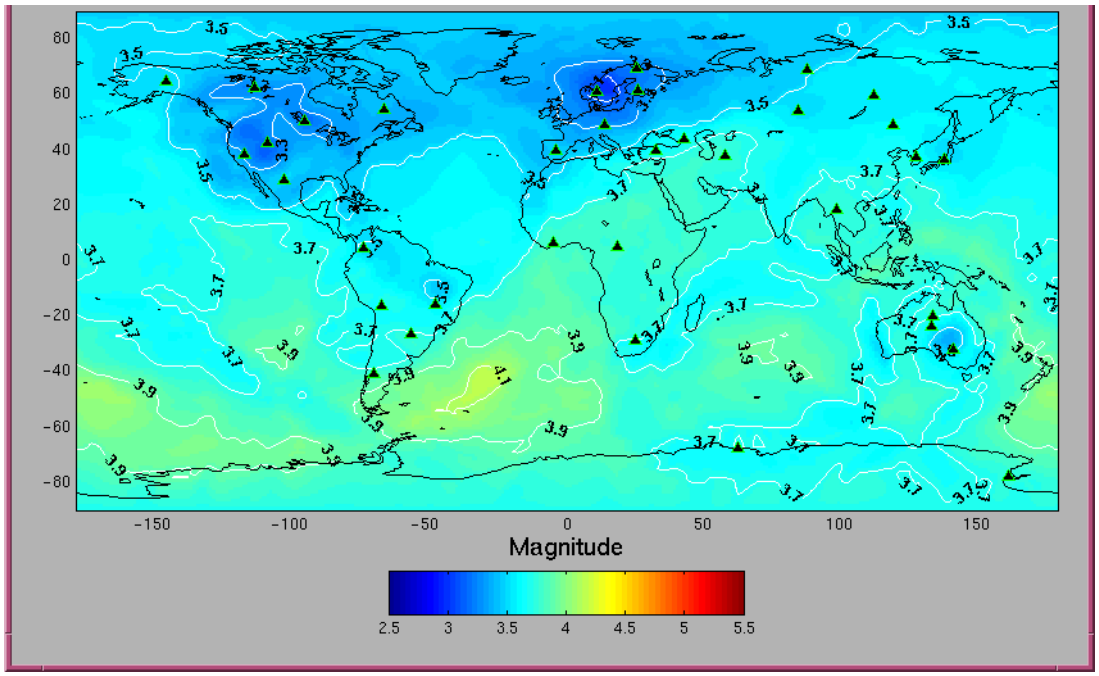

Fig. 6.1.6. Three-station detection capability of IMS primary stations on 7 July 2001.

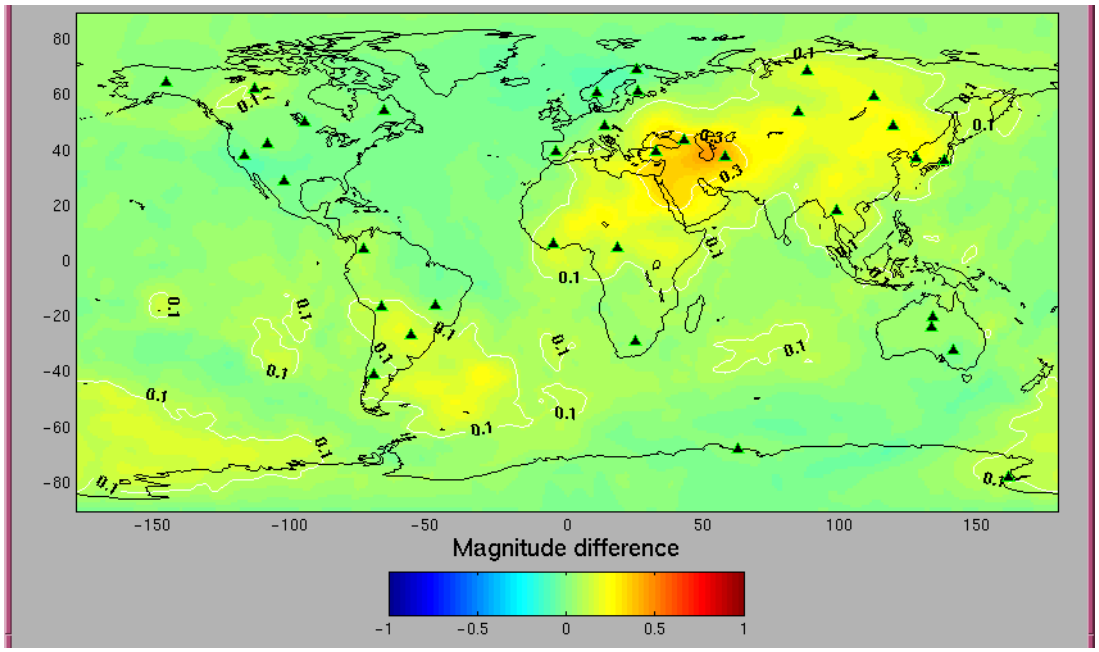

Fig. 6.1.7. Difference in detection capability between the current operational primary seismic network (Fig. 6.1.6) and full network (Fig 6.1.4).

The detection capability of the IMS primary seismic network in the coda of a large earthquake

At 09:38:43.5 on 7 July 2001 a m_b 5.7, M_S 7.6 earthquake occurred near the coast of Peru. Fig. 6.1.8 shows the average three-station network detection capability for a five minute time interval that starts 1 minute and 20 seconds after the origin time of the event. Notice the reduced detectability for the areas around the epicenter.

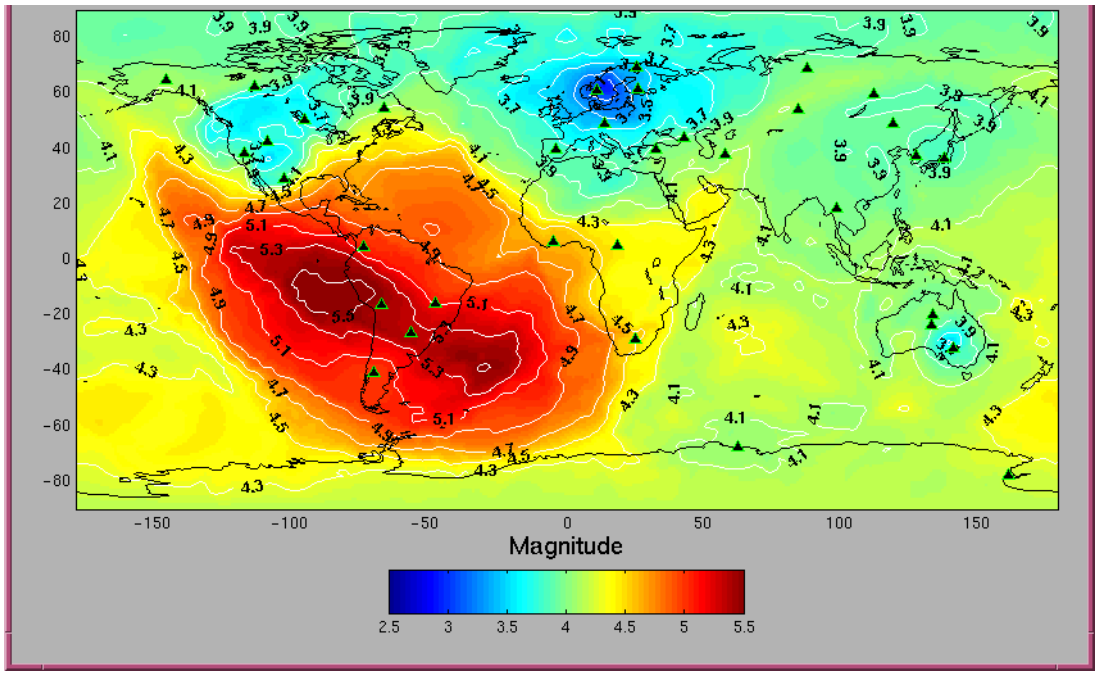

Fig. 6.1.8. Three-station detection capability of IMS primary stations 1 minute and 20 seconds after the occurrence of a m_b 5.7 earthquake near the coast of Peru.

In Fig. 6.1.9 we have plotted the difference in detectability between the time interval with the earthquake signals (Fig. 6.1.8) as compared to the detectability during quiet background noise conditions (Fig. 6.1.6). For large regions, including South America and adjacent areas, the detection performance is reduced by more than 1 magnitude unit. The maximum difference is 1.925 units in the vicinity of the epicenter. As time passes, the seismic signals will propagate to longer distances and reduce the detectability for larger regions of the Earth. However, due to the signal attenuation the degradation of the detection capability will be less than for regions closer to the event.

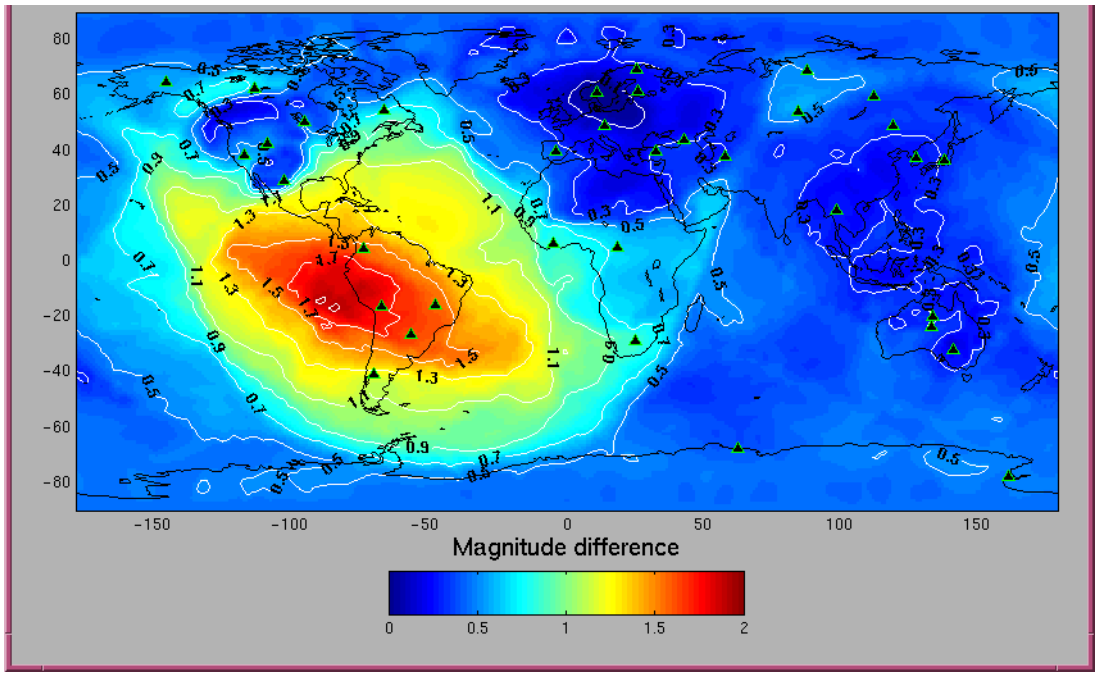

Fig. 6.1.9. Difference in detection capability between the levels given in Fig. 6.1.8 and 6.1.6.

Conclusions

We have found that the 35 stations of the primary seismic IMS network operational as of July 2001 have a three-station detection capability that is quite close to the projected performance of the 49 stations of the network. The largest difference of about 0.5 m_b units is found in south-west Asia. This can be explained by the fact that most of the sensitive array stations of the network are already in place. Another uncertainty is the noise levels assigned to the planned stations and to the stations that did not provide real noise data during the period under investigation. The assignment of realistic noise levels for planned stations is therefore a topic requiring additional studies.

This study also confirms the results provided by Kværna and Ringdal (1999) that large earthquakes and the corresponding coda energy can temporarily, over tens of minutes, significantly reduce the detection capability of the IMS network. During such conditions the use of high-frequency regional data, combined with less stringent event formation criteria (1 or 2 station only) will be important for CTBT verification purposes.

References

Kværna. T. and F. Ringdal (1999). Seismic Threshold Monitoring for Continuous Assessment of Global Detection Capability, Bull. Seism. Soc. Am., 89, 946-959.

Ringdal, F. and T. Kværna (1989). A Multichannel Processing Approach to Real Time Network Detection, Phase Association and Threshold Monitoring, Bull. Seism. Soc. Am., 79, 1927-1940.

Ringdal, F. and T. Kværna (1992). Continuous Seismic Threshold Monitoring, Geophys. J. Int., 111, 505-514.

Sereno, T.J., S.R. Bratt and G. Yee (1990). NetSim: A computer program for simulating detection and location capability of regional seismic networks, SAIC Annual Technical Report to DARPA, SAIC 90/1163, March 1990.

T. Kværna

6.2 Travel times and attenuation relations for regional phases in the Barents Sea region

This research is conducted under contract DTRA01-00-C-0107.

A database containing 42 events in the Barents Sea region has been compiled and analyzed with the aim of evaluating crustal models, travel times and attenuation relations in the context of performing regional detection threshold monitoring of this region. The 42 events are mostly located around the circumference of the study area due to the virtually aseismic nature of the Barents Sea itself. Regional P_n and S_n phases were observable for most events in the database, while P_g and L_g phases were only observable for events with ray paths within continental crust. This corroborates a number of previous observations of L_g-wave blockage across the Barents Sea. Three existing velocity models were evaluated, with a model having slightly lower S-velocities than earlier assumed in the upper mantle giving the overall best fit to the observed arrivals. In order to estimate magnitudes, short term average (STA) and spectral amplitude values were calculated in several frequency bands for all phase arrivals in the data base. There were no significant differences between spectral and STA amplitudes, so the latter were used as this parameter is more efficient to calculate in real-time processing. An inversion was performed in order to determine a P_n and S_n attenuation relation specific for this region. The resulting magnitudes based on P_n and S_n phases gave an internally consistent, reasonably stable set of values, which can be calibrated towards any existing global or regional scale. An attenuation relation was also determined for the L_g phase, but the low number of amplitude readings in this case renders the results less reliable.

Introduction

The Barents Sea region is an area which is of particular interest in the context of the comprehensive nuclear test ban treaty (CTBT), as it contains the former Soviet Union nuclear test sites on Novaya Zemlya. For this reason, it is of interest to perform regional seismic detection threshold monitoring in order to continuously assess the upper limit magnitude of events that could go undetected, and also to provide automatic locations for seismic events in the region with the best possible precision. The Threshold Monitoring (TM) method (e.g. Ringdal and Kværna, 1989; 1992; Kværna and Ringdal, 1999) uses continuous seismic data from a network of stations to calculate a threshold magnitude for each point in a grid, for which an event would have 90% probability of detection by the network. It is thus able to take varying noise levels, interfering signals from teleseismic events, data gaps, particularly favorable site-station transmission properties etc. into account, which traditional, static capability maps are incapable of doing (Ringdal and Kværna, 1992). However, for the threshold monitoring to be accurate, reliable travel time curves and attenuation relations are required for the target area. Ideally, calibration events should be available for all station/phase combinations at each target point. However, in practice, particularly in areas of low seismic activity such as the Barents Sea, it is necessary to rely on travel time curves calculated from a regional velocity model and regional attenuation relations. Still, a good coverage of seismic events is a requirement in order to determine mean regional values of such relations. In order to provide the necessary data for this region, we have compiled a database of recent events, and have attempted to extract the necessary information in spite of the less than optimal coverage.

Seismotectonic setting

The Barents Sea is an epicontinental sea, bordering on the Precambrian and Caledonian crust of northern Fennoscandia, the Kola Peninsula and northern Siberia to the south, and young passive margins to the north and west, formed during the Cenozoic opening of the Eurasian Basin and the Norwegian-Greenland Sea respectively (e.g. Faleide *et al.*, 1993). Large parts of the western margin and the oceanic crust to the west is covered by a huge sediment wedge deposited after the opening of the Norwegian-Greenland Sea, primarily during the Pliocene-Pleistocene age (Eidvin *et al*., 1993). The interior of the Barents Sea is underlain by large thicknesses of Upper Paleozoic to Cenozoic sediments, with accentuated Moho relief, leaving as little as ~4 km of crystalline basement under the deepest basins (Jackson *et al*., 1990; Faleide *et al.*, 1993).

The internal Barents Sea has very little seismic activity, implying a stable tectonic situation (Bungum and Lindholm, 1996). This has also been interpreted as a consequence of a relatively weak ridge-push force counteracted by tensional stresses related to Pliocene-Pleistocene erosional unloading (Fiedler and Faleide, 1996). The activity is significantly higher along the western Barents Sea margin, which is under weak oblique (NW-SE) compression from the north-Atlantic ridge, with the large Pliocene-Pleistocene sediment load likely being the most important stress-generating mechanism in these areas (Byrkjeland *et al*., 2000).

Northern Fennoscandia and the Kola Peninsula are areas of intermediate seismic activity, tending mainly toward earthquakes in the upper half of the crust. There appears to be some activity connected to a postglacial reverse and strike-slip fault system in northern Fennoscandia (Bungum and Lindholm, 1996), the stress tensor appears to have NW-SE compression approximately corresponding to the expected ridge-push direction (Hicks *et al*., 2000). There is also some seismic activity along the northern coast of the Kola Peninsula, while onshore northern Siberia has lower levels. The seismic activity in northern Fennoscandia is most likely tied to a combination of the tectonic ridge push force and constructive postglacial uplift stresses (Bungum and Lindholm, 1996). Novaya Zemlya and the Kara Sea to the east has some sporadic earthquake activity, as evidenced by some interesting events in recent years (e.g. Marshall *et al*., 1989; Ringdal *et al*., 1997; Bowers *et al*., 2001; Schweitzer and Kennett, 2002).

Database of seismic events

A total of 42 seismic events in the Barents Sea and northern Fennoscandia were used as the basis for this study. The events were selected to provide the best possible ray path coverage of the crust, although since large areas of the Barents Sea are in practice aseismic, there is a concentration of activity on the outer parts: Svalbard, western Barents Sea, northern Fennoscandia, the Kola Peninsula and Novaya Zemlya. The database consists of earthquakes, mining blasts and other explosions (both chemical and nuclear), and some events of unknown origin. Areas with large numbers of seismic events with similar locations were represented with a single event, in order to avoid introducing any bias towards these areas in the subsequent inversion.

In addition to waveform data from seismic array stations on mainland Norway (ARCES, NORES), we have also used available array data from Finland (FINES), Svalbard (SPITS), and the Russian Kola peninsula (APA). Data from the Amderma (AMD) station in northern Russia were available for 15 of the events, waveform data were also retrieved from the IRIS consortium for the Global Seismographic Network (GSN) seismic stations in Kevo, Northern Finland

(KEV), Lovozero on the Kola peninsula (LVZ) and Ny Ålesund on the Svalbard archipelago (KBS). The location of these nine stations used are shown along with the locations of the 42 selected seismic events in Fig. 6.2.1. The waveform data were re-analyzed, with emphasis placed on consistent phase identification and onset time picking of observable phases. Only phases that could be clearly observed and identified were analyzed and used. A preliminary relocation of the events was performed during the analysis, using the 'Fennoscandia' crustal model (Mykkeltveit and Ringdal, 1981) which is the model routinely used by NORSAR for seismic event location in northwestern Europe and the Barents Sea.

An investigation of which phases were observable on the different stations from various source areas was performed, in order to evaluate the geographical coverage for each phase. As expected, crustal phases (P_g and L_g) are in general only observable for paths that travel more or less exclusively within the shield areas, i.e. from onshore or coastal events in Fennoscandia and Svalbard. This confirms previous observations indicating the blockage of L_g phases that have paths crossing large sedimentary structures such as those encountered in the Barents Sea (e.g. Zhang and Lay, 1994; Baumgardt, 2001; Bowers *et al*., 2001). P_n and S_n phases are observable for most events with distances greater than 2-3 degrees. Fig. 6.2.2 shows phase maps for the ARCES array in northern Norway.

Crustal models and travel times

In order to be able to predict phase arrival times for a given origin in a threshold monitoring application, an accurate crustal velocity model is required. An evaluation of several available crustal models was therefore performed. Observed and theoretical travel times for two models are shown in Fig. 6.2.3, plotted according to epicentral distance after relocation with the corresponding model using HYPOSAT (Schweitzer, 2001). All depths were fixed at 10 km for this comparison. The Fennoscandia model (Mykkeltveit and Ringdal, 1981), shown in Table 6.2.1, gave a reasonably good travel time residuals, but there were some systematic discrepancies as clearly visible in Fig. 6.2.3. The L_g-phase arrivals have consistent and quite large negative residuals on average, while the S_n phases trend towards positive residuals. The P_n arrivals have quite large negative residuals, in particular around the 6 - 12 degree distance range. Two models from Schweitzer and Kennett (2002), named BAREY and BAREZ (Table 1) were also tested, with the BAREY model giving the lowest travel time residuals overall (Fig. 6.2.3). These two models were adapted from a model developed for the Barents and Kara Seas by Kremenetskaya *et al.* (2001) by making minor P-velocity adjustments and varying the P/S ratio in the upper mantle (Schweitzer and Kennett, 2002). The main differences between these two models are the S velocities in the upper mantle, which of course have the greatest effect on regional S phases propagating at these depths (S_n). The BAREY model has the lowest S velocities in the upper mantle while BAREZ has the highest. The Fennoscandia model has upper mantle S velocities between the other two models. As shown in Table 6.2.1, the velocity profiles for both P and S within the crust are virtually identical, with the Conrad discontinuity at 16 km and the Mohorovicic discontinuity at 40 km (Fennoscandia) and 41 km (BAREY/BAREZ) depth.

The small differences in upper mantle P velocities (Table 6.2.1) serve to reduce the observed P_n residuals after relocation. The resulting small differences in epicenter locations for the different models also have an effect on the travel times of crustal phases, most visible for the L_g onsets (Fig. 6.2.3). The BAREY model appears to be particularly accurate for paths from Novaya

Zemlya to Fennoscandia, which is the setting for which it was developed. The BAREZ model is slightly better for paths crossing the Barents Sea from Novaya Zemlya to the north-west (towards Svalbard and Bjørnøya), and also to the south (towards Amderma) (Schweitzer and Kennett, 2002). The BAREY model however provided the smallest overall travel time residuals for all paths in our data set. The geographic distribution of the travel time residuals for the Fennoscandia and BAREY models is shown in Fig. 6.2.4, showing the generally lower residuals, in particular for the S_n arrivals, obtained using the BAREY model.

Attenuation relations and magnitudes

In order to provide threshold magnitudes for a given location, it is essential to be able to convert observed amplitudes to event magnitudes at the target location. To this end an attenuation relation from Jenkins *et al.* (1998), based on Sereno (1990) is used:

$$M_L = \log A + \log\left(\left(\frac{\Delta}{200}\right)^{af+b}\right) \quad (1)$$

where A is amplitude in nanometers, Δ is the epicentral distance in km, f is the logarithmic center frequency of the passband at which the amplitude reading is taken, while a and b are phase-dependent constants. The value 200 represents a reference distance where the geometrical spreading changes from spherical to a more complicated function based on the phase analyzed (Sereno, 1990). Due to the fact that the decrease in seismic amplitude with epicentral distance is a combined effect of geometrical spreading, anelasticity and scattering, care must be taken in relating these coefficients to physical properties of the medium (cf. Alsaker *et al.*, 1991). However, this is not necessary for our purpose, as long as the relation as a whole is able to describe the amplitude/distance relation in a consistent and reasonably accurate manner. The relation was developed using spectral amplitudes, however for continuos processing it is more efficient to use time-domain short term average (STA) amplitudes. A comparison of STA amplitudes and spectral amplitudes in the same frequency bands for the selected events showed that they are in practice equivalent with regard to magnitude calculation ($A_{STA} \sim A_{SPEC}$). STA amplitudes were calculated in three frequency bands (2-4, 3-6 and 4-8 Hz) corresponding to three of the frequency ranges used in JENKINS *et al*. (1998), using a moving window with a step length of one sample and window lengths of 2 s length for P_n and 5 s for S_n and L_g. The maximum STA amplitude within 7.5 s (P_n), 10 s (S_n) and 15 s (L_g) after the observed phase onset was then selected. Only amplitude readings with a minimum signal-to-noise ratios (SNR) of 3.0 or greater for P_n and S_n and 2.5 or greater for L_g, compared to a noise window of 5 s length starting 10 s ahead of the observed onset time have been used. The SNR for L_g is almost always lower than for S_n or P_n, as the L_g phase arrives within the coda of the earlier onsets. Similarly, S_n arrivals generally show lower SNRs than P_n arrivals, although this can also depend on source effects and the relative noise situation at the seismic station.

Magnitudes calculated using equation (1) did reveal some inconsistencies between magnitudes calculated from different frequency bands, phases and stations, as shown in Fig. 6.2.5. The *a* and *b* coefficients used in this care were determined using data from eastern North America, central Asia and Australia by Jenkins *et al.* (1998) (Table 6.2.2), also applied by Bowers *et al.* (2001) for the Barents Sea. For ARCES it is clear that magnitudes calculated from STA values in the 2-4 Hz passband are systematically higher, by about 0.3 magnitude units on average, than magnitudes calculated in the 3-6 Hz passband, which again are almost 0.2 magnitude units

higher on average than magnitudes calculated from the 4-8 Hz passband. Similar discrepancies were observed at the other stations. As Fig. 6.2.5 also shows, there is a quite large, systematic offset between the P_n and S_n phase magnitudes calculated within the same frequency band at the same station. In addition, there are large discrepancies between magnitudes calculated from the same phase/frequency range at different stations. This implies that the relation does not accurately represent the attenuation of seismic waves for this set of reference events.

In order to provide an attenuation relation that better explains the measured amplitudes in the database, and also to determine station corrections for the nine stations used, an inversion of the available amplitude data was performed. Using equation (1), the STA amplitude A_{ijk} for phase i from event j measured at station k may be expressed as:

$$a_i f \log\frac{\Delta}{200} + b_i \log\frac{\Delta}{200} + S_{ik} - M_j = -\log A_{ijk} \tag{2}$$

where S_{ik} is the station correction for phase i at station k, and M_j is the event magnitude for event j. The parameters a_i and b_i are the coefficients from equation (1) for phase i. Equation (2) represents a set of linear equations, and can be written in matrix form:

$$Ax = D \tag{3}$$

where A represents the Jacobi matrix, x the vector of unknowns and D is the data vector. We used standard, least-squares techniques to solve equation (2).

A total of 863 amplitude readings with acceptable SNR (≥3.0) from P_n (548 readings) and S_n (315 readings) phases from the 40 seismic events that had sufficient data to be used, were inverted in order to yield the two relation coefficients and nine station corrections for each of the two phases, in addition to relative magnitudes for the 40 events. The individual events had between four and 40 amplitude readings contributing to the solution. The a_i and b_i values determined through this inversion are given in Table 6.2.2, while the corresponding station corrections S_{ik} are listed in Table 6.2.3. New magnitudes calculated using these results are plotted in Fig. 6.2.6, showing that the mean offset was reduced in all cases compared to the original calculations (Fig. 6.2.5). The scatter, expressed as the standard deviation, was marginally higher for some combinations, and reduced for others.

The magnitudes for the P_n and S_n phases calculated using the inversion results are internally consistent, and can thus be tied in to any other magnitude scale. To calibrate the scale in this case we have used five events in the Novaya Zemlya region with body wave magnitudes ranging from m_b 2.4 to 5.6 (Table 4) that have previously been studied in great detail (e.g. Ringdal and Kremenetskaya, 1999), giving a constant offset of -0.33. Applying this offset value and the estimated phase-dependant station corrections S_i (listed in Table 6.2.3) to equation (1), the final magnitude relation for P_n and S_n STA amplitudes yields:

$$M_{L(P_n, S_n)} = \log A + \log\left(\left(\frac{\Delta}{200}\right)^{a_i f + b_i}\right) + S_i - 0.33 \tag{4}$$

where A is observed STA amplitude within a frequency band with logarithmic center frequency f, Δ is epicentral distance, and a_i and b_i are phase-dependant constants given in Table 6.2.2. The

P_n and S_n magnitudes calculated using equation (4) were in general comparable to previously reported magnitudes for other, well studied events, as shown in Table 6.2.4.

A separate inversion was attempted in order to determine coefficients for the L_g phase for events and stations located within Fennoscandia, as L_g observations are limited to this area. The inversion gave seemingly acceptable results when applied to our small group of events, however, attenuation was extremely low for distances over around 500 km. Given this contrast to the general M_L relation for Norway from Alsaker *et al*. (1991), the inversion in this case appears to be unable to adequately constrain the required parameters. Data from more event/ station combinations in Fennoscandia are needed in order to provide a valid L_g STA-based magnitude relation for Fennoscandia. L_g magnitude relations are anyhow of little interest with regard to magnitude estimation for events in the Barents and Kara Seas due to the strong attenuation or blocking of L_g energy observed for events in this area.

Fig. 6.2.7 shows comparisons of corrected network magnitudes as calculated from individual phases. There are still clear discrepancies between P_n and S_n magnitudes for different source areas, which seem to be the result of different ray paths. Events that predominantly have ray paths within Fennoscandia have larger S_n magnitudes (relative to P_n), while the opposite is true for events that have ray paths crossing the sediment basins of the Barents Sea (Novaya Zemlya/ Kara Sea and the western Barents Sea/Mid-Atlantic ridge areas). Table 4 lists the date, location and P_n, S_n, and overall network magnitudes with number of readings and RMS values for the 42 events in the database. Magnitudes (M_L) estimated by NORSARs GBF system (Ringdal & Kværna, 1989) and reference magnitudes (m_b) for the five Novaya Zemlya events from Ringdal and Kremenetskaya (1999) are also given.

Data from the Amderma station

The seismic station in Amderma (AMD) has a unique and important location with regard to studying seismic activity in the eastern Barents Sea/Kara Sea area (Fig. 6.2.1). Data from this station have not been generally available, but waveform data for a number of events in the Barents Sea region were collected as part of a joint project between NORSAR and the the Kola Regional Seismological Centre in Apatity. These data covered a total of 15 of the 42 events in our database, of which phase arrivals could be identified for 13 of the events. These arrivals represent an important contribution to the evaluation of the models. The epicentral distances for the majority of the events in the database are larger than for the other stations used in this study, so only nine events had onsets with SNRs large enough to be included in the inversion of the attenuation relations. Magnitudes calculated from amplitude observations at AMD using the coefficients determined by the magnitude inversion in this study appear to correlate on average quite well to the other stations, although the scatter is somewhat higher. The higher scatter is most likely an effect of the significantly different location (and thereby differences in ray paths), and also the relatively low number of good amplitude readings for this station compared to the other stations used in this study.

Conclusions

The following main conclusions can be drawn from this study of regional phases in the Barents Sea region:

The pattern of L_g arrivals and associated amplitudes support the previously published indications that the deep sediment basins and Moho topography under the Barents Sea efficiently blocks L_g wave energy from crossing.

The 'BAREY' model (Table 6.2.1) from Schweitzer and Kennett (2002), based on a model for the Barents Sea area from Kremenetskaya *et al.* (2001), provides the smallest overall travel time residuals when locating events within the vicinity of the Barents- and Kara Seas.

The attenuation in the Barents Sea region differs somewhat from that observed in other stable tectonic regions, as evidenced by the fact that the coefficients given by Jenkins *et al*. (1998) for such regions do not give consistent magnitudes across frequencies, phases and stations for our amplitude observations from the events in the Barents Sea region.

Amplitude inversion has been used in this study to resolve new coefficients and station corrections for estimating M_L magnitudes from STA amplitude observations for P_n and S_n phases in the Barents Sea region (Tables 6.2.2 and 6.2.3). The number of L_g amplitude observations for raypaths within northern Fennoscandia was too low to provide a usable magnitude relation for L_g. A future study using a greater number of continental events could most likely provide a more stable relation for STA based L_g magnitudes.

The magnitudes determined using the relation in equation (4) are self-consistent, and can be tied in to any other global, regional or local magnitude scale. The relation given in equation (4) has been adjusted in order to comply with body wave magnitudes for five events at Novaya Zemlya from Ringdal and Kremenetskaya (1999).

The seismic station in Amderma can be tied in to the regional network in Fennoscandia and on the Svalbard archipelago using an appropriate crustal model, and is able to provide important information regarding the location of events in the eastern parts of the Barents Sea and the Kara Sea (Schweitzer and Kennett, 2002). Magnitudes calculated at this station are on the whole quite consistent with the other observations.

The BAREY velocity model (Schweitzer and Kennett, 2002), and attenuation relation given in equation (4), currently provide the best possible locations and magnitudes for events in the Barents Sea region, and can be used for a Threshold Monitoring implementation for this area. When more and better quality data become available it may be possible to further improve these results, although the aseismic nature of the Barents Sea will continue to pose problems with regard to a detailed study of seismic wave propagation within the Barents Sea itself.

E.C. Hicks
T. Kværna
S. Mykkeltveit
J. Schweitzer
F. Ringdal

References

Alsaker, A., Kvamme, L.B., Hansen, R.A., Dahle, A. and Bungum, H. (1991): *The M_L scale in Norway,* Bull. Seis. Soc. Am *81,* 379-398.

Baumgardt, D.R. (2001), *Sedimentary basins and the blockage of Lg wave propagation in the continents*, Pure Appl. Geophys. *158*, 1207-1250.

Bowers, D., Marshall, P.D., and Douglas, A. (2001): *The level of deterrence provided by data from the SPITS seismometer array to possible violations of the Comprehensive Test Ban in the Novaya Zemlya region*, Geophys. Jour. Int. *146*, 425-438.

Bungum, H., and Lindholm, C. (1996), *Seismo- and neotectonics in Finnmark, Kola and the southern Barents Sea part 2: Seismological analysis and seismotectonics*, Tectonophys. *270*, 15-28.

Byrkjeland, U., Bungum, H., and Eldholm, O. (2000), *Seismotectonics of the Norwegian continental margin*, Jour. Geophys. Res. *105*, 6221-6236.

Eidvin, T., Jansen, E., and Riis, F. (1993), *Chronology of Tertiary fan deposits off the western Barents Sea: Implications for the uplift and erosion history of the Barents Shelf*, Mar. Geol. *122*, 19-131.

Fiedler, A., and Faleide, J.I. (1996), *Cenozoic sedimentation along the southwestern Barents Sea margin in relation to uplift and erosion of the shelf*, Global Planet. Change *318*, 75-93.

Faleide, J.I., Vågnes, E., and Gudlaugsson, S.T. (1993), *Late Mesozoic-Cenozoic evolution of the south-western Barents Sea in a regional rift-shear tectonic setting*, Mar. Petrol. Geol. *10*, 186-214.

Hicks, E.C., Bungum, H., and Lindholm, C.D. (2000), *Stress inversion of earthquake focal mechanism solutions from onshore and offshore Norway,* Nor. Geol. Tidsskr. *80*, 235-250.

Jackson, H.R., Faleide, J.I., and Eldholm, O. (1990), *Crustal structure of the sheared southwestern Barents Sea margin*, Mar. Geol. *93*, 119-146.

Jenkins, R.D., Sereno, T.J., and Brumbaugh, D.A. (1998), *Regional attenuation at PIDC stations and the transportability of the S/P discriminant* (AFRL-VS-HA-TR-98-0046, Science Applications International Corporation, San Diego, Ca, USA).

Kværna, T., and Ringdal, F. (1999), *Seismic threshold monitoring for continuous assessment of global detection capability,* Bull. Seis. Soc. Am. *89*, 946-959.

Kremenetskaya, E., Asming, V., and Ringdal, F. (2001). *Seismic location calibration of the European Arctic,* Pure Appl. Geophys. *158,* 117-128.

Marshall, P.D., Stewart, R.C., and Lilwall, R.C. (1989), *The seismic disturbance on 1986 August 1 near Novaya Zemlya: A source of concern?* Geophys. Jour. Int. *98*, 565-573.

Mykkeltveit, S., and Ringdal, F. (1981), *Phase identification and event location at regional distance using small-apature array data*, In *Identification of seismic sources - Earthquake or underground explosions* (eds. Husebye, E.S. and Mykkeltveit, S.), pp. 467-481.

Ringdal, F., and Kremenetskaya, E. (1999), *Observed characteristics of regional phases and implications for P/S discrimination in the Barents/Kara Sea region*, In: *NORSAR Sci. Rep. 2-98/99*, Kjeller, Norway.

Ringdal, F., and Kværna, T. (1989), *A multi-channel processing approach to real time network detection, phase association, and threshold monitoring*, Bull. Seis. Soc. Am. *79*, 1927-1940.

Ringdal, F., and Kværna, T. (1992), *Continuous seismic threshold monitoring*, Geophys. J. Int. *111*, 505-514.

Ringdal, F., Kværna, T., Kremenetskaya, E., and Asming, V. (1997), *The seismic event near Novaya Zemlya on 16 August 1997*. Semiannual Technical Summary, 1 April-30 September 1997, NORSAR Sci. Rep. 1-97/98, Kjeller, Norway.

Schweitzer, J. (2001), *HYPOSAT - An enhanced routine to locate seismic events*, Pure Appl. Geophys. 158, 277-289.

Schweitzer, J., and Kennett, B.L.N. (2002), *Location studies for the Kara Sea event 16 August 1997*, Semiannual Technical Summary, 1 July - 31 December 2001, NORSAR Sci. Rep. 2-2001/2002, Kjeller, Norway.

Sereno, T.J. (1990), *Attenuation of regional seismic phases in Fennoscandia and estimates of arrival time and azimuth uncertainty using data recorded by regional arrays*, Tech. Rep. SAIC-90/1472, Science Applications International Corp.

Zhang, T., and Lay, T. (1994), *Effects of crustal structure under the Barents and Kara seas on short-period regional wave propagation for Novaya Zemlya explosions: empirical relations*, Bull. Seis. Soc. Am. *84*, 1132-1147.

Fennoscandia			BAREY			BAREZ		
Depth (km)	**V_P**	**V_S**	**Depth (km)**	**V_P**	**V_S**	**Depth (km)**	**V_P**	**V_S**
0.0	6.20	3.58	0.0	6.20	3.58	0.0	6.20	3.58
16.0	6.20	3.58	16.0	6.20	3.58	16.0	6.20	3.58
16.0	6.70	3.87	16.0	6.70	3.87	16.0	6.70	3.87
40.0	6.70	3.87	41.0	6.70	3.87	41.0	6.70	3.87
40.0	8.15	4.705	41.0	8.10	4.58	41.0	8.10	4.71
			70.0	8.23	4.65	70.0	8.23	4.78
95.0	8.15	4.705						
95.0	8.25	4.763						
210.0	8.30	4.792	210.0	8.26	4.67	210.0	8.26	4.80

Table 6.2.1. The Fennoscandia (Mykkeltveit and Ringdal, 1981), BAREY and BAREZ (Schweitzer and Kennett, 2002) crustal models. The main differences between the models are the slightly different velocities in the uppermost mantle.

	P_n		**S_n**	
	a	**b**	**a**	**b**
JENKINS *et al.* (1998)	0.08	1.44	0.12	1.85
This study	0.36±0.02	0.88±0.09	0.41±0.02	0.63±0.11

Table 6.2.2. The inversion results for the a and b coefficients (±1σ) for P_n and S_n phases used in the attenuation relation (equations 4). The values from Jenkins et al. (1998) are shown for comparison. Note that the new coefficients have a stronger frequency dependency (higher a values).

Station	P_n	S_n
AMD	0.05±0.07	0.01±0.07
APA	0.15±0.04	-0.16±0.05
ARCES	0.13±0.04	0.03±0.04
FINES	0.13±0.05	-0.01±0.05
KBS	-0.07±0.04	-0.02±0.07
KEV	-0.09±0.04	-0.37±0.05
LVZ	0.09±0.04	-0.29±0.05
NORES	0.13±0.05	0.09±0.07
SPITS	0.05±0.04	0.12±0.09

Table 6.2.3. .Station corrections (±1σ) in magnitude units obtained as part of the inversion.

Date/time	Lat.	Lon.	P_n (M_L)			S_n (M_L)			Network (M_L)			GBF (M_L)		Ref.
			Mag.	no	RMS	Mag.	no	RMS	Mag.	no	RMS	Mag.	no	(m_b)
1988-235:16.20.00.13	*66.64*	*79.38*	*5.10*	*1*	-	-	-	-	5.1	1	-	-	-	
1990-167:12.43.26.91	68.95	34.62	3.75	2	0.30	3.98	2	0.27	3.86	4	0.31	-	-	
1990-297:14.58.06.49	72.50	54.08	5.65	1	-	5.16	1	-	5.41	2	0.25	-	-	5.6
1991-157:12.46.11.32	65.57	22.88	3.18	2	0.20	3.41	2	0.12	3.29	4	0.20	-	-	
1991-236:10.56.29.65	65.73	31.69	3.48	1	-	3.65	1	-	3.57	2	0.09	-	-	
1992-366:09.29.25.84	73.77	54.24	3.02	1	-	2.71	1	-	2.87	2	0.16	2.25	1	2.7
1993-005:10.19.34.40	64.68	17.29	3.97	4	0.26	4.16	3	0.22	4.05	7	0.26	3.61	7	
1995-013:04.34.08.58	75.95	8.90	3.45	8	0.29	3.44	3	0.07	3.45	11	0.25	-	-	
1995-021:01.58.07.21	70.43	18.39	2.99	5	0.08	3.34	4	0.18	3.14	9	0.22	2.99	10	
1995-054:21.50.00.15	71.19	54.53	2.18	2	0.16	2.34	1	-	2.23	3	0.15	-	-	
1995-063:18.29.04.36	82.25	28.71	3.65	6	0.17	3.65	5	0.21	3.65	11	0.19	3.10	1	
1995-101:20.07.23.02	80.05	35.67	3.67	5	0.18	3.83	4	0.22	3.75	9	0.22	3.25	2	
1995-102:08.18.52.49	69.26	33.38	2.35	4	0.25	2.54	1	-	2.39	5	0.24	2.04	5	
1995-133:22.38.51.04	76.89	9.54	3.54	9	0.15	3.46	4	0.11	3.51	13	0.14	3.13	3	
1995-161:18.45.34.11	75.70	33.88	2.55	3	0.10	2.56	3	0.14	2.56	6	0.12	2.01	2	
1995-162:19.27.15.07	*75.65*	*33.78*	*3.29*	*3*	*0.18*	*3.33*	*2*	*0.27*	3.31	5	0.22	*2.93*	*2*	
1995-164:19.22.38.41	75.10	56.02	3.51	4	0.22	3.53	5	0.21	3.52	9	0.21	2.74	2	3.5
1995-184:12.49.32.76	69.64	25.07	2.90	3	0.13	3.21	1	-	2.98	4	0.17	2.94	9	
1995-185:03.26.24.87	79.94	94.76	3.71	2	0.13	3.73	3	0.06	3.72	5	0.10	3.15	1	
1995-241:22.12.19.06	77.14	22.33	3.75	4	0.12	3.53	2	0.09	3.67	6	0.15	3.54	3	
1995-261:03.26.06.18	66.51	30.64	2.86	6	0.19	3.14	2	0.05	2.93	8	0.20	2.96	11	
1995-313:01.10.23.59	66.73	33.51	2.91	6	0.08	3.06	3	0.08	2.96	9	0.11	3.12	11	
1995-329:19.41.26.68	77.17	18.14	3.65	6	0.35	3.72	5	0.05	3.68	11	0.26	3.50	5	
1996-013:17.17.23.57	75.02	56.02	2.46	2	0.16	2.42	2	0.24	2.44	4	0.20	1.90	2	2.4
1996-021:02.16.32.03	69.25	24.25	3.72	7	0.30	4.00	2	0.08	3.78	9	0.29	3.86	12	
1996-218:20.04.38.23	75.58	14.63	3.13	7	0.29	3.09	4	0.07	3.12	11	0.24	2.38	3	
1996-272:06.08.47.35	69.39	32.03	1.95	3	0.21	-	-	-	1.95	3	0.21	1.60	1	
1996-301:23.55.17.21	79.88	23.54	3.45	4	0.24	2.99	1	-	3.36	5	0.28	2.62	1	
1996-361:04.44.15.67	63.24	44.62	2.98	4	0.08	3.00	3	0.16	2.99	7	0.12	2.74	4	
1997-122:07.31.17.23	72.67	20.85	2.86	6	0.24	2.68	4	0.14	2.78	10	0.22	2.15	2	
1997-228:02.11.00.36	72.48	57.67	3.42	5	0.24	3.52	2	-	3.43	7	0.23	-	-	3.5
1997-279:12.33.27.04	76.44	24.01	3.77	4	0.07	3.83	3	0.15	3.8	7	0.12	3.27	5	
1997-279:21.17.31.53	73.84	10.78	3.26	5	0.18	2.75	1	-	3.17	6	0.25	2.96	2	
1997-279:21.29.18.26	73.38	7.42	3.83	4	0.11	3.41	1	-	3.75	5	0.20	2.95	5	
1999-229:04.44.37.19	67.85	34.15	3.99	6	0.25	3.90	3	0.08	3.96	9	0.22	3.90	13	
1999-290:12.07.16.70	70.43	18.64	3.55	7	0.20	3.90	1	-	3.59	8	0.22	3.79	13	
2000-225:07.30.41.31	69.66	37.38	3.41	8	0.35	3.14	3	0.03	3.34	11	0.32	2.80	8	
2000-316:02.01.06.65	75.35	16.76	3.52	6	0.33	3.93	4	0.22	3.68	10	0.35	3.46	4	
2000-341:00.34.40.15	76.17	8.77	3.86	3	0.14	3.27	1	-	3.71	4	0.29	2.94	4	
2000-360:03.50.28.47	73.32	14.01	3.68	8	0.19	3.64	5	0.14	3.66	13	0.18	3.39	9	
2001-090:11.30.55.35	66.41	13.67	3.90	8	0.25	4.16	6	0.10	4.01	14	0.24	4.00	13	
2001-122:15.59.43.93	67.23	24.70	2.93	5	0.07	3.20	2	0.05	2.97	12	0.12	3.07	10	

Table 6.2.4. Origin time and locations for the 42 seismic events after relocation using the BAREY model. Magnitudes (M_L) were calculated using the attenuation parameters determined through inversion, using amplitude observations in the 3-6 Hz frequency band. Mean magnitudes, no. of observations and RMS of residuals are listed for P_n and S_n phases, and also network magnitudes, which are the mean of all reported station magnitudes (P_n and S_n) for each event. Automatic network magnitudes (M_L) from NORSARs GBF system (Ringdal & Kværna, 1989) and the reference magnitudes (m_b) used to calibrate the magnitude scale (Ringdal & Kremenetskaya, 1999) are also shown. The two events marked in italic (1988-235 and 1995-162) could not be used as input to the inversion determining the attenuation relation for P_n and S_n.

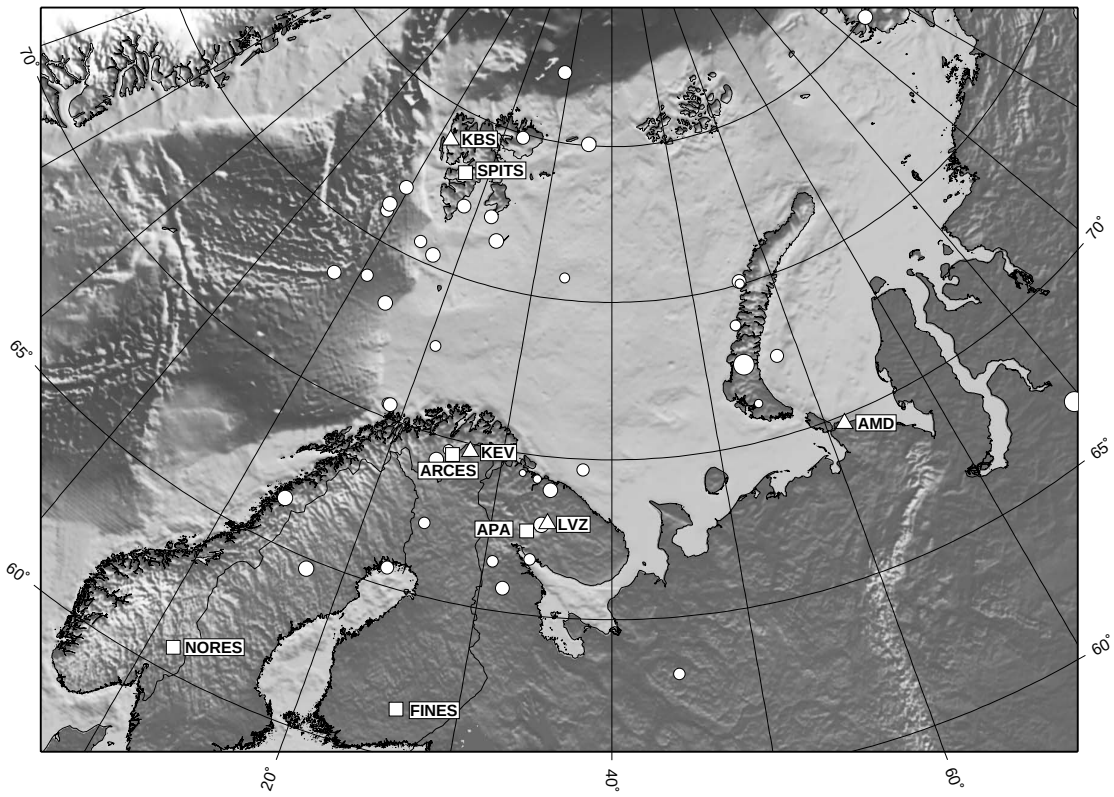

Fig. 6.2.1. Events (circles) and seismic stations used for deriving wave propagations characteristics of the Barents Sea and surrounding areas. Array stations are shown as squares, while 3C stations are shown as triangles. The event locations shown are after analysis and relocation using the BAREY model (Schweitzer and Kennett, 2002). The symbol size for the events are proportional to the network magnitudes in Table 6.2.3.

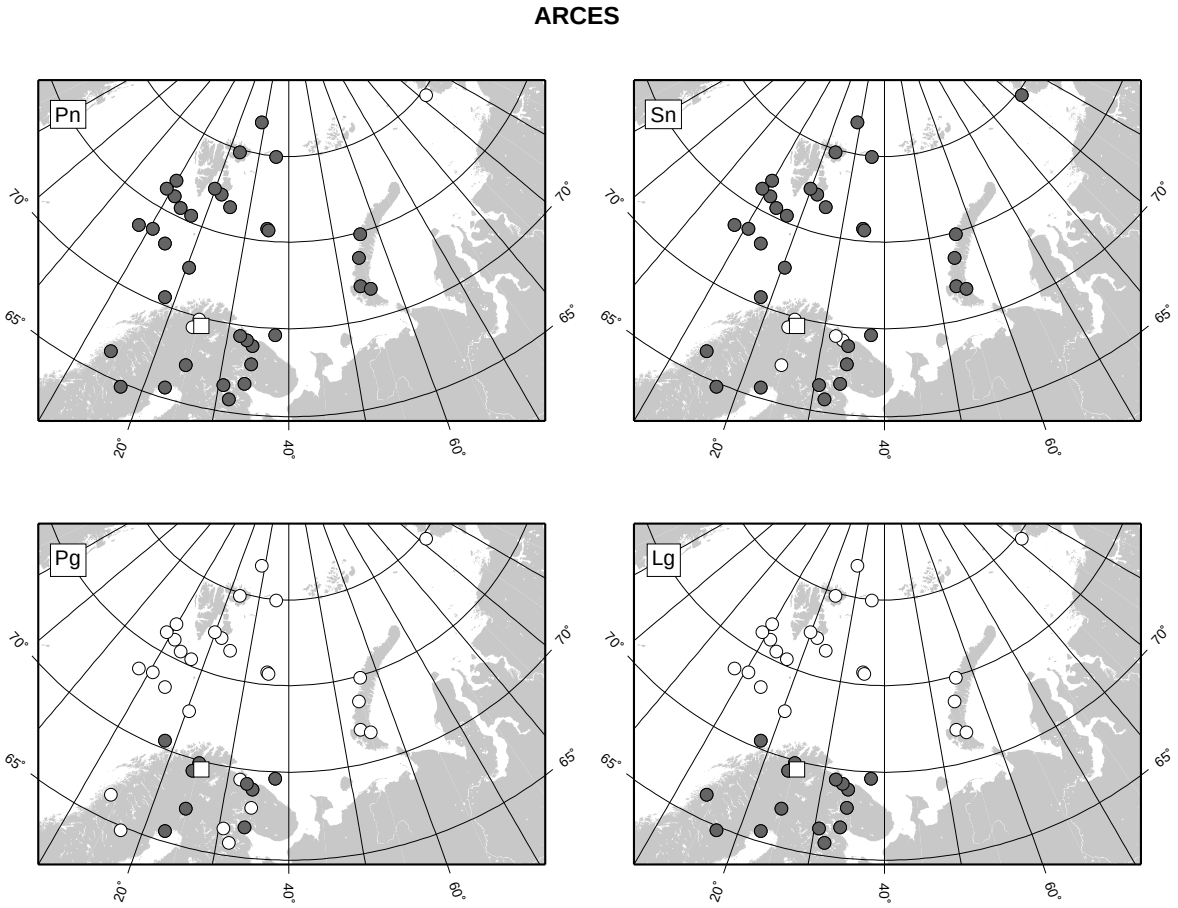

Fig. 6.2.2. Phase observations (dark circles) for P_n (upper left), P_g (lower left), S_n (upper right) and L_g (lower right) by the ARCES array (white square). The white circles represent events where the phase in question is not observed, but at least one other phase is observable.

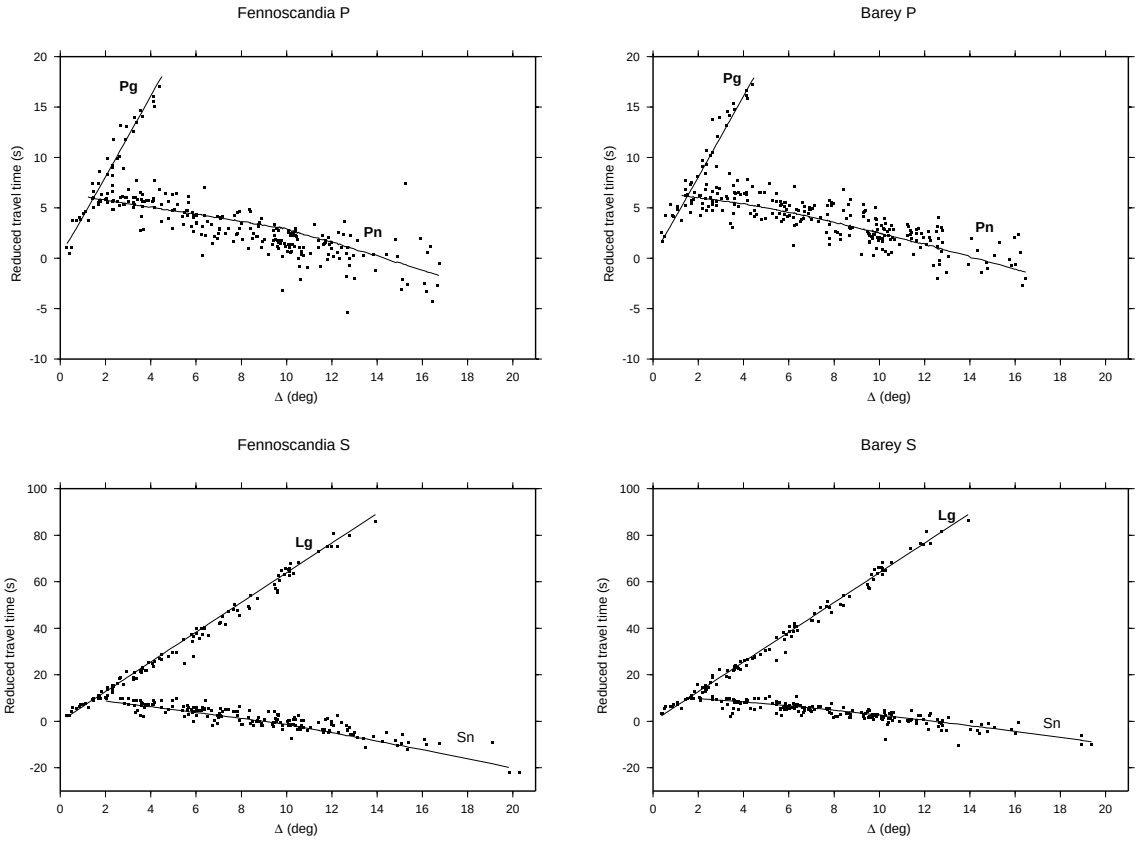

Fig. 6.2.3. Mykkeltveit and Ringdal (1981) and BAREY (right) (Schweitzer and Kennett, 2002) models. For the Fennoscandia model, P_n and L_g arrivals have mostly negative residuals while the S_n arrivals have positive residuals. The observations are distributed in a fairly symmetrical manner, and residuals are smaller (particularly for S phases) when the BAREY model is used. The travel times are reduced using 8.0 km/s for P and 4.5 km/s for S. Note that the vertical scales are different for the P and S plots.

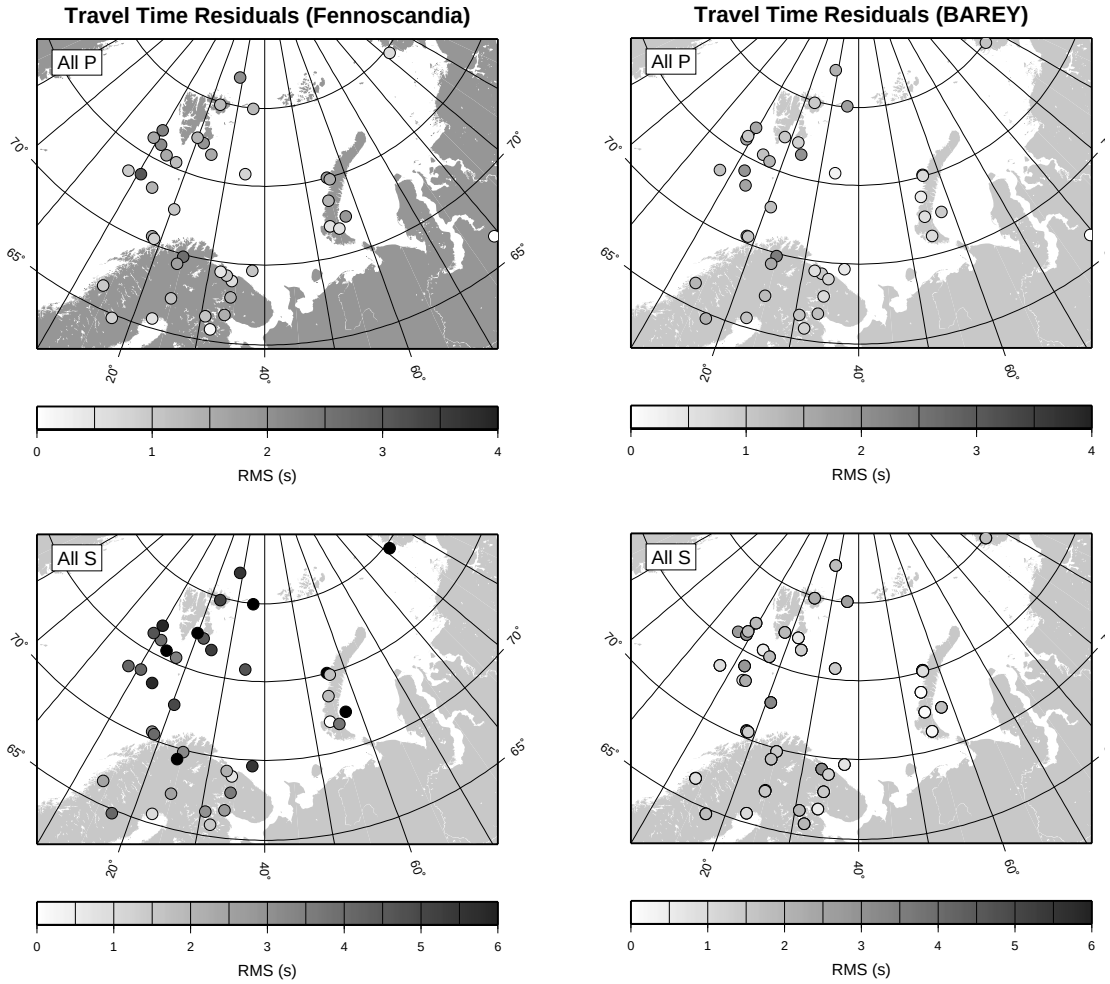

Fig. 6.2.4. RMS of travel time residuals for P (top) and S (bottom) phases for individual events located using the Fennoscandia (left) and BAREY (right) models, darker symbols indicate higher residuals. Events with larger residuals than 4.0 (P phases) or 6.0 (S phases) seconds are black.The residuals are generally smaller for locations using the BAREY model, in particular for the S phases.

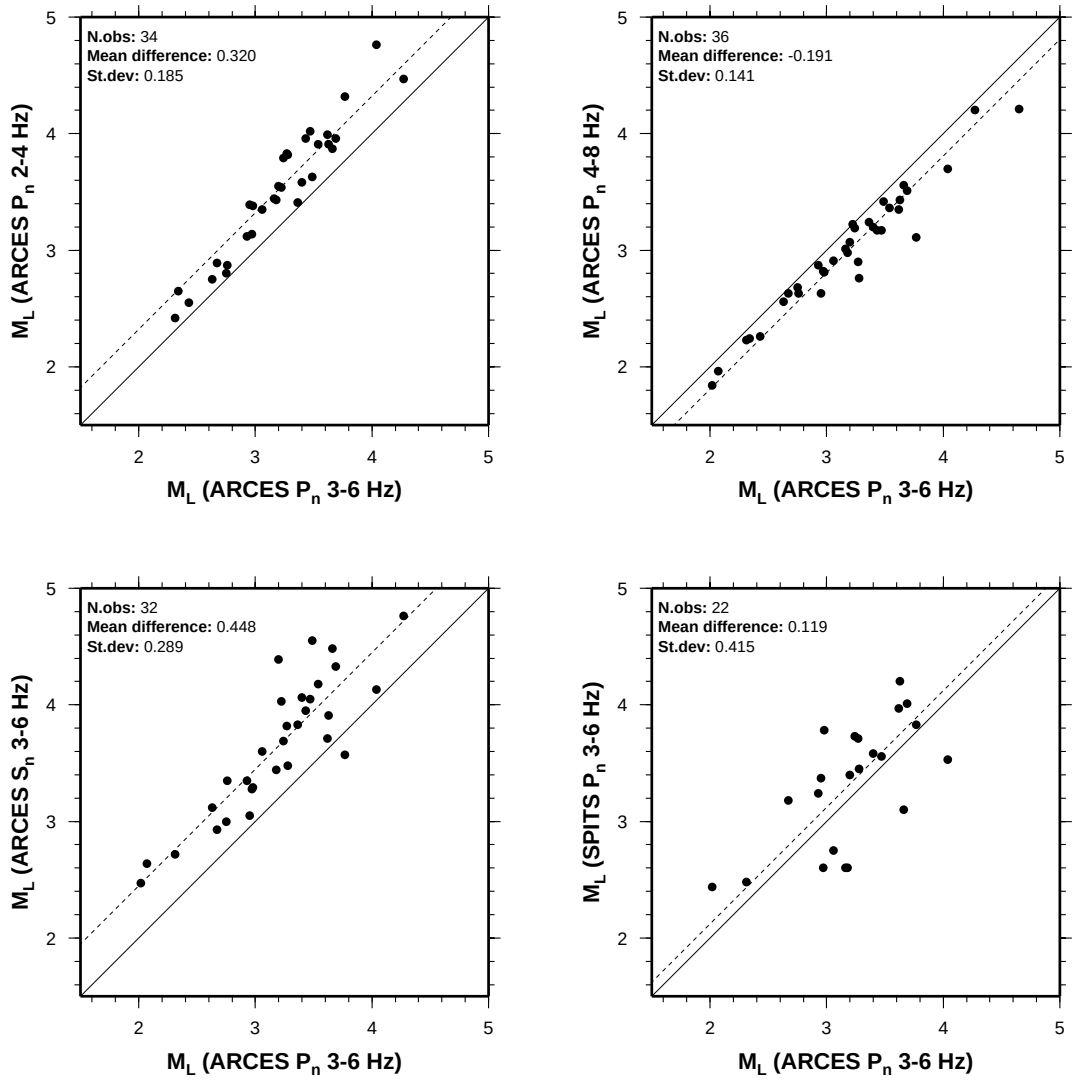

Fig. 6.2.5. Magnitudes calculated using the attenuation relation of Jenkins et al. (1998). Top: Comparison between different frequency bands at ARCES. Note the systematic trend towards lower magnitudes with increasing frequency. Lower left: Comparison between magnitudes calculated for P_n and S_n phases in the 3-6 Hz band at ARCES. The systematic offset is almost 0.5 magnitude units. Lower right: Comparison between P_n magnitudes in the 3-6 Hz band at ARCES and SPITS. The scatter (σ = 0.423) is quite large, with differences of up to a full magnitude unit for some events.

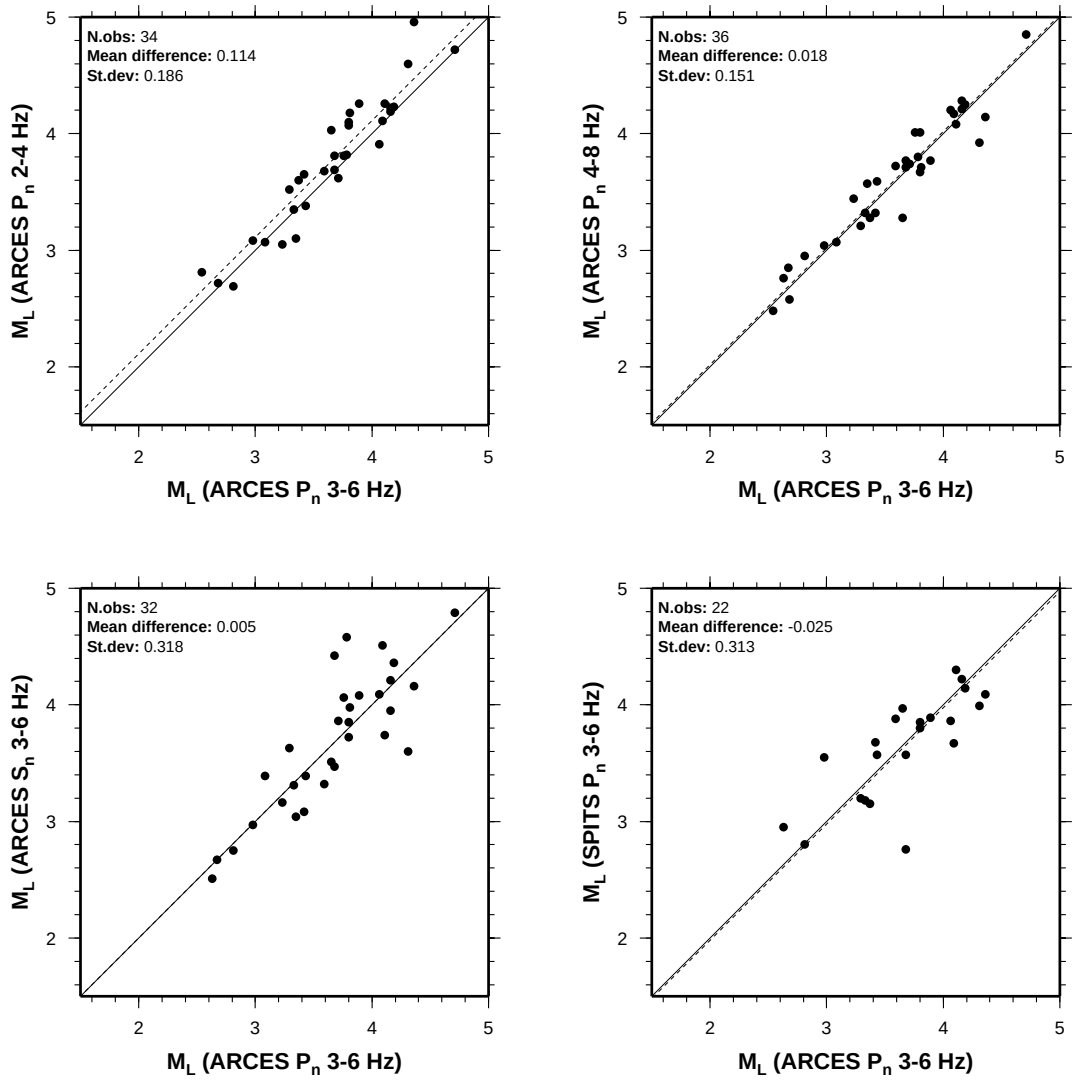

Fig. 6.2.6. Magnitudes calculated using the attenuation coefficients and station corrections from the inversion. Top: Comparison between different frequency bands at ARCES. The systematic frequency dependency as visible in Fig. 6.2.5 is significantly reduced. Lower left: Comparison between magnitudes calculated for P_n and S_n phases in the 3-6 Hz frequency band at ARCES. There is no obvious systematic offset, although the scatter is marginally increased compared to Fig. 6.2.5. Lower right: Comparison between P_n magnitudes in the 3-6 Hz frequency band at ARCES and SPITS. The average offset and scatter is reduced compared to Fig. 6.2.5.

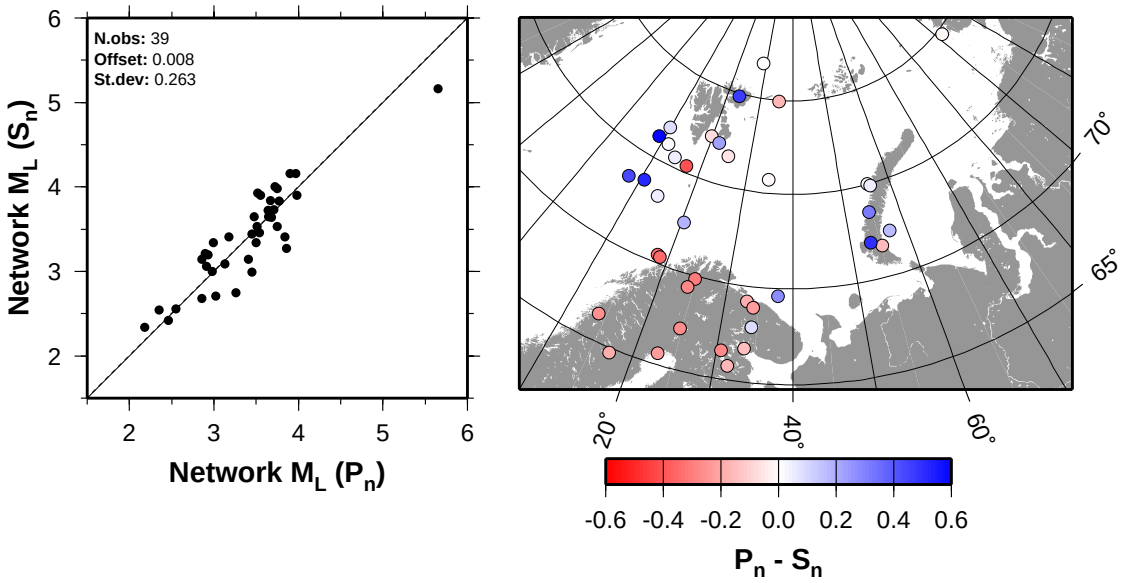

Fig. 6.2.7. Network event magnitude comparisons and maps of the geographical distribution of the magnitude differences for P_n vs. S_n. Note that S_n magnitudes are overestimated compared to P_n for events that have paths predominantly within the Baltic shield, while events with paths that cross the Barents Sea have larger P_n magnitudes compared to S_n.

6.3 Site-Specific Threshold Monitoring (SSTM) applied to the Lop Nor test site

Introduction

Continuous seismic threshold monitoring (TM) is a technique that has been developed at NORSAR over the past decade to monitor a geographical area continuously in time. Data from a network of arrays and single stations are combined and "steered" toward a specific area to provide a continuos assessment of the upper magnitude limit of seismic events that might have occurred in that area.The basic principles have been described by Ringdal and Kværna (1989, 1992), who showed that this method could be useful as a supplement to event detection analysis. The usefulness of the TM method for global network capability estimation has been shown by Kværna and Ringdal (1999). Examples of site-specific threshold monitoring (SSTM) applied to the former Soviet test site at Novaya Zemlya, and the Indian and Pakistani test areas have been demonstrated by Kværna et al. (2002a,b). We have also recently reported an application of this technique to the site of the "Kursk" accident in the Barents Sea.

The main purpose of the threshold monitoring technique is to highlight instances when a given threshold magnitude is exceeded, thereby helping the analyst to focus on those events truly of interest in a monitoring situation.The analyst can then apply traditional tools in detecting, locating and identifying the source of the disturbance.

In this paper we apply the SSTM technique to the Lop Nor test site in China. The emphasis will be put on detection (and location) of small seismic events with mb < 4.0, and the purpose is to evaluate the SSTM method as a potential monitoring tool. In contrast to most previous case studies, which have been based on recordings by seismic arrays at regional distances, we will in this study apply a combination of 3-component stations and arrays, at both regional and teleseismic ranges.

Our efforts so far, as reported in this contribution, comprises mainly a study of available seismic stations, selection of those stations which are most sensitive to seismic events in the Lop Nor general area, and tuning of the signal parameters of these stations so as to prepare processing recipes for the application of the threshold monitoring tool.

Development of processing recipes

For the successful implementation of SSTM, beams filtered in optimal frequency bands must be steered from the individual arrays towards the Lop Nor test site, and amplitude calibration constants developed from older events are applied to facilitate the calculation of continuous magnitude thresholds for the site. For single (or 3-component) stations, the vertical component was filtered in the optimal frequency band.

For the purposes of this study, 23 stations and arrays were initially chosen as shown in Fig. 6.3.1. For each of the stations data were collected from known nuclear tests at Lop Nor. The explosions used for the calibration is summarized in Table 6.3.1, however, for most stations only a few data sets with explosions were available for the calibration.

Event	Event	Event	Event
1990-146 M=5.5	1993-278 M=5.9	1995-135 M=6.0	1996-211 M=4.7
1992-142 M=6.5	1994-161 M=5.8	1995-229 M=5.9	
1992-269 M=5.0	1994-280 M=5.9	1996-160 M=5.8	

Table 6.3.1. Lop Nor nuclear test explosions used for the station calibration purpose (year, Julian day and magnitude of the explosion).

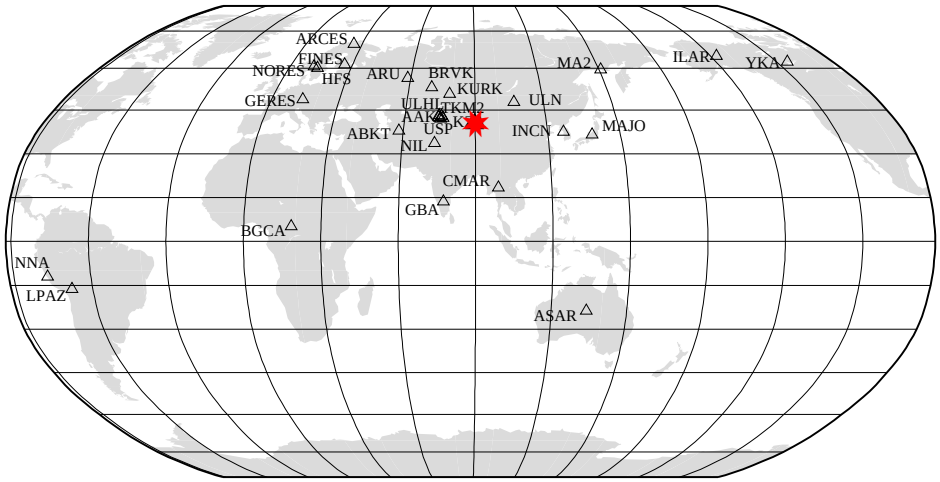

Fig. 6.3.1. Stations selected for SSTM calibration for the Lop Nor site (indicated with red star).

The calibration procedure

The development of the calibration parameters followed a 3-step procedure for the arrays listed in Table 6.3.2:

- Firstly the average azimuth and apparent velocity was obtained for the arrays. Generally, a higher power in the FK domain indicated also appropriate frequency bands.
- Through beamforming, the STA trace aimed at Lop Nor was computed for different frequency bands, and the optimal frequency band was defined based on maximum SNR.
- For the optimal beamforming parameters, the maximum corrected STA amplitude for the phase was computed and the corresponding magnitude corrections were computed.

The process is exemplified in Fig. 6.3.2, and shows the distribution of FK power with azimuth and apparent velocity in different frequency bands for the array CMAR. The final parameters extracted (and later applied in the beamsteering) from the data are apparent velocity and azimuth (for arrays), optimal frequency filtering band, phase travel time, phase amplitude and tolerance bands for these parameters. Table 6.3.2 summarizes some of the parameters obtained for the different stations and arrays.

Station	No. of records	Delta	P-travel-time	Calib. constant	Calib. St. deviation	Optimal Frequency Band	
AAK	7	10.48	155.6	3.32607	0.122042	1.5	4.0
ABKT	7	23.58	317.9	3.20032	0.131820	0.5	2.0
ARCES	7	42.47	478.2	3.80806	0.065702	2.0	6.0
ARU	6	24.43	322.8	3.27962	0.210574	0.5	2.0
ASAR	6	77.16	719.2	4.23516	0.209677	1.5	4.0
BGCA	1	71.7	687.2	2.24374	-	1.0	4.0
BRVK	4	16.87	239.6	3.35027	0.112567	1.0	4.0
CMAR	5	24.64	326.8	3.62734	0.298740	2.0	4.0
FINES	6	41.75	472.4	4.02934	0.208297	1.0	4.0
GBA	7	29.60	371.6	4.25127	0.178033	1.0	4.0
GERES	10	51.41	548.6	4.42041	0.241027	2.0	4.0
HFS	3	47.93	521.0	3.35685	0.063838	1.0	4.0
ILAR	8	65.57	645.9	3.69785	0.112615	0.5	2.0
INCN	1	29.5	307.7	1.80385	-	2.0	4.0
KURK	1	11.47	165.7	3.19758	-	1.0	4.0
KZA	2	9.92	149.8	1.92404	0.102790	2.0	4.0
LPAZ	5	147.8	1190.8	2.83462	0.050651	1.5	4.0
MA2	3	41.7	467.9	2.45095	0.991537	1.5	4.0
MAJO	2	38.50	443.3	2.37779	0.058921	2.0	4.0
NIL	4	14.38	209.0	2.42098	0.067611	1.0	4.0
NNA	6	147.9	1189.8	3.70520	0.108466	0.5	2.0
NORES	9	48.84	528.5	3.50340	0.245675	1.0	4.0
TKM2	1	9.68	146.0	1.96420	-	0.5	2.0
ULHL	2	9.18	139.8	1.87506	0.082691	1.0	4.0
ULN	1	14.64	216.4	1.60884	-	0.5	2.0
USP	3	10.51	156.6	2.44410	0.189674	1.0	4.0
YKA	1	74.6	702.4	4.77741	-	2.0	6.0

Table 6.3.2. The stations calibrated for the ACD Lop Nor experiment with main calibration values. For the shaded stations calibration parameters were developed, but these have not yet been implemented.

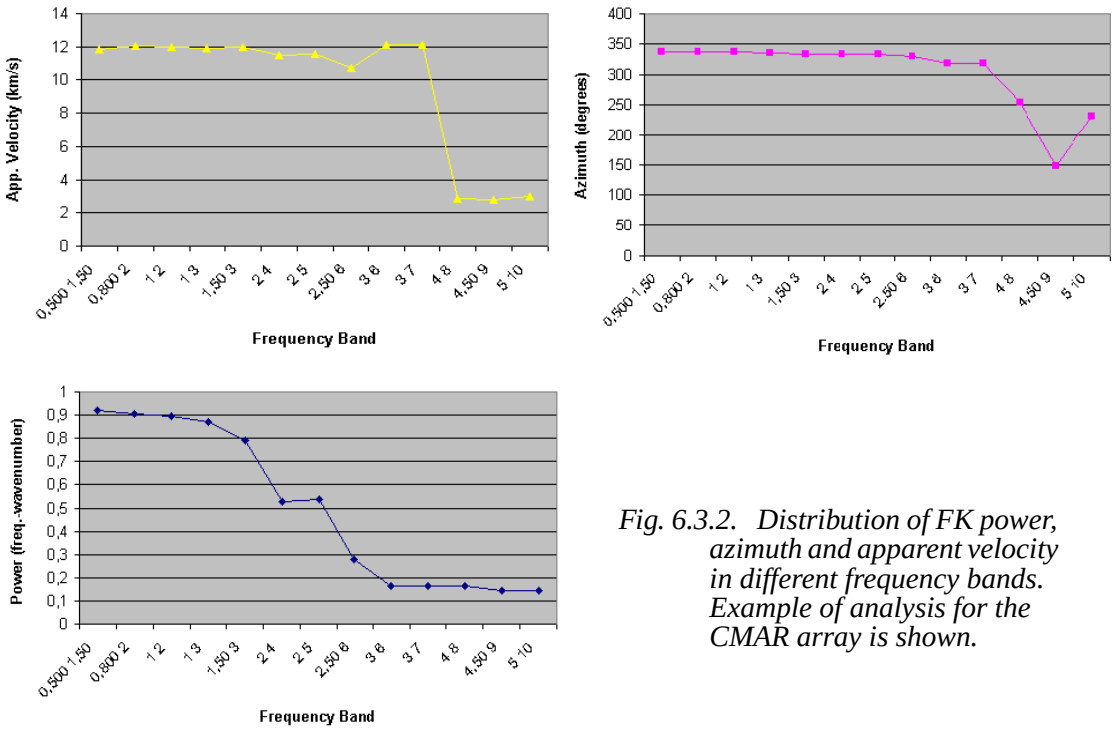

Fig. 6.3.2. Distribution of FK power, azimuth and apparent velocity in different frequency bands. Example of analysis for the CMAR array is shown.

Preliminary Results

Two performance tests were carried out. First, data for one day (September 10, 2001) was collected, and in these data the recordings of 4 explosions were scaled and embedded at some (but not all of) the stations (see Table 6.3.3). Secondly, a 10 day test period with data from August 2 through 11, 2001 was selected and data were collected for the stations. Fig. 6.3.3 shows examples of network results of these two performance tests.

Event	Time used	Scaling magn.	Stations *without* embedded, scaled data
1995/05/15	09/10/2001 05:01:19	mb 3.0	
1995/05/15	09/10/2001 09:15:13	mb 3.5	
1996/07/29	09/10/2001 06:37:43	mb 3.5	ULN, KURK
1996/07/29	09/10/2001 12:17:14	mb 3.0	ULN, KURK
1999/01/27	09/10/2001 13:25:08	mb 3.5	FINES, GERES, HFS, NORES, ULHL
1999/01/30	09/10/2001 14:23:03	mb 3.5	FINES, GERES, HFS, NORES, ULHL
1999/01/27	09/10/2001 16:59:57	mb 3.0	FINES, GERES, HFS, NORES, ULHL
1999/01/30	09/10/2001 20:59:58	mb 3.0	FINES, GERES, HFS, NORES, ULHL

Table 6.3.3. The four events/explosions scaled and embedded as eight events in the data for day 253 as shown in Figs. 6.3.3-6.3.6.

Figs. 6.3.4 and 6.3.5 shows the SSTM threshold traces for single stations and arrays respectively. In both figures, the data cover the one day (10 September 2001) which contained the scaled, embedded events, and the combined network trace (using all stations) is shown on top of each figure. It can be observed that the arrays generally have thresholds between magnitude 3.2 and 3.8, and that the network threshold is close to or better than 3.0 (based on both arrays and single stations). Some stations feature frequent data problems.

Fig. 6.3.6 shows a close-up figure of the detection parameters at ARCES for an hour where there is also an embedded event (13:25). It should be observed that the slowness and azimuth observed from the event are within the bands that are indicative for an event from the Lop Nor area (yellow shaded area).

From these tests the following preliminary observations can be stated:

- Out of the eight embedded explosions on day 253 six were flagged, and the two non-flagged could be clearly seen in the data.
- The quiet day (214) did not have any events flagged.
- On day 217 the SSTM method triggered on two large teleseismic events.
- In a monitoring situation, all peaks exceeding the threshold could be analyzed. The maximum number of such peaks during one day was 10-15 for the days processed. If such peaks were analyzed, all of the scaled events on day 2001-253 would have been found.

The above observations should be evaluated under the perspective that the calibration is a preliminary one, where the majority of the stations could only be calibrated with one or two events/explosions, and where only some of the calibrated stations were included in the performance test. Furthermore, the day with embedded events did not include embedded data for all the stations (see Table 6.3.3), and this did introduce a bias in the threshold monitoring results.

Conclusions

From the above we conclude that the Site-Specific Threshold Monitoring performance tests for the Lop Nor test site were successful. It is expected that these initial tests will be followed by more detailed studies, where in particular the calibration parameters will be more firmly established.

Conrad Lindholm
Tormod Kværna
Johannes Schweitzer

References:

Kværna, T. and F. Ringdal (1999). Seismic threshold monitoring for continuous assessment of global detection capability, Bull. Seism. Soc. Am., 89, No. 4, 946-959.

Kværna, T., F. Ringdal, J. Schweitzer and L Taylor (2002a). Optimized Seismic Threshold Monitoring - Part 1: Regional Processing, Pageoph, in Press.

Kværna, T., F. Ringdal, J. Schweitzer and L Taylor (2002b). Optimized Seismic Threshold Monitoring - Part 2: Teleseismic Processing, Pageoph, in Press.

Ringdal, F. and T. Kværna (1989). A multichannel processing approach to real time network detection, phase association and threshold monitoring, Bull. Seism. Soc. Am., 79, 1927-1940.

Ringdal, F. and T. Kværna (1992). Continuous seismic threshold monitoring, Geophys. J. Int., 111, 505-514.

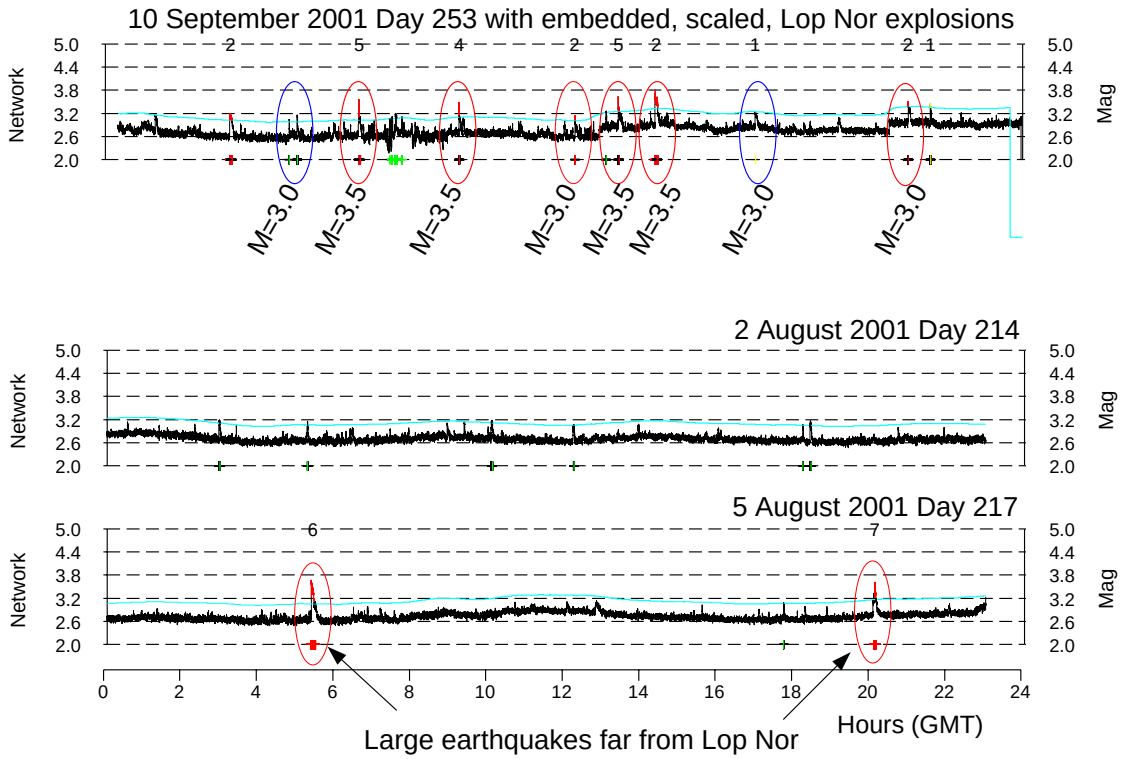

Fig. 6.3.3. The network traces from three different days. Upper trace from day 253 with embedded Lop Nor event recordings scaled to magnitudes 3.0 and 3.5. Red circles indicate that the SSTM analysis picked the events, while blue circles indicate that the events were not picked. Lower traces are from days 214 and 217. Day 214 is silent with no detections, while 217 show two detections from large earthquakes (teleseismic events far from Lop Nor).

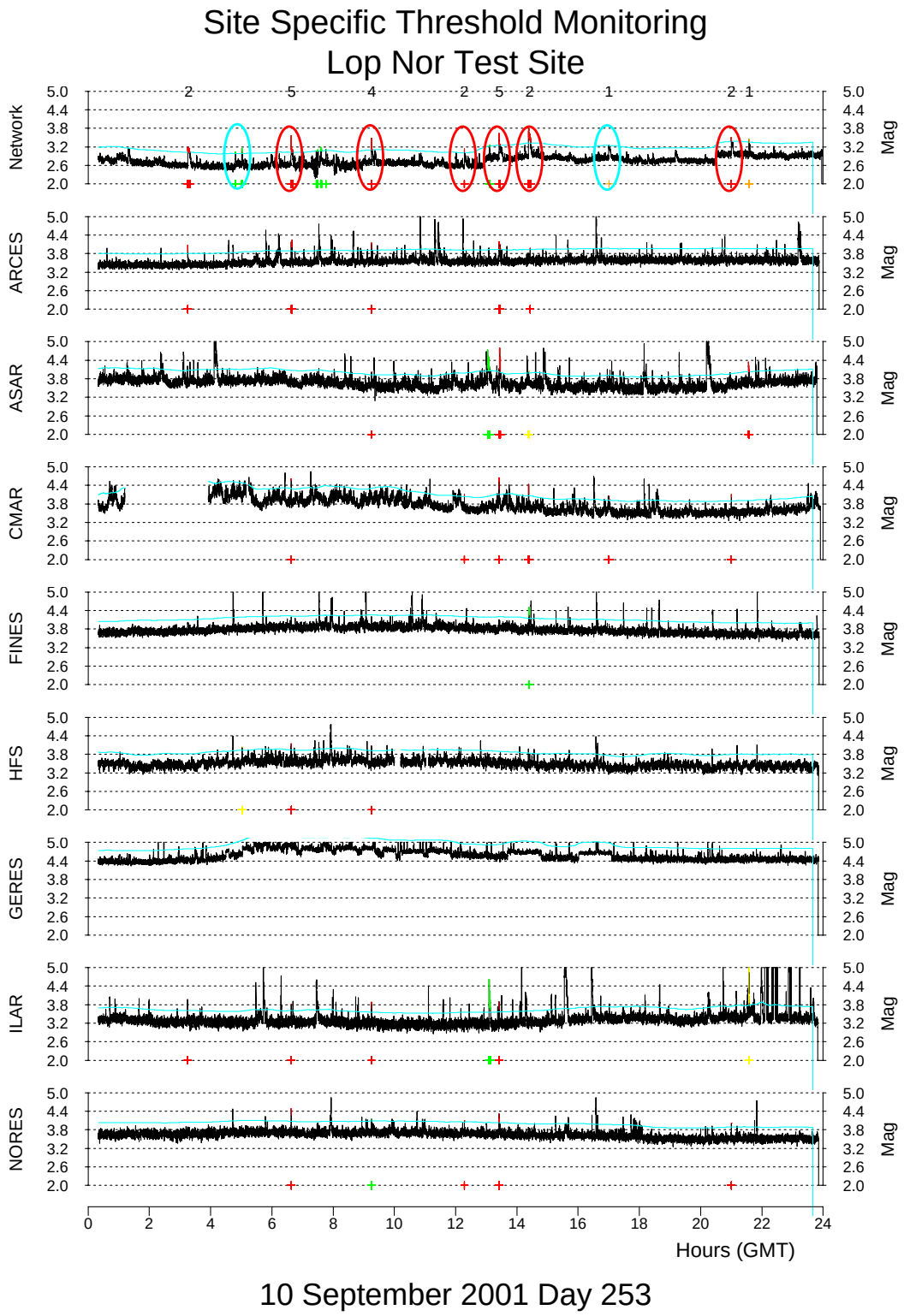

Fig. 6.3.4. Network and array TM traces for one day with embedded, scaled, events. Red circles indicate that the explosions were picked by SSTM, blue circles indicate that they were not picked.

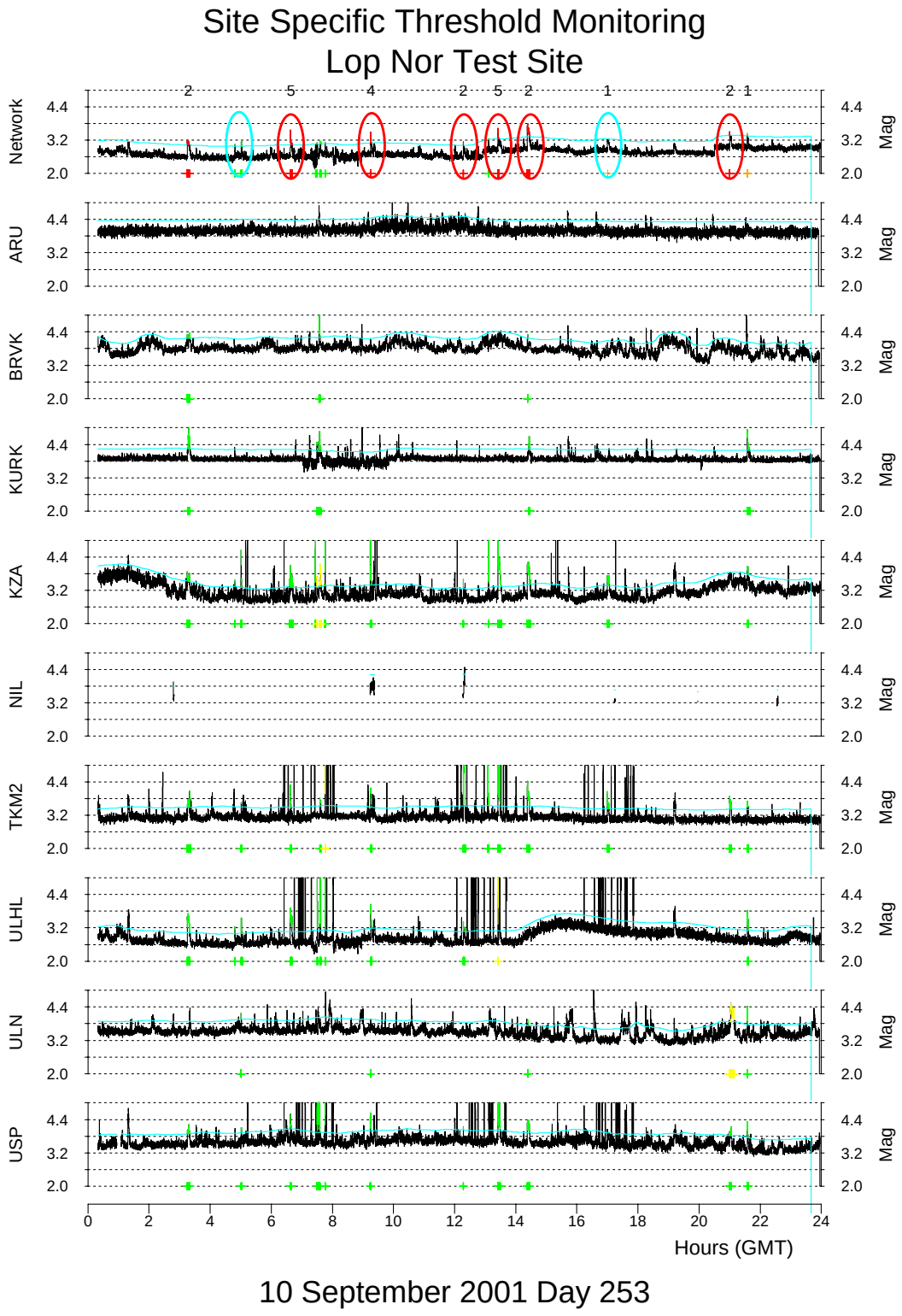

Fig. 6.3.5. Network and single station TM traces for one day with embedded, scaled, events. Red circles indicate that the explosions were picked by SSTM, blue circles indicate that they were not picked.

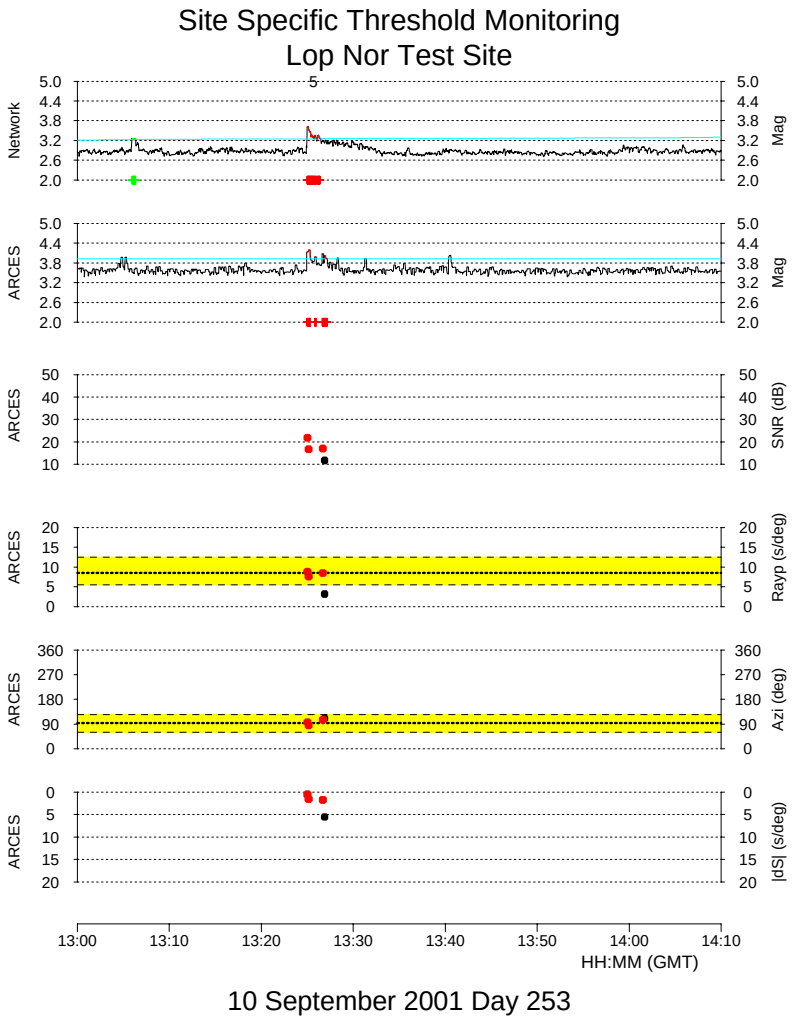

Fig. 6.3.6. Network and ARCES TM traces for one day and one hour with one embedded, scaled, event. The lower traces provide additional information for the ARCES station. The yellow shaded areas indicate the azimuth and slowness bands expected from a Lop Nor event.

6.4 Monitoring the seismicity of the Spitsbergen Archipelago

6.4.1 Introduction

The work described in this paper is a part of the KRSC - NORSAR cooperative activity aimed at a detailed study of seismicity in the Spitsbergen region. Part of the motivation for the study is to improve the quality and availability of well-located reference events ("ground truth data") for location calibration purposes, and to develop local velocity models for improved location accuracy.

Spitsbergen and the adjacent areas are parts of a geologically complex region with moderate to high seismicity. The main seismicity in the area is associated with the North-Atlantic Ridge, and especially the Knipovich Ridge situated at a distance less than 400 km from the archipelago (Sundvor and Eldholm, 1979, Mitchell et. al., 1990). In addition, some coal mines are located in the area of Spitsbergen, causing occasional induced seismicity. In this study we describe some of our observation of unusual features of seismic events and wave propagation in the area and our preliminary attempts to develop local travel time models.

6.4.2 Station Network and Geology

The Spitsbergen (Svalbard) Archipelago is characterized by a very complicated geological structure. The simplified map in Fig. 6.4.1 shows the delineation of the four major geologic units:

- local Tertiary basin sediments;

- Carboniferous through Cretaceous platform cover sequence;

- Devonian basin sediments;

- metamorphic basement rocks;

The complexity of geological structure and underwater topography causes difficulties in location and interpretation of seismic events. We will return to some illustrations of this problem later.

Local seismicity has been observed in Spitsbergen for a considerable time by a seismic network comprising digital and analog seismic stations (see Fig. 6.4.1). The analog stations BRB and PYR were operational from about 1976 to 1990, and were then closed down. Recently, a digital station has been reinstalled at the BRB location. The station KBS operated as an analog station until the 1980s, and is now a digital broad-band station. The array SPI is part of the International Monitoring System, and has been in operation since 1992.

Maps of seismic events in and near Spitsbergen for the period 1964 - 2001 are shown in Fig. 6.4.2. The locations for years 1964-1998 are taken from ISC bulletins whereas those for 1998-2001 are taken from NORSAR Reviewed Regional Seismic Bulletin. Even though the NORSAR regional bulletin covers a much shorter time interval than the ISC bulletin, the observed seismicity patterns in the two plots are remarkably similar. In particular, a segment of the mid-atlantic ridge to the west can be observed, and pronounced seismic zones in Nordaustlandet (northeast) and Heerland (southeast) can also be identified on both maps.

The temporary seismic network shown in Fig. 6.4.1 was installed in Spitsbergen in 1979 (Bungum et. al, 1982) and operated during that year. A map of seismic events detected and located by this network is shown in Fig. 6.4.3.

6.4.3 Travel time model

In 2001 a digital seismic station GBV 316B was installed in Barentsburg (Kremenetskaya et. al, 2001b). A large number of mining rockbursts and explosions have been recorded (distances 2-5 km from the station). Based on these events we have estimated P and S velocities in the upper layer and obtained values of 4.54 and 2.52 km/sec, respectively. Such values are usual for sediments.

We used the calibration event 28.01.2001 with known coordinates (78.066 N, 14.324 E) to extend the model to larger distances. This event, which has been described by Kremenetskaya et. al (2001b), was well-recorded by the SPI and KBS stations (Fig 6.4.4).

We tried to modify the BARENTS travel time model adding a layer of sediments with the velocities mentioned above and fitting the depth of this sedimentary layer as well as the Moho depth. As a preliminary result, which seems to provide the best fit to the data, we obtained the following:

Table 6.4.1. Velocity model SPITS0

Depth (km)	Vp (km/s)	Vs (km/s)
0-2	4.54	2.52
2-10	6.20	3.44
10-30	6.70	3.72
30-55	8.10	4.50
55-210	8.23	4.57
>210	Same as IASPEI 91	

This model is similar, although not identical to the model presented in Kremenetskaya et. al. (2001a). We re-located the event using the BARENTS model and the SPITS0 model. The results are shown in Table 6.4.2, and demonstrate that the location error decreases from 16 km using the Barents model to less than 1 km using the SPITS0 model. While this kind of performance cannot be expected on a general basis, it is nevertheless encouraging.

Table 6.4.2. Re-locating the calibration event 28.01.2001

Model	Latitude	Longitude	Error (km)
Ground Truth	78.066	14.324	0.0
SPITS0	78.072	14.317	0.7
BARENTS	77.93	14.045	16

6.4.4 Earthquakes in Heer Land

The Norwegian Government has recently approved the operation of a new coal mine in the Svea area close to the Heerland seismic zone. In a report to the Norwegian Parliament (JD Report No. 9 (1999-2000)) it was stated that “rockfalls” occurred several times in the Svea mine during experimental operation in 1997-1998. To clarify the situation regarding local seismicity we relocated a set of seismic events that occurred in this area using the travel time model mentioned above. The results are shown in Fig. 6.4.5 and Table 6.4.3.

Table 6.4.3. List of relocated Heer Land earthquakes

Number	DATE	TIME	Latitude	Longitude	ML
1	1997/04/28	06.09:48	77.7	17.1	1.8
2	1997/05/29	06.42:41	77.7	17.8	2.0
3	1998/02/03	05.40:33	77.8	17.6	1.5
4	1998/05/17	19.55:57	77.8	17.6	1.5
5	1998/09/10	21.57:37	77.8	18.1	1.8
6	1998/10/13	11.10:45	77.8	18.0	1.8
7	1998/11/11	07.37:37	77.8	17.9	1.8
8	1998/11/26	05.50:42	77.9	17.9	3.0
9	1998/11/26	14.12:36	77.7	17.7	1.9
10	2001/07/31	11.59:20	77.8	17.1	2.1
11	2002/01/20	08.53:21	77.9	16.9	1.6

Although the location errors here could amount to several kilometers (see below) it is possible to see that most of the earthquakes occurred in a compact zone. To contour this zone more exactly it would be desirable to install a set of additional seismic stations. This would also be useful in recording possible rockbursts associated with future mining operations.

6.4.5 Limits of the model application and possible sources of location errors

There are some indirect arguments in favor of the SPITS0 model in regions of Svalbard covered by sediments. Thus, some geologists estimate the thickness of sediments to be up to 2 km. In addition, the estimates of apparent velocities computed by sensors of the SPI array for very close events (2-5 km from the array) are in the range 4.4 - 5.2 km/sec which is more or less in agreement with the model.

It is clear that in a place with such complicated geological structure as Svalbard one should be very careful when using 1-D models. Thus, it is impossible to use the 1-D model SPITS0 to locate Svalbard events with more distant stations like ARCESS. An example is shown in Fig. 6.4.6.

One more striking example of location problems is the earthquake which occurred on 29.12.2001 at 14.24 GMT in Nordaustlandet. It was recorded by KBS and SPI, and the recordings are shown in Fig. 6.4.7.

Multiple onsets of P waves are clearly seen, especially for the KBS recording, where one can identify up to 4 different P onsets. In contrast to typical Pn and Pg onsets, say, for Khibiny explosions recorded at ARCESS, the amplitudes of the P onsets for this event are very different.

To explain such features, careful modelling, probably 3-dimensional, is required. We might expect that if the P wave has several onsets, then the S wave should have the same, too. But we have not been able to find them in the waveforms. The reason might be that first S onsets are masked by the coda of the P waves. It means that the error of estimation of time difference between P and S onsets could amount to as much as 5-10 seconds or more. And, therefore, the location error by a single station could amount to many tens of kilometers.

The result of locating this event is shown in Fig. 6.4.8. Lines of location do not cross at the same point. The backazimuth calculated by the SPI array using beamforming is significantly different from that corresponding to the estimated location.

For weaker events these first weak onsets of P waves might be unnoticeable, which of course could influence the location accuracy.

After having looked through recordings for events in typical seismic regions of the Svalbard Archipelago, we have found that such weak first P onsets are typical for almost all areas, except some events occurring in the ridge zone to the West of Svalbard.

6.4.6 Anomalies in P/S ratios

The complex geological conditions in the Svalbard area manifest themselves in extremely high variability of P/S ratios. We have noticed this in particular for events occurring in the ridge zone and around Bear Island.

Thus, for example, KBS recordings of two earthquakes occurring very closely to each other are shown in Fig. 6.4.9. (3.12.2001 at 1.45:49 GMT, 78.33 N, 8.24 E and 3.01.2002 at 22.50:40 GMT, 78.4 N, 7.6 E). The P/S ratios for these two events differ by about a full order of magnitude, even though the events are very close together and of similar magnitudes.

6.4.7 Conclusions

1. A preliminary 1-dimensional travel time model has been developed for Spitsbergen.
2. Taking into account the very complicated geology and underwater topography in and near Spitsbergen, it is necessary to use a 3-dimensional model or some kind of regionalization for improving locations;
3. Multiple onsets of P and probably S waves can strongly increase location errors. Such onsets are not uncommon for Spitsbergen earthquakes;
4. The complexity of the geology manifests itself also in a great variability of P/S ratios of earthquakes in the Spitsbergen region. Study of this variability could help to “calibrate”

the P/S ratio as a discriminant between earthquakes and explosions or find conditions under which such discriminants fail;

5. Study of all the unusual phenomena mentioned above would require the development of more advanced techniques for analysis of seismic events.

E. Kremenetskaya
S. Baranov
V.E. Asming
F. Ringdal

References

Asming, V.E., E.O. Kremenetskaya & F. Ringdal (1998): Monitoring seismic events in the Barents/Kara Sea region, *Semiannual Technical Summary, 1 October 1997 - 31 March 1998*, NORSAR Sci. Rep. 2-97/98, Norway.

Bungum, H, B.J. Mitchell and Y. Kristoffersen (1982): Concentrated earthquake zones in Svalbard, Tectonophysics, 82, 175-188.

Kremenetskaya, E., V. E. Asming and F. Ringdal (2001a): Seismic location calibration of the European Arctic. *Pure and Applied Geophysics*, 158 No. 1-2, 117-128

Kremenetskaya E., S. Baranov, Y. Filatov, V. Asming and F. Ringdal (2001b): Study of seismic activity near Barentsburg mines (Spitsbergen). In: Semiannual Tech. Summ., 1 October 2000 - 31 March 2001, NORSAR Sci. Rep. 2-2000/2001, Kjeller, Norway.

Stortingsmelding nr. 9 (1999-2000) Svalbard, JD Report No. 9 to the Norwegian Parliament (1999-2000).

Mitchell, B.J., H. Bungum, W.W. Chan and P.B. Mitchell(1990): Seismicity and present-day tectonics of the Svalbard region. Geophys. J. Int., 102, 139-149.

Sundvor E. and O. Eldholm (1979): The western and northern margin off Svalbard. *Tectonophysics*, 59, 239-250.

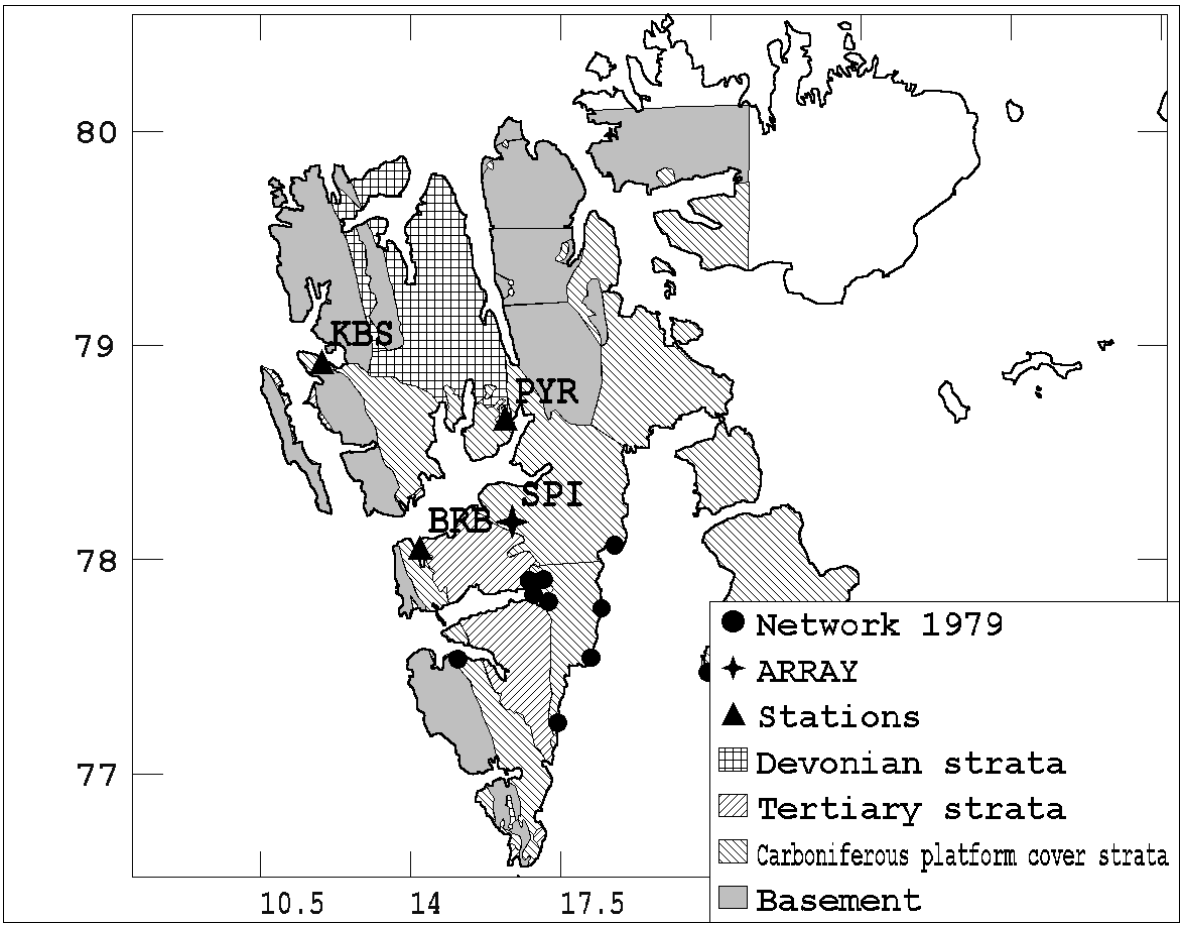

Fig. 6.4.1. Geology of the Spitsbergen Archipelago. Location of seismic stations are indicated.

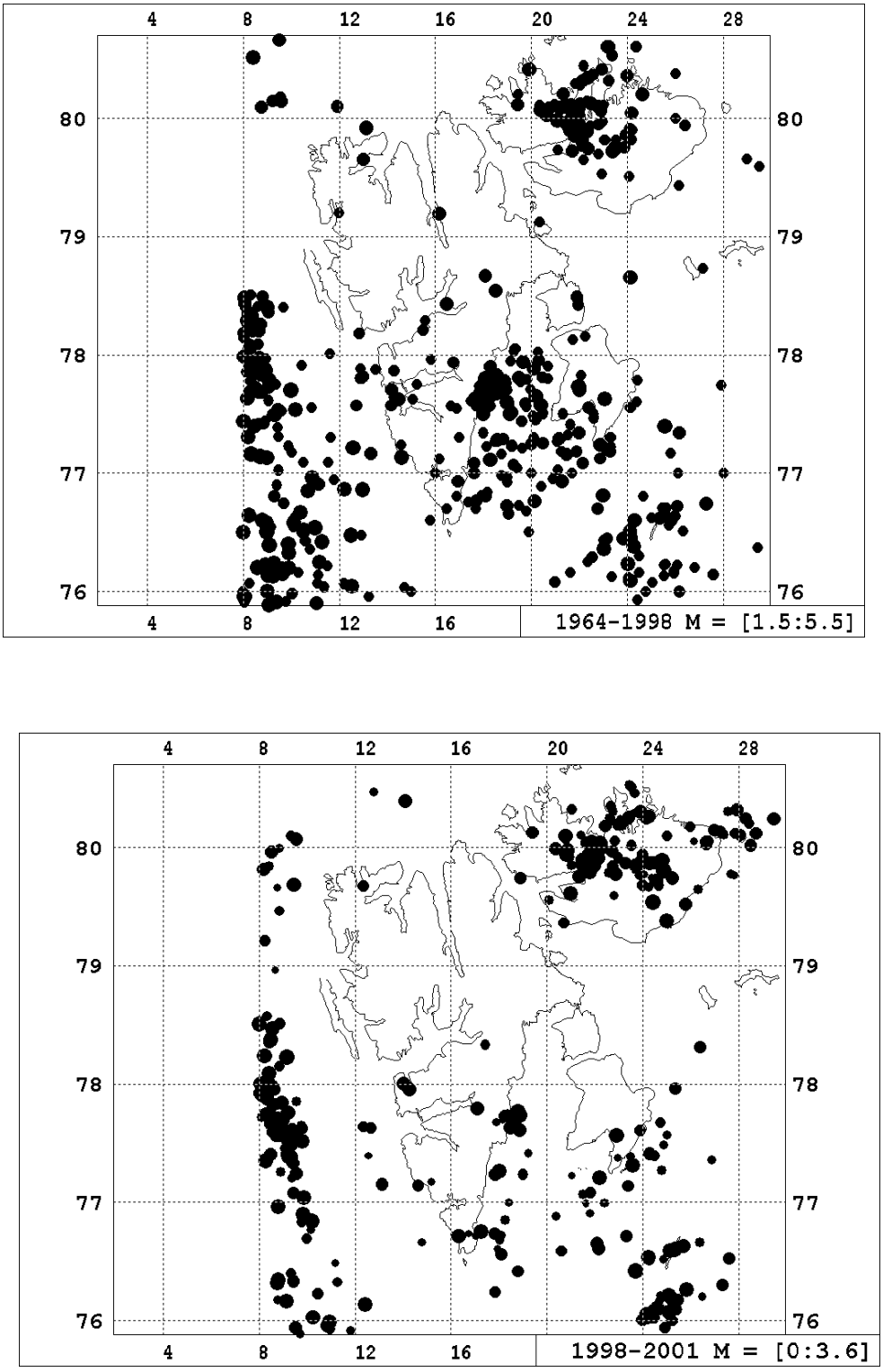

Fig. 6.4.2 Seismicity of Spitsbergen during 1964-1998 using ISC data (top) and during 1998-2001 using NORSAR Reviewed Bulletins (bottom).

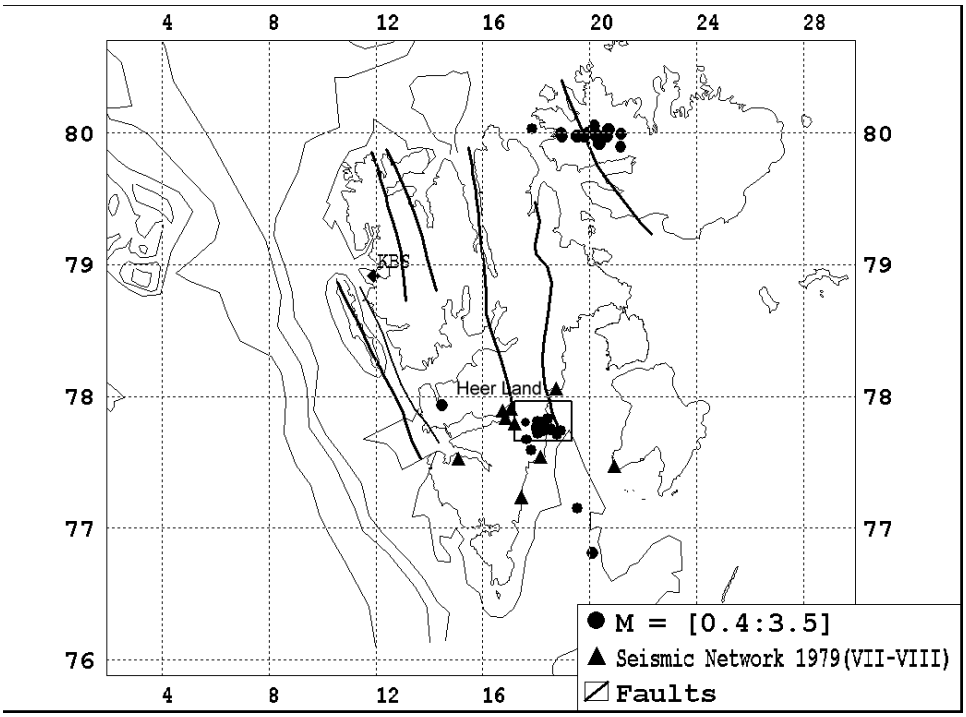

Fig. 6.4.3.Seismic events detected and located by the temporary network in 1979.

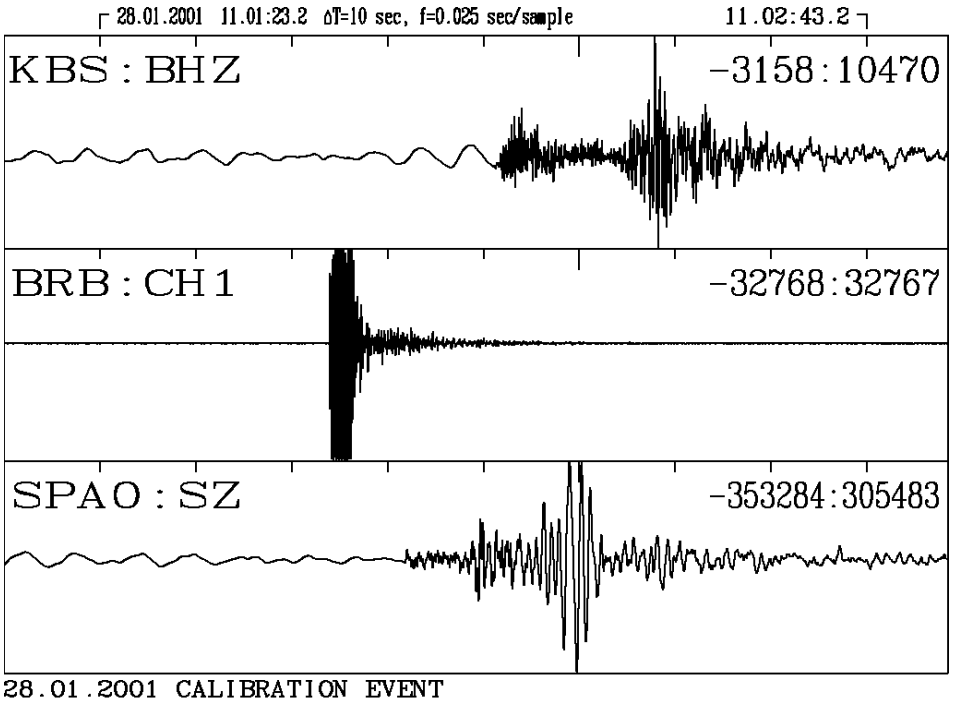

Fig. 6.4.4. Recordings of the calibration event 28.01.2001.

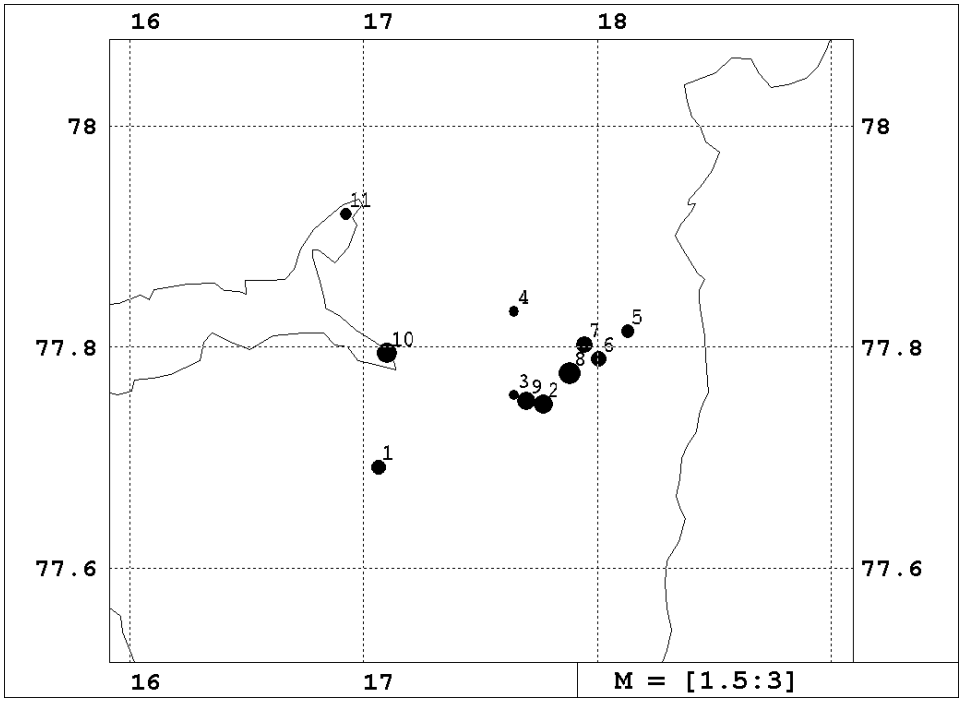

Fig. 6.4.5. Location of Heerland earthquakes.

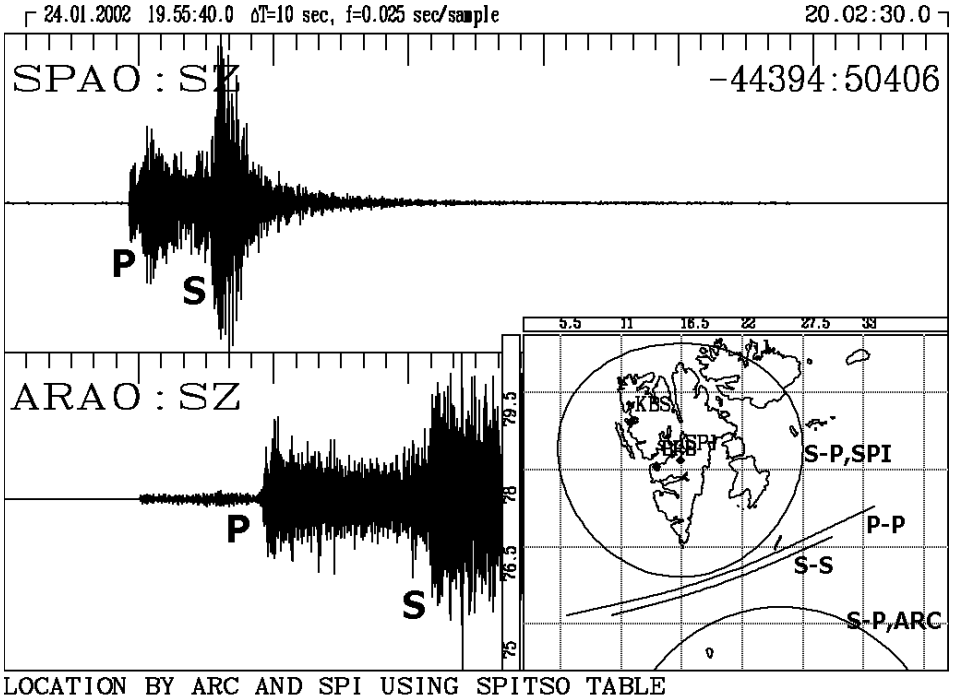

Fig. 6.4.6. Example of difficulty in obtaining location of event south of Spitsbergen using the SPITS0 model (isolines do not intersect).

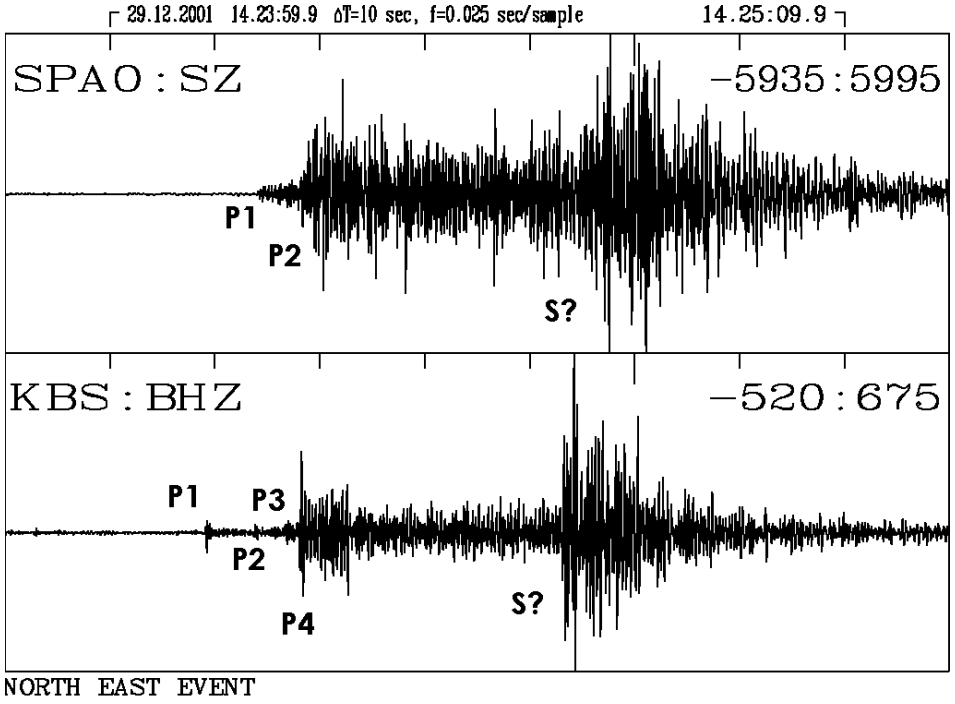

Fig. 6.4.7. Recording of the 29.12.2001 earthquake in Nordaustlandet.

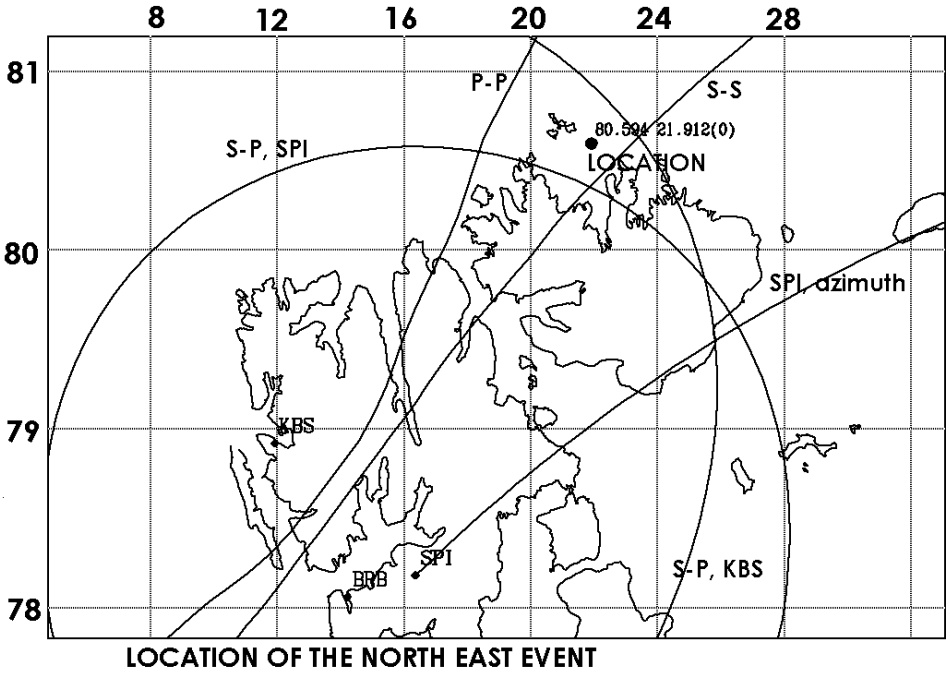

Fig. 6.4.8. Example of difficulty in obtaining location of an event in Nordaustlandet using the SPITS0 model (isolines do not intersect).

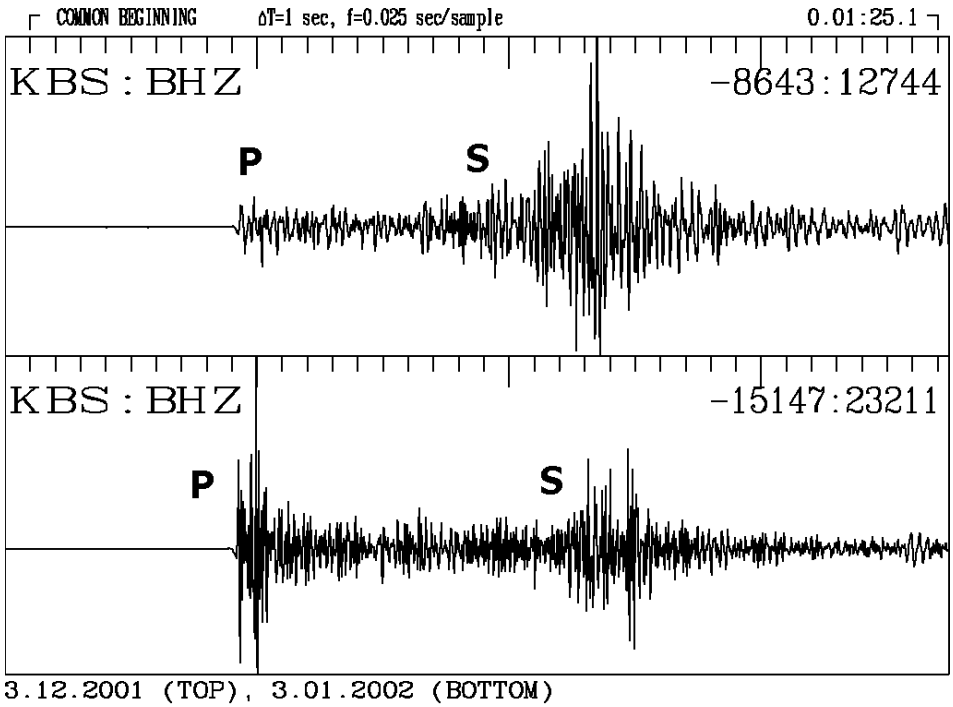

Fig. 6.4.9. Example of differences in P/S ratios for earthquakes located closely together. (3.12.2001 at 01.45.49 GMT; 78.33N 8.24E; and 3.01.2002 at 22.50.40 GMT; 78.4N 7.6E).

6.5 Comparison of location procedures – The Kara Sea event of 16 August 1997

Introduction

A seismic event in the Kara sea to the east of Novaya Zemlya on 16 August 1997 has been the subject of considerable discussion, because the very limited set of stations available to the International Seismological Centre (ISC) and the Reviewed Event Bulletin (REB) of the Experimental International Data Centre (EIDC) are inadequate to constrain the depth effectively. Could this event have been an underwater explosion?

A more comprehensive data set has been assembled by repicking all available records from the event, including the station AMD at the northern end of the Urals which lies the closest to the event at about 400 km range. The distribution of seismic stations, which observed this event is shown in Fig. 6.5.1, the station coordinates are listed in Table 6.5.1, and the full phase list with arrival time, slowness and azimuth readings are presented in Table 6.5.2.

Many of the stations lie in Fennoscandia, but azimuthal control is improved by a set of stations in the western Barents Sea and in Russia. The total data set contains many S readings; even where these have significant reading uncertainties (see Table 6.5.2), they can help to provide control on position and depth through the sensitivity of the differential S-P times to distance.

A sequence of location experiments have been undertaken to compare the results of using both different velocity models to describe the travel times of the phases and also to make a comparison between the use of a linearized location algorithm (HYPOSAT – Schweitzer, 2001) and a fully non-linear scheme (shakeNA – Sambridge and Kennett, 2001). For direct comparisons between the two methods we have used a standard least-squares misfit criterion, but have also examined the influence of more robust choices for data misfit when using the non-linear location scheme.

Observed data and tested models

We have employed the global reference models *JB* (Jeffreys and Bullen, 1940), *PREM* (Dziewonski and Anderson, 1981), *IASP91* (Kennett and Engdahl, 1991), and *AK135* (Kennett *et al.*, 1995), and also considered two regional models derived from the *Barents* model of Kremenetskaya *et al.* (2001). The *barey* model is very similar to the *Barents* model with a P- to S-velocity ratio close to 1.78, while the *barez* model has identical P velocities as *barey* model but faster S wavespeed with a P- to S-velocity ratio of 1.72 (see Fig. 6.5.2). We have found that the *barey* model gives a good representation of paths from the Kara Sea to Fennoscandia but that the *barez* model is more suitable for paths from the Kara Sea to Spitsbergen, Bear Island, and to Northern Siberia.

All of the listed observations in Table 6.5.2 were used during our study. However, the final inversions were made without some of these data: The S onsets at KTK1 and TRO were not used because we had no direct P observation of these in trigger mode operated stations. The P onset at MOR8 was not used because we suspect an absolute timing error at MOR8 (for all inversion results the residuum of this P onset is anomalously large). The ISC used a reading for NB2, which is a reported analysis on the beam calculated for the whole NORSAR array. Instead of recalculating this beam, we analyzed the onsets individually on all available 3C

broadband traces (NAO01, NB201, NC303, and NC602) of the NORSAR array. However, NC602 is co-located with the centre element (NRA0) of the NORES array and therefore we skipped the NC602 reading for our final analyses. The pIDC published in the REB an Sn-onset time for station ARU. We requested the ARU data from the pIDC to reanalyze also these records. However, after carefully checking the 3C data around the presumed and reported onset time, we could not confirm any Sn onset from the theoretically backazimuth and rejected this reading. However, this spurious onset was also listed in the ISC bulletin but never used as defining observation at the EIDC or at the ISC. Our final inversion therefore employs 23 P-phase and 13 S-phase readings from 23 different seismic stations at a distance range of about about 3˚ to 21˚.

Results with the Neighbourhood Algorithm shakeNA

The non-linear location procedure using the Neighbourhood Algorithm (NA) is based on an exploration of the 4-D hypocentral parameter space to find models with good fit to the data. At each stage the algorithm makes use of all the prior information to define a partition of the parameter space into Voronoi cells around each sampled point describing the region which lies closest to that point. To find effective location estimates the algorithm is used in a fairly focused way with an initial sampling of 9 points in the entire specified volume and then 9 new points in each iteration randomly sampling the current two “best” Voronoi cells, *i.e.* those containing the points with the least misfit. In this mode the progress of the non-linear inversion resembles the convergence of a cloud of points towards single goal.

The NA scheme was applied to a zone 16 deg across in longitude and 8 deg across in latitude and extending to 120 km deep, centred in the Kara Sea, and up to 20 s variation in origin time was also allowed. Despite the large initial domain convergence is rapid and low misfits can readily be achieved in about 30 iterations. The misfit levels for the two global reference models *AK135*, *IASP91* is comparable but *AK135* provides a slightly better fit. A variance reduction of about 30% can be achieved by using the region-specific models, *barey* and *barez.*

In Fig. 6.5.3 we show the central portion of the parameter space (a 20 km square about the same reference point) for the *barez* model. The NA algorithm has been extended here to 60 iterations to provide a further exploration of the zone of better misfit, the group of black models have a very similar level of misfit and define a ‘consistency region’ indicated with the gray polygons which indicates the variability allowed in the event location. This consistency region is defined with the aid of an auxiliary weighting function, based on analogues from statistical physics. It is easier to derive a threshold scheme for the weighting function than for the misfit itself, because the shape of the weighting function is known and only scaling varies. There is only a marginal difference between the levels of misfit for the solutions indicated with black symbols. The solution with best fit to data is indicated with the open diamond, but a more useful quantity is generally the ensemble weighted average indicated with the gray cross.

We believe that the robust statistic tends to suppress the influence of outliers and in doing so finds an alternative region of good fit with a different combination of depth and origin time. The sensitivity of the data misfit to subareas of the hypocenter space and indeed groups of solutions with very similar levels of misfit can exist. This is illustrated with Fig. 6.5.4, where we show the central portion of the parameter space for model *IASP91*. Clearly subregions of equally good misfit levels can be identified, notably in depth.

The epicentral areas of all four models tested with the NA algorithm are plotted in Fig. 6.5.5 and Table 6.5.3 lists the corresponding numerical results. The polygons give always the consistency region of the solution for each model. In addition two plotted two solutions: once the one with the absolute minimal misfit as open symbols and once the mean of the whole assemble of solutions defining the 'consistency region' as small filled symbols. The shakeNA locations for the standard Earth models *IASP91* and *AK135* are very close and clearly separated by about 20 km from the solutions using the regional models *barey* and *barez*, the latter show somewhat smaller consistency regions.

For a quantitative measure of the quality of an event location we have calculated two different parameters: the root-mean square (RMS) of all defining onset times and a weighted mean misfit of all observed parameters (WMF). The WMF values are calculated by calculating the mean of the residuals weighted by the standard deviation of the observation. RMS and WMF are also listed for each hypocenter determination in Table 6.5.3.

The presence of sets of solutions with very similar levels of fit poses problems when using a linearized inverse scheme because the algorithm will tend to be pulled towards one particular epicentral subregion or depth range (*e.g.* depending on where it was initiated), and unlike the non-linear scheme will not be able to escape to find a better point. If we are unlucky there is the possibility of approaching the minimum from a direction such that the next iteration overshoots its target and then returns to near the earlier point at the subsequent iteration. Such oscillations are difficult to tame.

In both, the non-linear and the linearized inversions, we found that the patterns of residuals when using either the *barey* or *barez* models reveal an inconsistency for S waves between paths to Spitsbergen and Siberia one side and Fennoscandia on the other side. Either one group or the other group of paths is well fitted, but always with significant residuals for the second group. This suggests the use of different models for the two sets of paths.

Discussion of the HYPOSAT results

To get the results of the HYPOSAT inversions comparable with the shakeNA results, the HYPOSAT inversions were restricted to a strict least-squares scheme without using special stations corrections or travel-time differences between the phases observed at one stations. All error ellipses for the epicenter were calculated for a 90% significance level after projecting the corresponding uncertainties of source time and event depth in consideration of the covariance matrix into the epicentral-error space. The iteration process was stopped when two sequential solutions were closer than 0.5 km to each other. To force a stable result, the program itself removes some observations during the iterations of the inversion when the residuals became too large. Therefore the number of defining parameters changes slightly for the different solutions.

We tested the same models as for the shakeNA scheme. The epicenters are plotted together with the shakeNA results in Fig. 6.5.5, and Table 6.5.3 again lists the corresponding numbers. The HYPOSAT epicenters are plotted with large filled symbols and their corresponding error ellipses as broken lines. The error ellipses and epicenters for the standard Earth models *IASP91* and *AK135* overlap very well with the shakeNA results. However, because of the inadequate velocity models, for both models the inversions were oscillating between a source depth in the middle crust and below the Mohorovicic discontinuity and the program fixed the depth.

Because of this source parameter reduction we also get a dimension reduction of the covariance matrix and consequently relatively small error ellipses, although the RMS and WMF values are relatively large.

For the models *barey* and *barez* the data were consistent enough that HYPOSAT inverted also for the event's depth. As in case of shakeNA, the models can only explain a subset of data, depending on the actual ray paths. For *barey* the S-phase observations on Spitsbergen and on the Bear Island could not be modeled and the error ellipse become very large. The hypocenter itself lies within the shakeNA results. For *barez* all residuals of the S observations in Fennoscandia became very large and were refused as defining parameters. Consequently, the data set became more homogeneous and the error ellipse smaller. The agreement with the shakeNA solutions for *barez* is worse but both the consistency region and the error ellipse show some overlap.

The data set for this Kara Sea event shows a bimodal distribution in observed travel times. Therefore, the original HYPOSAT code was extended such that it can now jointly apply two different travel-time tables after choosing the best travel-time table for each path (see Table 6.5.2). For a final solution — here called *comb* (Fig. 6.5.5, in red) — we applied all possibilities of HYPOSAT (i.e. station elevation corrections, inverting for travel-time differences, and choosing the travel-time table with respect to the paths) and the result was a location with a very small error ellipse and very small data residuals.

To find out, how sensitive our *comb* location is for data from the nearest station AMD, we ran several tests. Starting with a depth of 0 km, we inverted the data with different combinations of AMD contributions, *i.e.* without any AMD observations, only with the Pn or only with the Sn onset, and with both onsets with or without also inverting the travel-time difference Sn-Pn. The result of these tests was that only if we include **both** the Pn and the Sn onset time (in any combination) at AMD, we could resolve the event depth as about 20 km.

Finally, we tested if the source depth as estimated for solution *comb* is depending on the start depth of the inversion. Therefore a start solution close to the epicentral area with start depth of 0, 10, 20, and 30 km was chosen for the inversion. In all cases the inversion converged to a depth between 15 and 20 km and using the start depth as fixed depth the result for 20 km had the smallest residuals.

In conclusion, the location estimations from the different techniques agree quite well and show some overlap of their confidence regions or error ellipses. From this we conclude that the event cannot be shallower than 10 km and is most likely in the lower crust at about 20 km depth.

Comparison with data centre solutions

The international data centres pIDC (REB), NEIC (PDE), and ISC located the discussed Kara Sea event. They all used slightly different observations and published different solutions. All these solutions are listed in Table 6.5.4, and Fig. 6.5.6 shows the epicenters (REB: diamond, PDE: hexagon, ISC: point) with their published error ellipses in black together with our *comb* solution for all available data in red (see Table 6.5.3). The number of defining observations for the ISC location is relatively large because the ISC used in its inversion the data from the arrays SPITS, FINES, and NORES twice as defining: once under the array-beam name and once under the name of the central site of the array (SPA0, FIA0, and NRA0).

The precise travel-time curves, location algorithms and applied data uncertainties of the data centre solutions are unknown to us. Therefore, it is difficult to compare our solutions with the data centre solutions. We choose the following approach for our experiment: to use only those of our readings, which were made at the same stations as listed in the ISC bulletin (all entries marked with a 'C' in Table 6.5.2). Then we relocated the event (see Fig. 6.5.6 and Table 6.5.1) with HYPOSAT for the different standard Earth models *JB* (Jeffreys and Bullen, 1940, gray, point), *PREM* (Dziewonski and Anderson, 1981, blue, hexagon), *IASP91* (Kennett and Engdahl, 1991, red, triangle), and *AK135* (Kennett *et al.*, 1995, blue, square) and for the three models derived for the Barents Sea region (*barey* (rhomb), *barez* (triangle), and *comb* (point), all in green), where *comb* is again the combined usage of *barey* and *barez*.

Because this subset of data have no resolution for the event's depth, we used here a fixed depth of 18 km which came from our *comb* solution for the whole data set. In addition we listed in Table 6.5.4 the number of defining parameters used for the locations, the RMS values of all as defining used onset times, and the epicentral distance to our *comb* solution from table Table 6.5.3. To get some feeling about the quality of the different solution we calculated again the WMF values. For the data centre solutions we used the data uncertainties as given in Table 6.5.2 but the residuals as published in the bulletins. In the REB as well as in the ISC bulletin an Sn reading from station ARU is listed but was not used to locate the event. To calculate the WMF value for the REB solution, this residual of -20.8 s was ignored.

All relocations for the three global models *JB*, *IASP91*, and *AK135* are very close and from the data centre solutions only the REB solution lies within their definitely larger error ellipses. The relatively small error ellipse of the REB solution is mainly because the Sn onsets with their large residuals were not used as defining for the solution. In our relocations (including *PREM*) all onsets were used and contribute with their residuals to the larger error ellipses. In all these solutions the P-type onsets are more or less equally well explained but not the Sn onsets. Because this could be a depth effect we also relocated the event with a fixed depth at 0 km and at 10 km. For all four global models (*JB*, *PREM*, *IASP91*, and *AK135*) the residuals were smallest for the fixed depth at 18 km.

The smallest residuals were obtained for the new regional models (see the green locations on the map). The worst of these solutions is for model *barez*, of which we know that it explains best the readings from stations in the western Barents Sea, at AMD, and at NRIS. The subset of data, used in this experiment, contains such readings only from the SPITS array. All other readings are from Fennoscandia or the Kola Peninsula. For these data model *barey* explains better the Sn-onset times. Consequently the location with model *barey* has smaller residuals. The residuals and the error ellipse for model *comb* are the smallest and this solution is the closest to our *comb* solution. This is a clear effect of using path specific velocity models.

Conclusion

This study has shown both the importance of S wave information in assessing the depth of regional events, and the need to get a good regional velocity model for both P and S in order to place the strongest constraints on the location of the event.

The conclusions from our experiment of comparing the different data centre solutions with our results are that using only a limited data set but an adequate travel-time model one can locate the event in the Kara Sea relatively close to our *comb* location. In this case the depth resolution

is of course negligible. The relative small error ellipses are a problem which arises when using only a limited number of data. Then the data errors do not usually follow a normal distribution but are biased in one direction and suggest high resolution and accuracy.

The location estimates for the whole data set from the different techniques agree quite well, with some overlap of the estimated confidence regions. The event cannot be shallower than 10 km and is most likely in lower crust around 20-30 km depth. Such deep crustal events are often attributed to the long-term effects of ice-unloading from the last glaciation and were previously observed around Novaya Zemlya (*e.g.* Marshall *et al.,* 1989). That this event was not an underwater explosion is also confirmed by the occurrence of an aftershock in the same epicentral area about four hours later (Ringdal *et al.,* 1997) and the fact that the observed seismic signals do not show bubble pulse reverberations, typical for underwater explosions.

Johannes Schweitzer

Brian Kennett, RSES, Australian National University

References

Dziewonski, A.M. and Anderson D.L. (1981): Preliminary reference Earth model. Phys. Earth Planet. Inter. **25**, 297-356.

Jeffreys, H., and Bullen, K.E., (1940): Seismological tables. British Association for the Advancement of Science, London 1940, 50 pp.

Engdahl, E.R., R. van der Hilst, and R. Buland (1998): Global teleseismic earthquake relocation with improved travel times and procedures for depth determination. Bull. Seism. Soc. Amer. **73**, 1271-1302.

Kennett, B.L.N., and Engdahl, E.R. (1991): Travel times for global earthquake location and phase identification. Geophys. J. Int. **105**, 429-466.

Kennett, B.L.N., Engdahl, E.R., and Buland, R. (1995): Constraints on seismic velocities in the Earth from traveltimes. Geophys. J. Int. **122**, 108-124.

Kremenetskaya, E., V. Asming, and F. Ringdal (2001): Seismic Location Calibration of the European Arctic. Pure appl. geophys. **158**, 117-128.

Marshall, P.D., R.C. Stewart, and R.C. Lilwall (1989): The seismic disturbance on 1986 August 1 near Novaya Zemlya: A source of concern? Geophys. Jour. Int. **98**, 565-573.

Ringdal, F., T. Kværna, E.O. Kremenetskaya, and V.E. Asming (1997): The seismic event near Novaya Zemlya on 16 August 1997. In: NORSAR Semiannual Tech. Summ. 1 April - 30 September 1996, NORSAR Sci. Rep. **1-97/98**, Kjeller, Norway, 110-119.

Sambridge, M.S., and B.L.N. Kennett (2001): Seismic Event Location: Nonlinear Inversion Using a Neighbourhood Algorithm. Pure appl. geophys. 1**58**, 241-257.

Schweitzer, J. (2001): HYPOSAT – An enhanced routine to locate seismic events. Pure appl. geophys. **158**, 277-289.

Table 6.5.1. Stations and their coordinates used in this study (see also Fig. 6.5.1). A star indicates if the reading(s) of this station were used or listed by international agencies or in this study.

Station	Latitude [˚]	Longitude [˚]	Elevation [m]	PIDC	NEIC	ISC	This study
AMD	69.7667	61.6833	200.0	-	-	-	*
APA0	67.6061	32.9931	200.0	-	-	*	*
ARU	56.4302	58.5625	250.0	*	-	*	-
BJO	74.5055	19.1883	18.0	-	-	-	*
FINES	61.4436	26.0771	150.0	*	*	*	*
HFS	60.1342	13.6956	265.0	*	*	*	*
JOF	62.9182	31.3124	180.0	-	-	-	*
KAF	62.1128	26.3061	205.0	-	*	*	*
KBS	78.9256	11.9417	74.0	-	-	-	*
KEF	62.1672	24.8703	215.0	-	-	-	*
KEV	69.7553	27.0067	81.0	-	-	-	*
KJN	64.0853	27.7119	250.0	-	-	-	*
KTK1	69.0117	23.2371	340.0	-	-	*	*
MOR8	66.1713	14.4411	445.0	-	-	*	*
NAO01	60.8442	10.8865	426.0	-	-	-	*
NB201	61.0495	11.2939	613.0	-	-	-	*
NB2	61.0397	11.2148	717.0	-	-	*	-
NC303	61.2251	11.3690	401.0	-	-	-	*
NC602	60.7353	11.5414	305.0	-	-	-	*
NORES	60.7353	11.5414	302.0	*	*	*	*
NRIS	69.0061	87.9964	498.0	*	*	*	*
NUR	60.5090	24.6514	102.0	-	*	*	*
PKK	60.0052	24.5169	10.0	-	-	-	*
PVF	60.5451	25.8616	45.0	-	-	-	*
SDF	67.4203	26.3936	276.5	-	-	-	*
SPITS	78.1777	16.3699	323.0	*	*	*	*
SUF	62.7192	26.1506	185.0	-	-	-	*
TRO	69.6325	18.9281	15.0	-	-	*	*
VAF	63.0422	22.6715	55.0	-	-	-	*

Table 6.5.2. All reread parameters as onset times, backazimuths (BAZ), and ray parameters (P) and their standard deviations σ of first P- and S-type onsets. Epicentral distances (Δ) and azimuths (AZI) were calculated with respect to the *comb* solution of Table 6.5.3. To find this and all other solutions of this table, all with an 'I' marked data were inverted. For the *comb* solutions, we used model *barey* for all travel-time relevant parameters except for the observations indicated with a '2' - in this case model *barez* was applied. A 'C' marks data used for the comparison of the results of this study with the solutions published by international data centres (see Table 6.5.4).

Station	Δ [°]	AZI [°]	Phase	Hour	Minute	Second	σ Time [s]	BAZ [°]	σ BAZ [°]	P [s/°]	σ P [s/°]	Remarks
AMD	2.917	151.2	P	02	11	48.50	0.10	-	-	-	-	I-2
AMD	2.917	151.2	S	02	12	21.15	0.20	-	-	-	-	I-2
APA0	9.623	252.7	P	02	13	17.14	1.50	72.7	25.0	9.03	4.0	I-C
APA0	9.623	252.7	S	02	15	02.84	2.00	53.5	25.0	19.24	4.0	I-C
BJO	11.041	299.3	P	02	13	35.98	3.00	-	-	-	-	I-2
BJO	11.041	299.3	S	02	15	30.60	5.00	-	-	-	-	I-2
FINES	16.227	244.1	P	02	14	46.33	1.75	33.2	15.0	10.90	1.5	I-C
FINES	16.227	244.1	S	02	17	37.83	3.00	-	-	-	-	I-C
HFS	20.856	257.2	P	02	15	42.82	0.50	28.0	15.0	9.42	2.0	I-C
JOF	16.606	239.6	P	02	14	09.86	1.00	-	-	-	-	I
JOF	16.606	239.6	S	02	16	33.42	2.00	-	-	-	-	I
KAF	15.617	245.2	P	02	14	36.00	2.00	-	-	-	-	I-C
KBS	12.704	321.0	P	02	13	57.47	1.00	-	-	-	-	I-2
KBS	12.704	321.0	S	02	16	08.06	2.00	-	-	-	-	I-2
KEF	15.957	247.3	P	02	14	42.72	0.75	-	-	-	-	I
KEV	10.209	270.3	P	02	13	25.19	0.50	-	-	-	-	I
KEV	10.209	2703	S	02	15	13.18	2.50	-	-	-	-	I
KJN	13.664	248.0	P	02	14	12.32	2.00	-	-	-	-	I
KJN	13.664	248.0	S	02	16	39.60	2.00	-	-	-	-	I
KTK1	11.738	270.5	S	02	15	50.37	2.50	-	-	-	-	C
MOR8	16.141	269.4	P	02	14	41.42	1.50	-	-	-	-	C
NAO01	21.132	261.5	P	02	15	45.44	0.60	-	-	-	-	I
NB201	20.847	261.4	P	02	15	43.07	0.60	-	-	-	-	I-C
NC303	20.687	261.6	P	02	15	41.27	0.50	-	-	-	-	I

Station	Δ [˚]	AZI [˚]	Phase	Hour	Minute	Second	σ Time [s]	BAZ [˚]	σ BAZ [˚]	P [s/˚]	σ P [s/˚]	Remarks
NC602	21.021	260.6	P	02	15	44.57	0.50	-	-	-	-	-
NORES	21.021	260.6	P	02	15	44.55	0.50	37.1	15.0	10.08	1.2	I-C
NRIS	10.521	91.5	P	02	13	30.19	1.00	-	-	-	-	I-2-C
NRIS	10.521	91.5	S	02	15	19.35	1.50	-	-	-	-	I-2-C
NUR	17.395	244.2	P	02	15	02.00	2.00	-	-	-	-	I-C
PKK	17.853	243.5	P	02	15	07.90	1.50	-	-	-	-	I
PVF	17.033	242.6	P	02	14	58.18	1.50	-	-	-	-	I
SDF	11.703	260.7	P	02	13	45.17	1.00	-	-	-	-	I
SDF	11.703	260.7	S	02	15	50.75	2.00	-	-	-	-	I
SPITS	11.731	318.0	P	02	13	44.85	0.50	103.0	15.0	11.98	2.5	I-2-C
SPITS	11.731	318.0	S	02	15	45.45	1.50	95.0	15.0	19.86	2.5	I-2-C
SUF	15.173	246.8	P	02	14	31.29	1.00	-	-	-	-	I
SUF	15.173	247.8	S	02	17	13.10	3.00	-	-	-	-	I
TRO	12.730	276.7	S	02	16	15.40	2.50	-	-	-	-	C
VAF	15.915	252.2	S	02	17	29.83	2.00	-	-	-	-	I
VAF	15.915	252.2	P	02	14	41.05	1.50	-	-	-	-	I

Table 6.5.3. The new hypocenter solutions for the 16 August 1997 Kara Sea event as plotted in Fig. 6.5.6. Listed are the source parameters and the number of data used by HYPOSAT as defining for onset times (OT), backazimuths (BAZ), ray parameters (RP), and travel-time differences (TTD). In the header line, the maximum possible number of these parameters is given in parenthesis. WMF is the weighted mean misfit for all available travel-time observations and RMS was calculated from all defining onset times. An 'F' together with the estimated depth indicates that the depth was fixed by the program. 'M' indicates the used method: NA-B - the shakeNA with smallest misfit, NA-M - the mean of all solutions in the consistency region, and H - the HYPOSAT solution.

Model	Lat [°]	Lon [°]	D [km]	σ D [km]	Time	OT (36)	BAZ (7)	RP (7)	WMF (36)	RMS [s]	EE [km^2]	M
AK135	72.382	57.356	30.4	29.1 -31.6	02:11:02.85	36	7	7	2.63	4.61	-	NA-B
AK135	72.391	57.371	29.4	29.1 -31.6	02:11:02.65	36	7	7	2.64	4.60	-	NA-M
AK135	72.366	57.367	34.4 F	13.2 - 51.7	02:11:03.26	36	5	1	2.64	4.58	252	H
IASP91	72.365	57.342	35.0	32.1 - 36.0	02:11:03.37	36	7	7	2.83	4.97	-	NA-B
IASP91	72.373	57.360	34.2	32.1 - 36.0	02:11:03.21	36	7	7	2.84	4.99	-	NA-M
IASP91	72.288	57.246	37.3 F	18.5 - 62.2	02:11:04.12	29	5	1	2.89	2.69	247	H
BAREY	72.383	57.740	30.3	27.8 - 31.0	02:11:03.76	36	7	7	1.21	1.80	-	NA-B
BAREY	72.389	57.753	29.7	27.8 - 31.0	02:11:03.66	36	7	7	1.21	1.79	-	NA-M
BAREY	72.394	57.802	39.8	10.1	02:11:04.88	30	4	1	1.35	1.27	1858	H
BAREZ	72.427	57.868	21.5	21.1 - 24.5	02:11:02.91	36	7	7	1.66	3.67	-	NA-B
BAREZ	72.427	57.874	22.2	21.1 - 24.5	02:11:03.01	36	7	7	1.68	3.66	-	NA-M
BAREZ	72.342	57.644	15.9	7.6	02:11:02.80	28	4	1	1.56	1.32	402	H
COMB	72.331	57.616	17.6	5.2	02:11:03.01	35	5	1	0.90	1.27	238	H

Table 6.5.4. Hypocenter solutions for the 16 August 1997 event in the Kara Sea as published by international data centres and the event locations performed for comparison with our results. Listed are source parameters including the fixed depth, the number of as defining used P- and S-onset times, backazimuths (BAZ), ray parameters (P), and travel-time differences (TTD). In parenthesis the maximum possible number of for this solution available data is given, respectively, such values are not available for NEIC and ISC. RMS is calculated from the defining onset times, WMF is the weighted misfit for all possible travel-time observations (in case of data centre solutions for all onsets, for which residuals were published), and Δ gives the epicentral distance between this solution and the *comb* solution of Table 6.5.3. EE lists the size of the error ellipse as plotted in Fig. 6.5.6. For further details see text.

Model	Lat [°]	Lon [°]	D [km]	Time	P	S	BAZ	P	TTD	RMS [s]	WMF	Δ [km]	EE [km^2]
REB	72.6484	57.3517	0	02:10:59.9	5(5)	-(4)	3(5)	3(5)	-(3)	0.20	1.77	36.5	179
PDE	72.835	57.225	10	02:10:59.77	7(7)	-(3)	-(?)	-(?)	-(3)	1.42	0.93	57.8	963
ISC	72.6171	56.9353	10	02:10:59.18	13(13)	-(9)	-(?)	-(?)	-(6)	1.30	1.08	39.3	358
J-B	72.6272	57.7404	18	02:10:57.27	10(10)	6(6)	7(7)	7(7)	4(4)	5.31	2.41	44.4	642
PREM	72.4919	57.5754	18	02:11:02.04	10(10)	6(6)	7(7)	6(7)	4(4)	4.34	1.88	18.0	502
IASP91	72.6331	57.7468	18	02:11:00.22	10(10)	6(6)	7(7)	7(7)	4(4)	5.79	2.74	30.7	649
AK135	72.6253	57.7464	18	02:11:00.30	10(10)	6(6)	7(7)	7(7)	4(4)	5.26	2.52	33.2	533
BAREY	72.5378	57.7625	18	02:11:02.55	10(10)	6(6)	7(7)	7(7)	4(4)	1.92	1.05	23.6	128
BAREZ	72.4819	57.7912	18	02:11:03.02	10(10)	6(6)	7(7)	7(7)	4(4)	3.80	1.53	17.9	262
COMB	72.4329	57.5582	18	02:11:03.35	10(10)	6(6)	7(7)	7(7)	4(4)	1.61	0.93	11.6	116

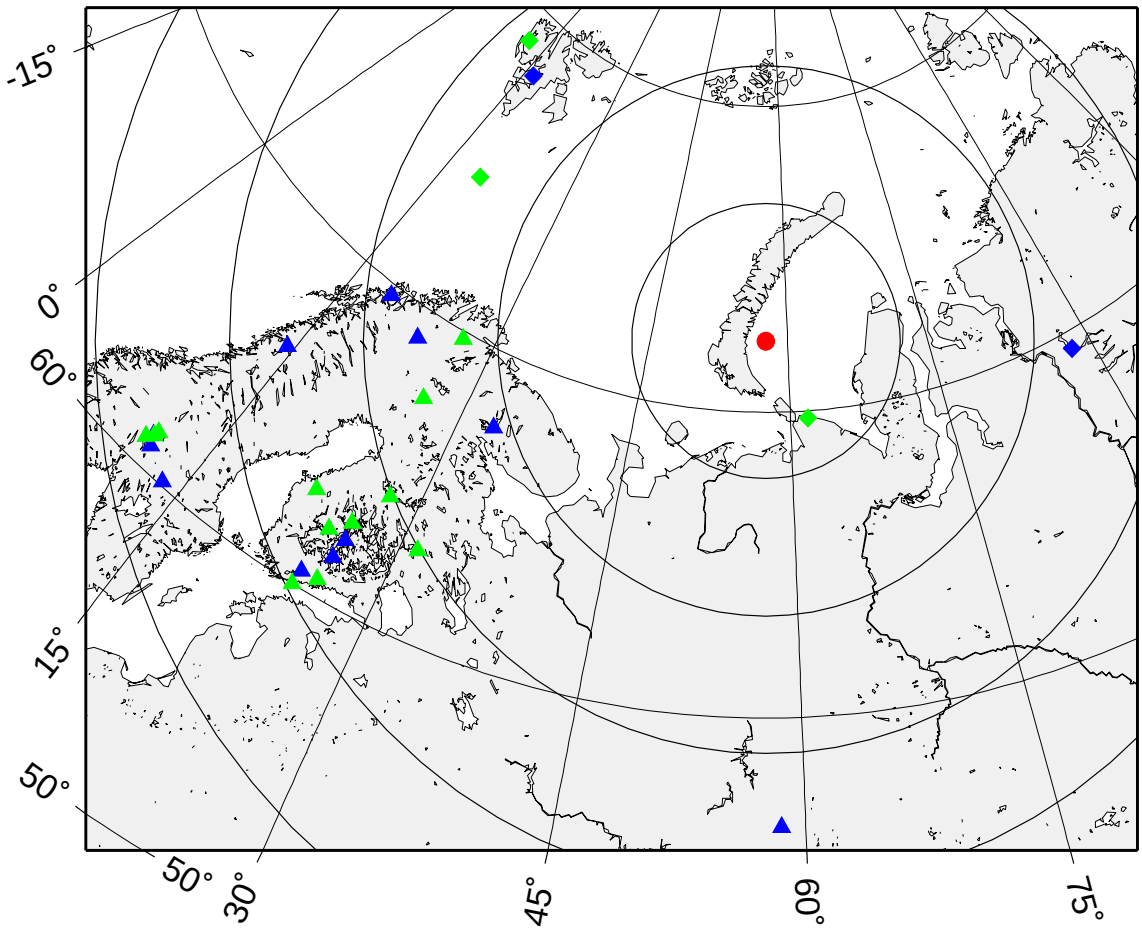

Figure 6.5.1: *Seismic stations (triangles and diamonds) which observed the Kara Sea event of 16 August 1997 (red point). Triangles (diamonds) were used for stations for which model barey (barez) gave the best results when calculating travel times for the joint model 'comb'. Blue symbols show stations, which contributed with parameter data to the bulletins of the international data centres, and green symbols represent stations with additionally analyzed data (this study). The circles show distances from the event in steps of 500 km.*

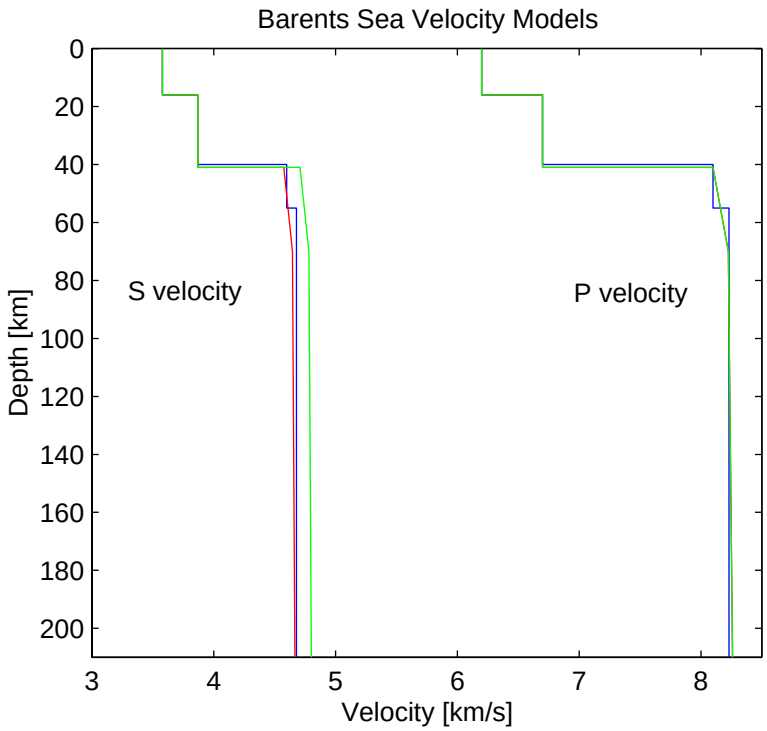

Figure 6.5.2: *Plot of regional velocity models used in this study. The models barey (red) and barez (green) were both derived from the barents model (blue, Kremenetskaya et al., 2001).*

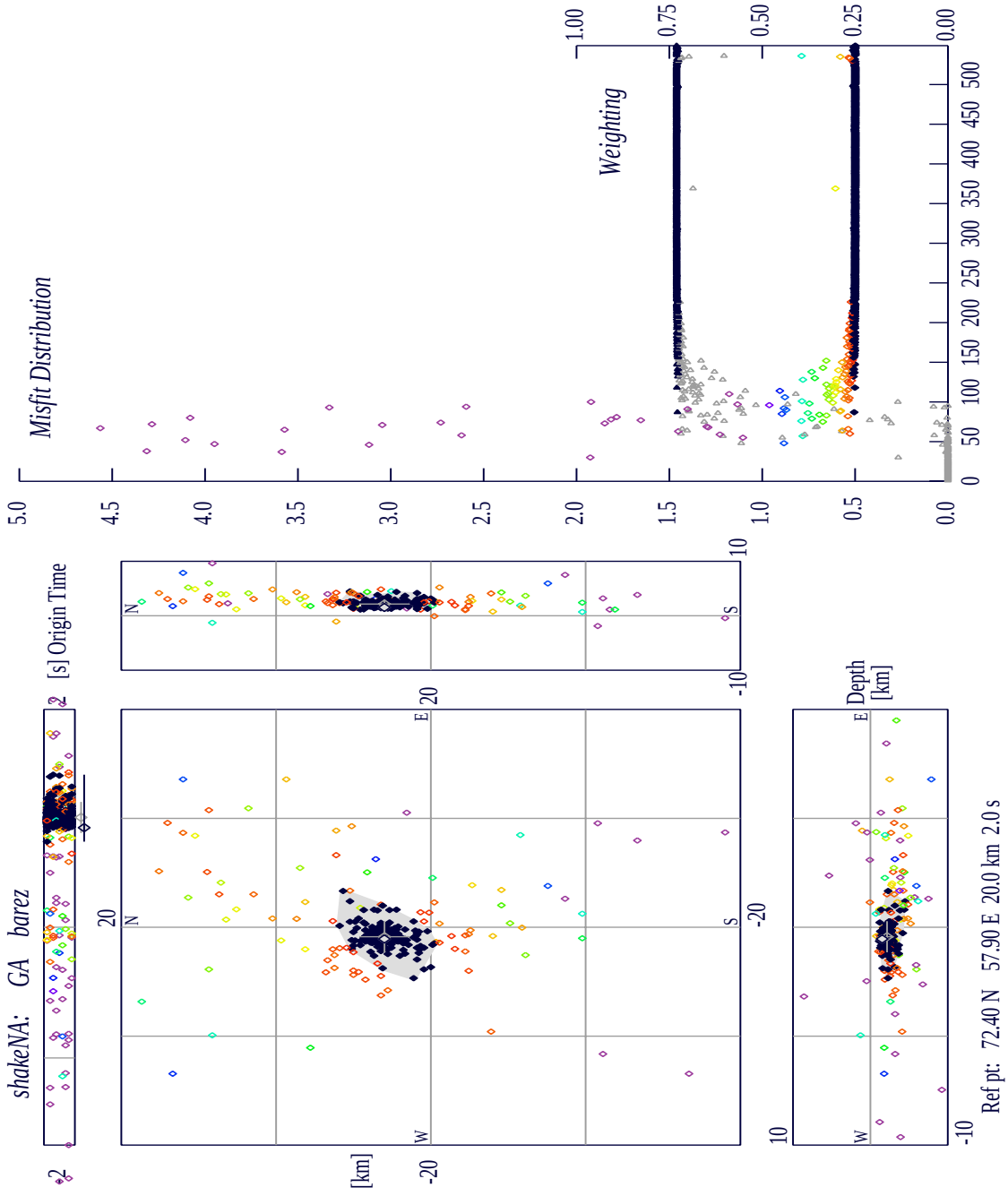

Figure 6.5.3: *Progress of the shakeNA program to a location estimate for the barez model shown as a map view and depth slices around the central portion of the sampled region.. The misfits are colour coded and the region of acceptable misfits is indicated with black symbols. The estimate of the consistency region associated with these acceptable models is indicated with grey shading. The right hand panel shows the misfit distribution and the approach to convergence. New models are generated as the iterations proceed and not all are as good as earlier models.*
The ensemble properties indicated by the grey marker and cross give a good indication of the location and its uncertainities.

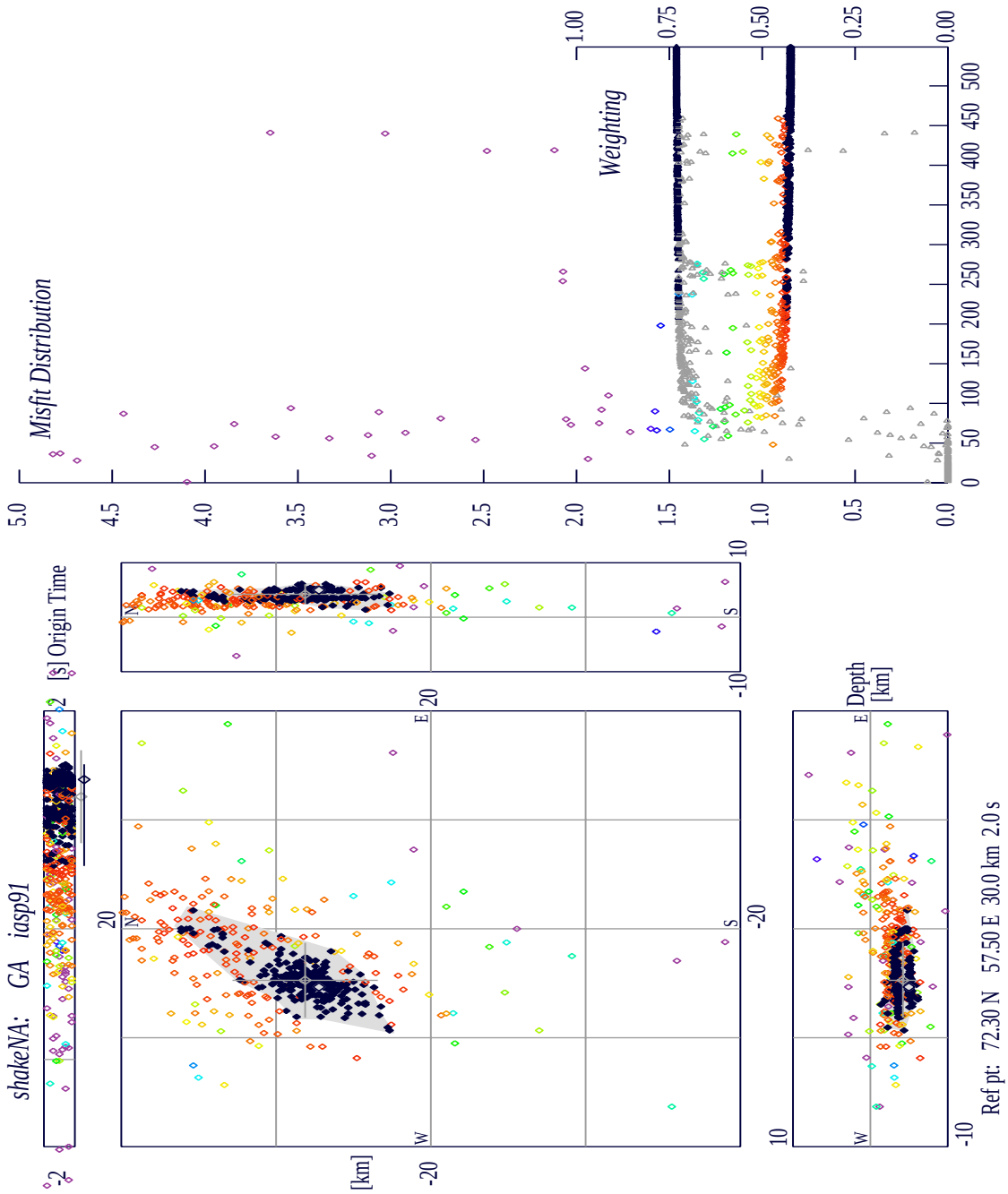

Figure 6.5.4: *same as Fig. 6.5.3 for model IASP91.*

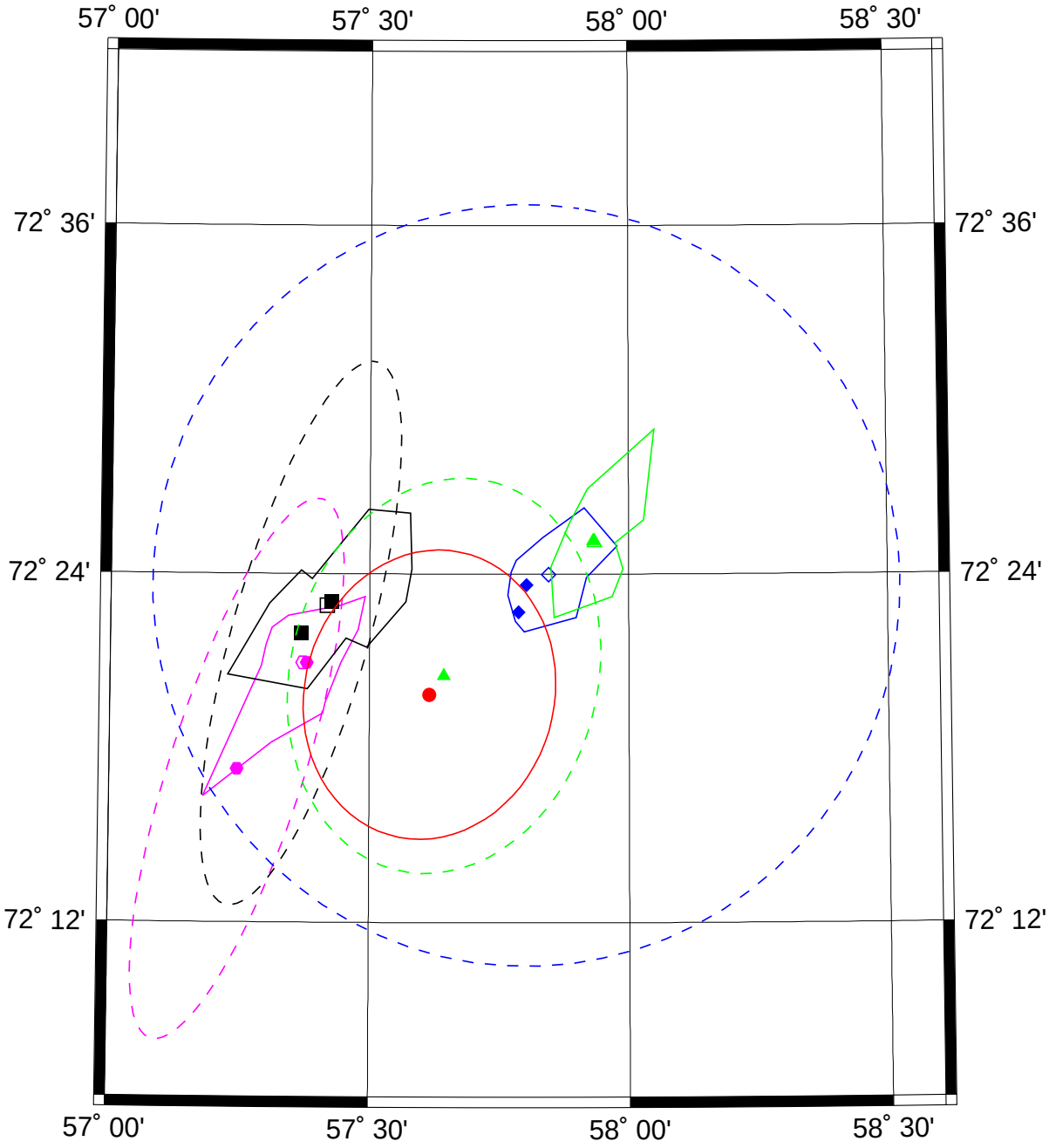

Figure 6.5.5: *Shows the NA (polygons) and the HYPOSAT (error ellipses) inversion results for the full data set and the different velocity models IASP91 (black), AK135 (magenta), barez (blue), barey (green), and 'comb' (red). For more details see text and Table 6.5.3.*

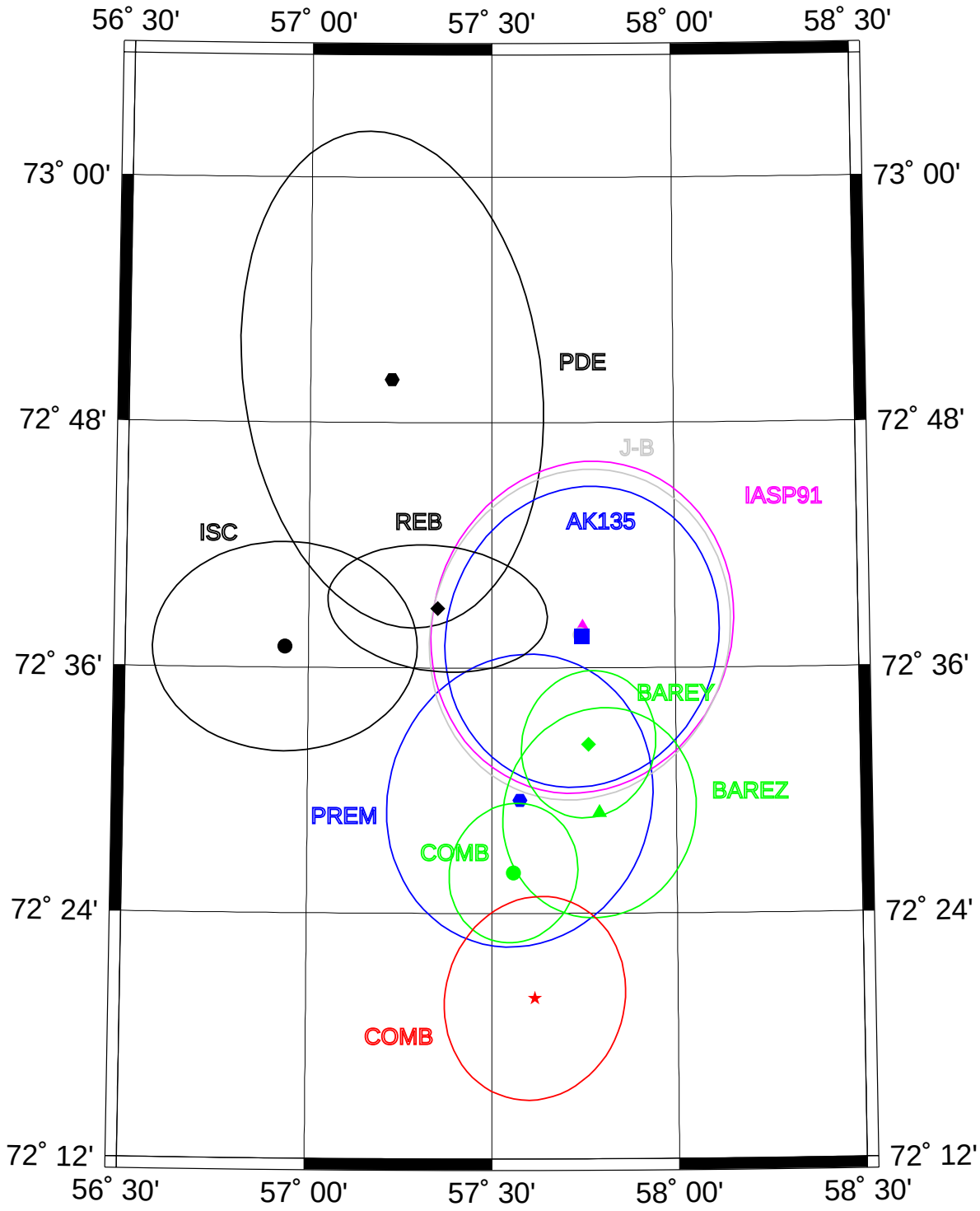

Figure 6.5.6: *Epicenters and error ellipses for the Kara Sea event of 16 August 1997 as published by data centres, and as estimated by our relocation experiment using only a limited set of data. For more details see text.*

6.6 Some results derived from the seismic signals of the accident of the Russian submarine Kursk

Introduction

In several studies different authors have used the observed seismic signals from the accident of the Russian submarine Kursk to investigate in detail the concomitant circumstances of this tragedy. Especially the location capabilities of the seismic networks and the yield of explosions, which presumably destroyed the submarine, were investigated in detail (Ringdal *et al.*, 2000; Koper *et al.*, 2001a, b; Savage and Helmberger, 2001; Northrop, 2001). The results of these studies were used to launch different theories on the presumed cause and sequence of events of the accident. In this short note, focus is on some new aspects resulting from a study of the seismic signals.

Relative location of the two seismic events

From analysis of ARCES data it became very soon clear that two different seismic events occurred about 2 minutes and 16 seconds apart in the same area, which later was confirmed as the Kursk submarine accident area. The first of these two events (Kursk-1) was about two magnitude units smaller than the second one (Kursk-2), which had a local magnitude of about 3.5 (Ringdal *et al.*, 2000); for details see Table 6.6.1. To get a better understanding of the accident, the relative location between these two events is investigated.

We assume that the sources of both events were in the submarine or in the surrounding water. In this case, S-waves can only be generated from P energy converted at the bottom of the Barents Sea. Events occurring at different depths in the water will have approximately the same S-P time difference at recording stations. Our event locations can therefore only provide information on the horizontal positions as projected down to the sea bottom. By measuring with high accuracy the time difference between both events at many stations and for different phases we should in principle be able to provide information on the relative horizontal position between Kursk-1 and Kursk- 2. Therefore, we will calculate relative coordinates of Kursk-1 with respect to the well located Kursk-2 event by applying the master-event location technique.

The Kursk-1 was best observed at ARCES and correlation analysis between different onsets for the two events show correlation coefficients of up to 0.78 (see Table 6.6.2). This indicates similar but not identical propagation effects and source characteristics for Kursk-1 and Kursk-2. The correlation method was used to measure the travel-time differences between the two events accurately. The first event was less visible at other stations than at ARCES, but using the correlation method, signals from the first event could also be identified at the Apatity array, the FINES array, and at the 3C-broadband stations APZ9, KEV, and LVZ. For this analysis all data were resampled to a common digitalization rate of 400 samples per second and the time difference of all interpretable signals was measured with an assumed accuracy of 0.005 s (two samples). To take into account the inversion the different signal-to-noise ratios of the Kursk-1 signals, the measured time differences were weighted with the observed correlation coefficients. Both P-type and S-type onsets were used to measure the source-time difference. These time differences scatter around a mean value of 135.76 s, and details with respect to each station and phase are listed in Table 6.6.2.

Then the master-event location technique was applied and the deviations in the time differences were inverted for a relative horizontal location between the two events. For this the 12 measured time differences could be inverted by applying the generalized-matrix inversion. The data

were weighted with the standard deviations calculated from the corresponding correlation coefficient. The inversion reduced the variance of the residuals by 42.7%. Table 6.6.3 shows the results of the inversion, where the horizontal distance between Kursk-1 and Kursk-2 was estimated at about 145 m.

Observations by analyzing the seismic signals of the Kursk events

As mentioned before, many authors have tried to estimate the yield of the explosions, which hit the Kursk submarine. Koper *et al*. (2001a, b) and Savage and Helmberger (2001) proposed a simple explosion-like source for Kursk-2. However, it was also observed that all readable first movements of the first P signals have a negative motion for this event (Koper et al. (2001a,b); Northrop (2001)). As an example, Fig. 6.6.1 shows the clear negative first motions on the array beams of ARCES and FINES. This does not fit with the idea of an explosion source. Koper *et al*. (2001a, b) rejected Northrop's (2001) argument against an explosion source mostly by pointing to the presence of a bubble signal as observed in the spectra of Kursk-2 in the frequency range between 1 and 6 Hz (Fig. 6.6.2, red curve). The wide amplitude maximum around 9 Hz is interpreted as the signal of the surface reflection and its reverberations in the water layer. For a water depth of about 115 m as in the Kursk accident area we can expect destructive interference for the frequencies 6.3 and 12.6 Hz and constructive interference for the frequencies 9.5 and 15.8 Hz. This is exactly what is seen in Fig. 6.6.2 (red curve), supporting our presumption that Kursk-2 happened close to the sea bottom. Fig. 6.6.2 also shows the spectra for Kursk-1 (blue curve) and an equally long noise sample observed just before the Kursk accident. It can easily be seen that the data of Kursk-1 are very close to the noise level. Any modulation due to a bubble pulse is not visible; maybe a slight amplitude increase for the frequency range of the surface reflection / water-layer reverberations signal can be seen.

As reported by Ringdal *et al.* (2000) and in several press reports, the Russian navy conducted a series of underwater explosions in the Kursk accident area during autumn and winter 2000/ 2001. For the largest of these explosions with a magnitude of about 2.5 (*i.e.* about one magnitude unit smaller than Kursk-2, see Table 6.6.1) we can clearly observe a positive first motion at ARCES and at FINES (Fig. 6.6.1). In addition, we cannot identify a bubble-pulse related modulation of the lower part of the spectrum (compare the green with the red curve in (Fig. 6.6.2). The signals from the surface reflection / water-layer reverberations at about 9 Hz are now more clearly visible than for Kursk-2 but we cannot see the outstanding amplitude minimum at about 6 Hz. We can also identify further amplitude maxima at about 11 and 15 Hz. By interpreting these frequency modulations as signals from the bubble pulse and assuming an identical explosion depth as for Kursk-2, we are led to a relatively small yield estimate of about 15 kg TNT equivalent for this explosion (after relations published in Gittermann et al. (1998)). This is far too small to produce a magnitude 2.5 event.

We observe these apparent discrepancies:

- clear negative first-motion onsets for Kursk-2 and spectral evidence of a bubble pulse for a proposed simple explosion inside of a submarine.
- clear positive first-motion onsets for an underwater explosion with no bubble pulse.

Because both signals came from the same source area, propagation effects can be excluded as cause for the observed discrepancies. This leads to the conclusion that the source history of Kursk-2 is quite complex. It also indicates that an explosion inside a closed steel container, possibly still in a gas volume, cannot be described with the standard model of an explosion source in water as done, e.g., for the Dead Sea explosions in 1999. Therefore, a source function with an initially implosive signal may be considered, as also proposed by Northrop (2001). In

the following, the size of an imploding volume will be estimated, which would explain all observed seismic energy of this event (as an extreme case).

Following Müller (1973, 2001) the seismic moment M_0 of a volume change ΔV due to an explosion (or implosion) can be modeled by $M_0 = (\lambda + 2\mu) \cdot \Delta V$, with the Lamé's parameters λ and μ. From the observed local magnitude 3.5 of Kursk-2 a seismic moment can be deduced of about $M_0 = 9 \cdot 10^{13}$ Nm. The modeled implosion source can be described as the collapse of a gas volume at normal atmospheric pressure inside the submarine due to the sudden pressure change (about 100 m water column) after a leakage. For water and gas the shear modulus $\mu \equiv 0$. Then λ becomes identical to the bulk modulus κ and the seismic moment can be written as $M_0 = \kappa \cdot \Delta V$.

The change of the gas volume ΔV due to the pressure change from one atmosphere to the pressure at about 100 m water depth can be written after applying Boyle-Mariotte's law for ideal gasses as $\Delta V = V \cdot \frac{\Delta p}{p}$, with the relative pressure change $\frac{\Delta p}{p}$, and the original volume V. The equation for the volume to be collapsed to radiate a specific seismic moment is then:

$$V = \frac{M_0 \cdot p}{\kappa \cdot \Delta p}$$

For 100 m water depth, the relative pressure change is about a factor of 10 and the bulk modulus for sea water is about $\kappa = 2.14 \cdot 10^9$ N/m^2. Putting all results together, we get for the collapsed volume a value of approximately V = 4200 m^3. Following published specifications of the Kursk (*e.g.* Federation of American Scientists: http:www.fas.org/nuke/guide/russia/theater/949.htm), the 150 m long Kursk submarine had a submerged water displacement in the range 16 400 to 24 000 tons, which corresponds with a total volume of about 16 700 to 24 400 m^3. In the case that the energy from Kursk-2 was radiated only by one imploding volume, about 20 to 26% of the whole submarine must have been cataclysmically flooded during this event. This volume corresponds well with news reports that about the first third (bow) of the submarine was heavily damaged.

Discussion

The application of the master-event analysis between the two seismic events connected with the Kursk accident suggests that the submarine moved about 145 m to the north-west during the 135.8 s between the two events. The azimuth of this movement is about 302°. After the accident not only the exact position of the Kursk submarine became known but also the direction in which the submarine was lying on the sea bottom (Lind, 2002). This direction was reported as 288°. This is in good agreement with our results about the relative movement of the submarine during the time interval between Kursk-1 and Kursk-2. How much the corresponding change in depth was, cannot be resolved. Assuming a pure horizontal movement, the minimum average velocity of the submarine was about 1.1 m/s (or 2.2 knots). In case the first event occurred when the submarine was close to the surface and the second event occurred when the submarine was close to the bottom of the Barents Sea, the depth difference would be about 100 m. Then, the total change in position was about 180 m and we get a maximum average velocity of about 1.3 m/s (or 2.6 knots). Both extreme average values for the velocity of the submarine

during the accident suggest that the submarine was already in a more or less motionless state when it was hit by the first event.

The observed differences between the explosion events during autumn and winter 2000/2001, and the proposed simple explosion-like source derived for Kursk-2 are obvious. The spectral analysis of the signals from Kursk-2 and the observed negative first motion of the onsets clearly indicate a very complex source function.

Johannes Schweitzer

References

Gittermann, Y., Z. Ben-Avraham, and A. Ginzburg (1998): Spectral analysis of underwater explosions in the Dead Sea. Geophys. J. Int. **134**, 460-472.

Koper, K. D., T. C. Wallace, St. R. Taylor, and H. E. Hartse (2001a): Forensic seismology and the sinking of the Kursk. EOS, Trans. Amer. Geophys. Union **82**, 37, 45-46.

Koper, K. D., T. C. Wallace, St. R. Taylor, and H. E. Hartse (2001b): Reply. EOS, Trans. Amer. Geophys. Union **82**, 244.

Lind, B. (2002). Personal communication with Bjørn Lind, Norwegian Radiation Protection Authority.

Müller, G. (1973): Seismic moment and long-period radiation of underground nuclear explosions. Bull. Seism. Soc. Amer. **63**, 847-857.

Müller, G. (2001): Volume change of seismic sources from moment tensors. Bull. Seism. Soc. Amer. **91**, 880-884.

Northrop, J. (2001). Comment. EOS, Trans. Amer. Geophys. Union **82**, 244.

Ringdal, F., T. Kværna, and B. Paulsen (2000): Seismic events in the Barents Sea and near the site of the Kursk submarine accident on 12 August 2000. NORSAR Semiannual Tech. Summ. 1 April - 30 September 2000, NORSAR Sci. Rep. No. **1-2000/2001**, Kjeller, Norway, 77-88.

Savage, B. and D. V. Helmberger (2001): Kursk explosion. Bull. Seism. Soc. Amer. **91**, 753-759.

Table 6.6.1. Source parameters for the analyzed events (three first lines). The depth of all events are unknown. The epicenter of Kursk-2 is assumed to coincide with the known location of the Kursk submarine on the sea bottom after the accident (provided in the fourth line).

Event	Date	Time	Latitude [º]	Longitude [º]	Depth [km]	Magnitude (NORSAR)	Reference
Kursk-1	12.08.2000	07.28.26.6	69.6160	37.5740	?	1.50	This study
Kursk-2	12.08.2000	07.30.42.4	69.6166	37.5708	?	3.50	This study
Explosion	15.11.2000	06.23.16.8	69.703	37.001	?	2.49	NORSAR
Submarine	12.08.2000	--	69.6166	37.5708	0.115	--	Lind (2002)

Table 6.6.2. The table shows the data used for the master-event inversion:
App.vel. is the applied apparent velocity for this observation,
Cor.coeff is the measured cross-correlation coefficient between Kursk-1 and Kursk-2 for the phases considered,
δt is the measured time difference,
δt-M is the measured time difference after removing the mean value,
Residuum is the time difference after the inversion, and
σ-δt is the assumed uncertainty of the measured time difference.

Station	Backazimuth	Phase	App. vel.	Cor. coeff.	δt	δt-M	Residuum	σ-δt
APA0	219.938	Pn	7.91	0.455	135.770	0.0088	0.0057	0.0110
APA0	219.938	Lg	3.56	0.407	135.755	-0.0063	0.0128	0.0123
APZ9	216.610	Lg	3.56	0.311	135.805	0.0438	0.0150	0.0161
ARCES	273.839	Pn	8.61	0.656	135.760	0.0188	0.0071	0.0119
ARCES	273.839	PnPn	8.14	0.755	135.757	-0.0013	-0.0098	0.0076
ARCES	273.839	Sn	5.72	0.780	135.743	-0.0043	-0.0103	0.0066
ARCES	273.839	Lg	4.12	0.774	135.740	-0.0183	-0.0147	0.0064
FIA0	214.939	Pn	8.07	0.421	135.780	-0.0213	-0.0204	0.0065
KEV	276.374	Pn	8.62	0.496	135.747	-0.0143	-0.0104	0.0101
KEV	276.374	Lg	3.07	0.734	135.731	-0.0303	-0.0291	0.0068
LVZ	210.569	Pn	7.74	0.675	135.769	0.0078	0.0087	0.0074
LVZ	210.569	Lg	3.71	0.770	135.778	0.0168	0.0181	0.0065

Table 6.6.3. Results of the master-event location between Kursk-1 and Kursk-2 and associated standard deviations σ. The distances are given relative to Kursk-1.

	Kursk-1 > Kursk-2 [km]	σ [km]
East-West	-0.123	0.021
North-South	0.076	0.013

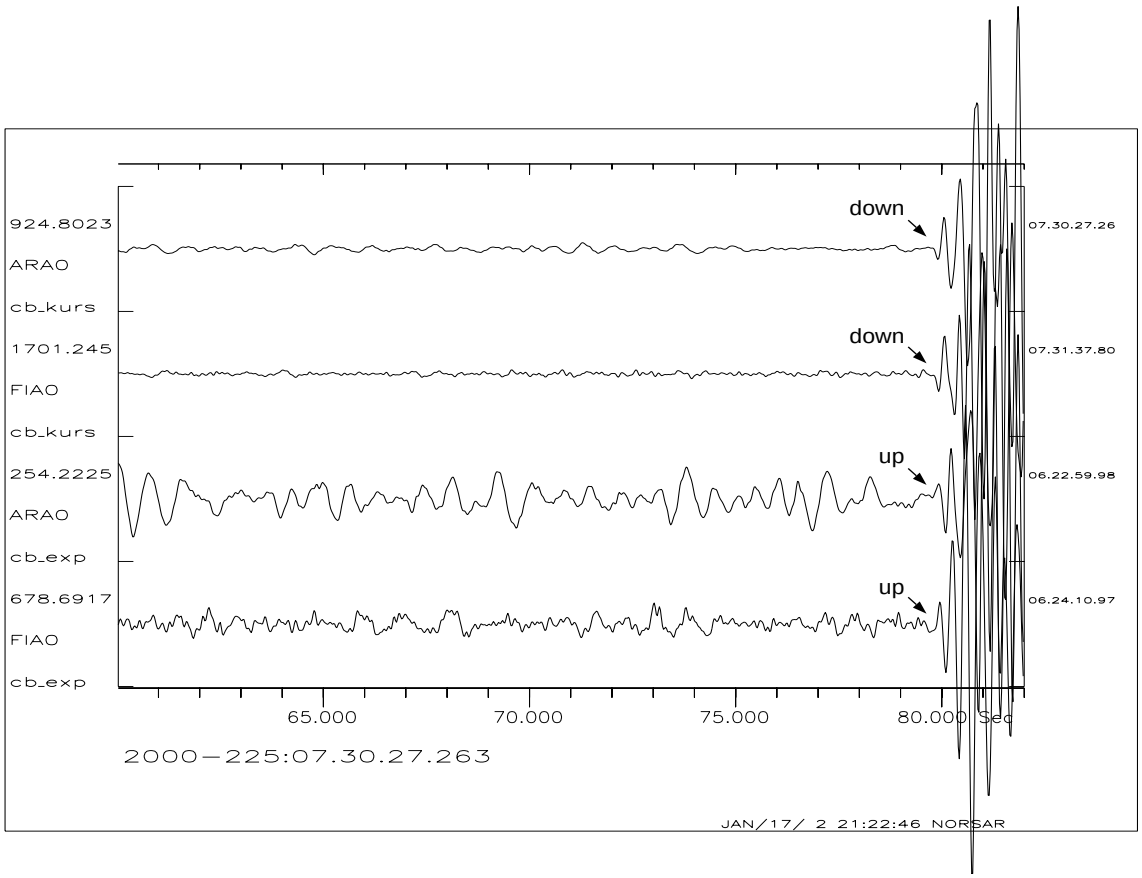

Fig. 6.6.1. Butterworth band-pass (1.5 - 8 Hz) filtered beams of Kursk-2 (_kurs) and the discussed explosion in the Barents Sea (_exp) as observed at the regional arrays ARCES and FINES. The source details are listed in Table 6.6.1.

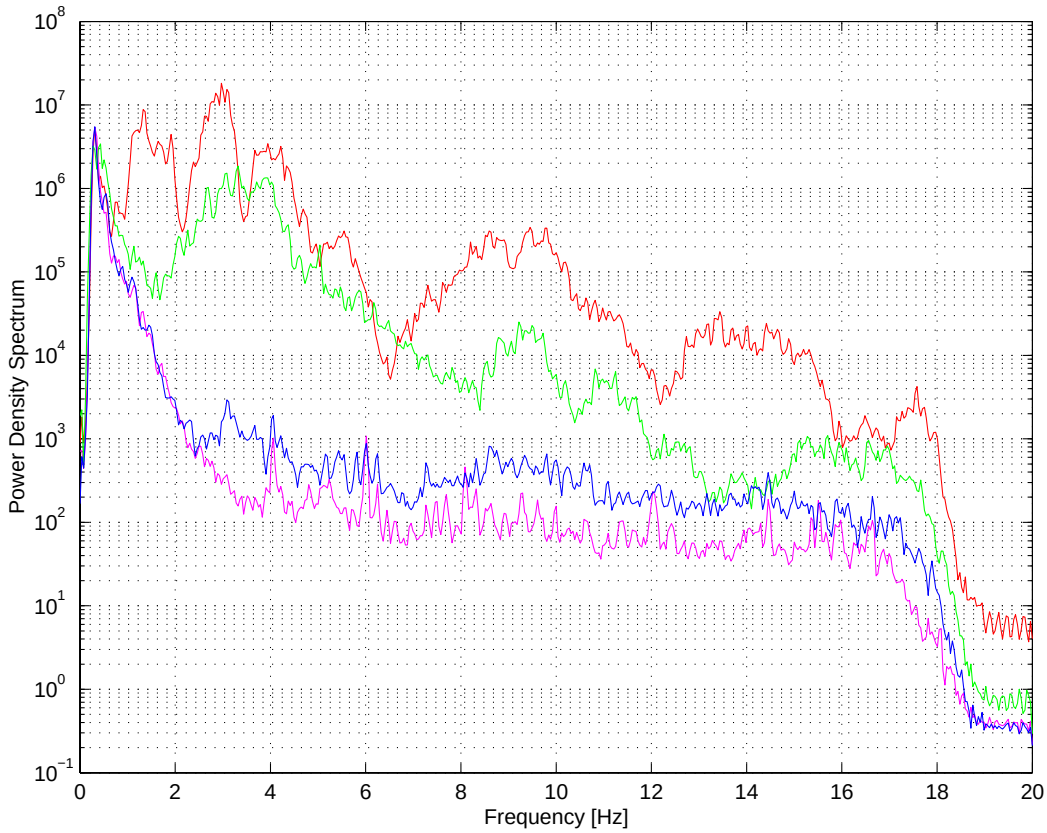

Fig. 6.6.2. Power density spectra from the Kursk main event (Kursk-2, red), the Kursk precursor event (Kursk-1, blue), the magnitude 2.5 explosion in the Barents Sea close to the Kursk site (green), and a noise sample measured just before the Kursk accident (magenta). All spectra are mean spectra of all three components of the central site ARA0 of the ARCES array. The time series were all 90 s long, starting with the P onset, and including most of the Lg wave train. The data were not filtered or processed before calculating the power density spectra using the Welch method.